PASSIVITY-BASED ADAPTIVE BILATERAL TELEOPERATION CONTROL FOR UNCERTAIN MANIPULATORS WITHOUT JERK MEASUREMENTS

Ivanko Yannick Yanque Tomasevich

Tese de Doutorado apresentada ao Programa de Pós-graduação em Engenharia Elétrica, COPPE, da Universidade Federal do Rio de Janeiro, como parte dos requisitos necessários à obtenção do título de Doutor em Engenharia Elétrica.

Orientadores: Fernando Cesar Lizarralde
Antonio Candea Leite

Rio de Janeiro
Junho de 2017

PASSIVITY-BASED ADAPTIVE BILATERAL TELEOPERATION CONTROL
FOR UNCERTAIN MANIPULATORS WITHOUT JERK MEASUREMENTS

Ivanko Yannick Yanque Tomasevich

TESE SUBMETIDA AO CORPO DOCENTE DO INSTITUTO ALBERTO LUIZ
COIMBRA DE PÓS-GRADUAÇÃO E PESQUISA DE ENGENHARIA (COPPE)
DA UNIVERSIDADE FEDERAL DO RIO DE JANEIRO COMO PARTE DOS
REQUISITOS NECESSÁRIOS PARA A OBTENÇÃO DO GRAU DE DOUTOR
EM CIÊNCIAS EM ENGENHARIA ELÉTRICA.

Examinada por:

_____
Prof. Fernando Cesar Lizarralde, D.Sc.

_____
Prof. Antonio Candea Leite, D.Sc.

_____
Prof. Bruno Vilhena Adorno, Ph.D.

_____
Prof. Ramon Romankevicius Costa, D.Sc.

_____
Prof. José Paulo Vilela Soares da Cunha, D.Sc.

RIO DE JANEIRO, RJ – BRASIL
JUNHO DE 2017

*A mis padres Justo y Liliana y a
mi hermano Mirko, por su amor
y confianza.*

Agradecimentos

CONTROLE ADAPTATIVO BASEADO EM PASSIVIDADE PARA TELEOPERAÇÃO BILATERAL DE MANIPULADORES INCERTOS SEM MEDIÇÃO DO JERK

Ivanko Yannick Yanque Tomasevich

Junho/2017

No presente trabalho, considera-se o problema de teleoperação bilateral de um sistema robótico cooperativo do tipo *single-master* e *multiple-slaves* (SM/MS) capaz de realizar tarefas de transporte de carga na presença de incertezas paramétricas no modelo cinemático e dinâmico dos robôs. A arquitetura de teleoperação está baseada na abordagem de duas camadas em estrutura hierárquica, onde as camadas superior e inferior são responsáveis por assegurar as propriedades de transparência e estabilidade respectivamente. O problema de transporte de carga é formulado usando a abordagem de controle de formação onde a velocidade de translação desejada e a força de interação são fornecidas ao robô mestre pelo operador, enquanto o objeto é manipulado pelos robôs escravos com uma força constante limitada. Primeiramente, desenvolve-se um esquema de controle adaptativo cinemático baseado em uma lei de adaptação composta para solucionar o problema de controle cooperativo de robôs com cinemática incerta. Em seguida, o controle adaptativo dinâmico de robôs cooperativos é implementado por meio de uma estratégia de controle em cascata, que não requer a medição da derivada da força (o qual requer a derivada da aceleração ou jerk). A teoria de estabilidade de Lyapunov e o formalismo de passividade são usados para estabelecer as propriedades de estabilidade e a convergência do sistema de controle em malha-fechada. Resultados de simulações numéricas ilustram o desempenho e viabilidade da estratégia de controle proposta.

PASSIVITY-BASED ADAPTIVE BILATERAL TELEOPERATION CONTROL FOR UNCERTAIN MANIPULATORS WITHOUT JERK MEASUREMENTS

Ivanko Yannick Yanque Tomasevich

June/2017

Advisors: Fernando Cesar Lizarralde
     Antonio Candea Leite

Department: Electrical Engineering

In this work, we consider the bilateral teleoperation problem of cooperative robotic systems in a Single-Master Multi-Slave (SM/MS) configuration, which is able to perform load transportation tasks in the presence of parametric uncertainty in the robot kinematic and dynamic models. The teleoperation architecture is based on the two-layer approach placed in a hierarchical structure, whose top and bottom layers are responsible for ensuring the transparency and stability properties respectively. The load transportation problem is tackled by using the formation control approach wherein the desired translational velocity and interaction force are provided to the master robot by the user, while the object is manipulated with a bounded constant force by the slave robots. Firstly, we develop an adaptive kinematic-based control scheme based on a composite adaptation law to solve the cooperative control problem for robots with uncertain kinematics. Secondly, the dynamic adaptive control for cooperative robots is implemented by means of a cascade control strategy, which does not require the measurement of the time derivative of force (which requires jerk measurements). The combination of the Lyapunov stability theory and the passivity formalism are used to establish the stability and convergence property of the closed-loop control system. Simulations and experimental results illustrate the performance and feasibility of the proposed control scheme.

Contents

List of Figures

Abbreviations and Symbols

Abbreviations and Acronyms

Symbol	Description	Units
n	Number of robot manipulators	$[\frac{p}{u}]$
c_i	Contact point on the object of the end-effector	[m]
$\mathbb{E}_s$	Inertial frame	$[\frac{p}{u}]$
$\mathbb{O}$	Object frame	$[\frac{p}{u}]$
p_{ci}	Position of the contact point c_i	[m]
p_o	Position of the object	[m]
p_i	Position of the end-effector	[m]
R_o	Rotation matrix of the object	$[\frac{p}{u}]$
δ_i	Object deformation vector	[m]
f_i	Reaction force vector	[N]
P	Potential function of deformation	$[\frac{p}{u}]$
m_o	Object mass	[kg]
q_i	Vector of joint angles	[rad]
n_i	Number of joints	$[\frac{p}{u}]$
ℓ_i	Number of kinematic parameters	$[\frac{p}{u}]$
b_i	Kinematic parameter vector	[m]
Z_i	Forward kinematic regressor matrix	$[\frac{p}{u}]$
W_i	Differential kinematics regressor matrix	$[\frac{rad}{s}]$
J_i	Position part of the manipulator Jacobian	$[\frac{m}{rad}]$
u_i	Velocity control signal	$[\frac{m}{s}]$
k_i	Forward kinematics map	[m]
ϵ_i	Prediction error	[m]
Γ_k	Kinematic adaptive gain matrix	$[\frac{ms}{radN}]$
w_1	Vanishing input signal	$[\frac{m}{s}]$
ε_i	Vanishing perturbation term	$[\frac{m}{s}]$
v_i	Cartesian control signal	$[\frac{m}{s}]$
K_v	Control gain matrix	$[\frac{m}{Ns}]$
λ_i	Cutoff frequency	$[\frac{rad}{s}]$

Symbol	Description	Units
M_i	Inertia matrix	$[\frac{Nms^2}{rad}]$
C_i	Coriolis matrix	$[\frac{Nms}{rad}]$
g_i	Gravity vector	[N m]
τ_i	Vector of generalized torques	[N m]
Γ_d	Dynamic adaptation gain matrix	[p/u]
σ_i	Measure of tracking accuracy	$[\frac{rad}{s}]$
Y_i	Dynamic regressor matrix	$[\frac{p}{u}]$
a_i	Dynamic parameter vector	$[\frac{p}{u}]$
m_i	Number of dynamic parameters	$[\frac{p}{u}]$
F_i	Kinetic regressor matrix	$[\frac{p}{u}]$
w_2	Fictitious external input	[N m]
K_d	Positive definite gain matrix	$[\frac{Nms}{rad}]$
E_m	Energy at the master side	$[J]$
E_s	Energy at the slave side	$[J]$
E_c	Energy at the communication channel	$[J]$
E_T	Total energy of the system	$[J]$
E^+	Received energy	$[J]$
E^-	Send energy	$[J]$
E_d	Desired energy level	$[J]$

Symbols

Accents

$(\quad)_i$	Of the i-th robot manipulator
$(\quad)_f$	Filtered
$(\quad)^d$	Desired
$(\quad)^r$	Reference
$(\quad)^\mathsf{T}$	Transpose
$(\quad)^\dagger$	Pseudo-inverse
$(\vec{\quad})$	Unit vector
$(\hat{\quad})$	Estimation
$(\tilde{\quad})$	Error or difference
$(\dot{\quad})$	First derivative
$(\ddot{\quad})$	Second derivative

Operators and Standard Functions

- t denotes time

- $\vec{x}$, $\vec{y}$, $\vec{z}$ are the unit vectors along the X, Y and Z axis, respectively.

- $S(.)$ denotes the (3×3) skew-symmetric matrix operator performing the cross product.

- I and O denote the identity and zero matrices, respectively.

- $Q(\vartheta, \vec{r})$ denotes the unit quaternion expressing a rotation of angle ϑ around an axis r.

List of Tables

Chapter 1

Introduction

Nowadays robots are making a great impact on many aspects of modern life, from the exploration of deep space and underseas, to industrial manufacturing and healthcare. They are slowly transitioning from fantastic elements of science fiction to become tools that improve the quality of life of the people.

In many situations it is more convenient to have a robot instead of a human to perform a desired task. This happens when this tasks need to be performed in remote, inaccessible and/or hostile environments for humans. In these cases a robot controlled remotely by a human operator can be used; this way, the human operator capabilities of planning, decision and expertise can be exploited while the operator remains in a safe environment (Niemeyer et al. (2016)).

Multi-arm robotic systems have been focus of attention from the early stages of robotic research, mainly due to the typical limitations in applications of single-arm robots. Several tasks like handling large or heavy objects, or the assembly of multiple parts are unsuited for the application of single-arm robots and gave rise to the adoption of multiple arms robotic systems working cooperatively (Caccavale and Uchiyama (2016)).

1.1 Motivation

In the last decades, human operators have been able to carry out grasp and manipulation tasks of several different types of objects, located in remote and harsh environments, in a safe and intuitive manner by using *telerobotics*, *teleoperation* or *telemanipulation* systems (Niemeyer et al. (2016)). These terminologies are generally used as synonymous although they have slightly different meanings: telerobotics highlights the remote control by operators, teleoperation emphasizes the task-level operations and telemanipulation stresses the object-level manipulation (Niemeyer et al. (2016)).

In this context, the control architecture can be classified as *direct*, *shared* and

supervisory. In the direct control, the motion of the slave robot is directly controlled by the user using the master robot interface (unilaterally or bilaterally), without intelligence or autonomy. In shared control, the task execution is shared between the direct control and local sensory feedback loops with low levels of intelligence and autonomy. In supervisory control, the user and the slave robots are connected with a high level of local intelligence and autonomy (Niemeyer et al. (2016)). In the direct control framework, bilateral teleoperation is considered when reaction forces from the slave robots are reflected back to the master robots and inserted into the input torque of the masters.

The teleoperation of cooperative manipulators present several problems. One of them is the presence of kinematic and dynamic uncertainties in the manipulators, due to the use of sensors or tools in the end-effectors, imperfections in the parts or bad calibration. This problem can be coped adaptive control laws that provide an estimative of the uncertain parameters and achieve stable behavior of the overall controller.

Also, when multiple arms hold an object, the internal force within the object needs to be measured or estimated and regulated for stable grasping while avoiding damage. A control scheme that considers the force exerted by the teleoperated manipulators is thus necessary.

Other problems arise due to the time delays that appear in the communication channel. The delay of a network specifies how long it takes for a bit of data to travel across the network from one node or endpoint to another. It is typically measured in multiples or fractions of seconds. Delay may differ slightly, depending on the location of the specific pair of communicating nodes (Wikipedia (2017)).

Time delays lead to loss of passivity of the overall system. Several methods have been proposed to cope with this problem, generally at the expense of performance.

Teleoperation of cooperative manipulators has applications in many areas, such as:

- Medicine : Where teleoperators are used to perform minimally invasive surgeries at distance in a reduced workspace with increased precision and haptic feedback (Cavusoglu et al. (2002); Guo et al. (2015)).

- Education and Training : Where telemanipulators are used for training and to perform experiments in remote laboratories (Nudehi et al. (2005); Shahbazi et al. (2015)).

- Chemical and Nuclear : Where telemanipulation handle toxic or radioactive materials, which would be expensive and dangerous for human operators to handle (Kuban and Martin (1984)).

- Undersea : Where underwater telemanipulators are used to explore and perform tasks in locations inaccessible or dangerous to human divers (Khatib et al. (2016); Stuart et al. (2017)).

- Aerospace : Assembly and maintenance of spacecrafts, where they prevent cosmonauts to perform tasks in hostile conditions of the outer space (Diftler et al. (2011); Mehling et al. (2007)).

Some teleoperation applications in medicine, industrial maintenance, space and undersea exploration are shown in Fig. 1.1. The *Zeus*, robot during Lindberg operation; the *DaVinci*, telerobotic surgical system; *Mascot IV*, performing maintenance to the Joint European Torus (JET); *Sofie*, robotic master-slave system for minimally invasive surgery (MIS); *Centaur*, Nasa mobile humanoid design for field work; *Robonaut 2 units A and B*, currently aboard the International Space Station; *Ocean One*, dual arm underwater robot.

1.2 Objective

In this work, a cooperative control strategy derived from formation control (Bai and Wen (2010)) is used to teleoperate multiple manipulators holding a common object with a desired grasping force. Adaptive control laws are proposed to cope with the kinematical and dynamical uncertainties considered in the robotic manipulators (Slotine and Li (1988)). To tackle the hybrid velocity and force control problem a cascade control strategy is applied (Hsu et al. (2007)), this allows to cascade the kinematic control scheme with the dynamic control law.

The problem of loss of passivity due to time delays during teleoperation is tackled using an scheme that monitors the incoming and outgoing energy and enforces passivity of the teleoperated system by using energy tanks (Franken et al. (2011)).

The objective of this Thesis is to develop a methodology for the teleoperated control of cooperative manipulators performing load transportation. Here it is considered that an operator provides a desired velocity and grasping force to the remotely located slaves which present uncertainties in their kinematic and dynamic parameters.

1.3 Teleoperation

Telerobotic systems allow human operators to manipulate objects located in a remote environment, thus allowing the execution of complex tasks and avoiding risky situations for the human operator. This is called Telemanipulation, where the greek word *Tele* means at a distance. The operator interacts with a master
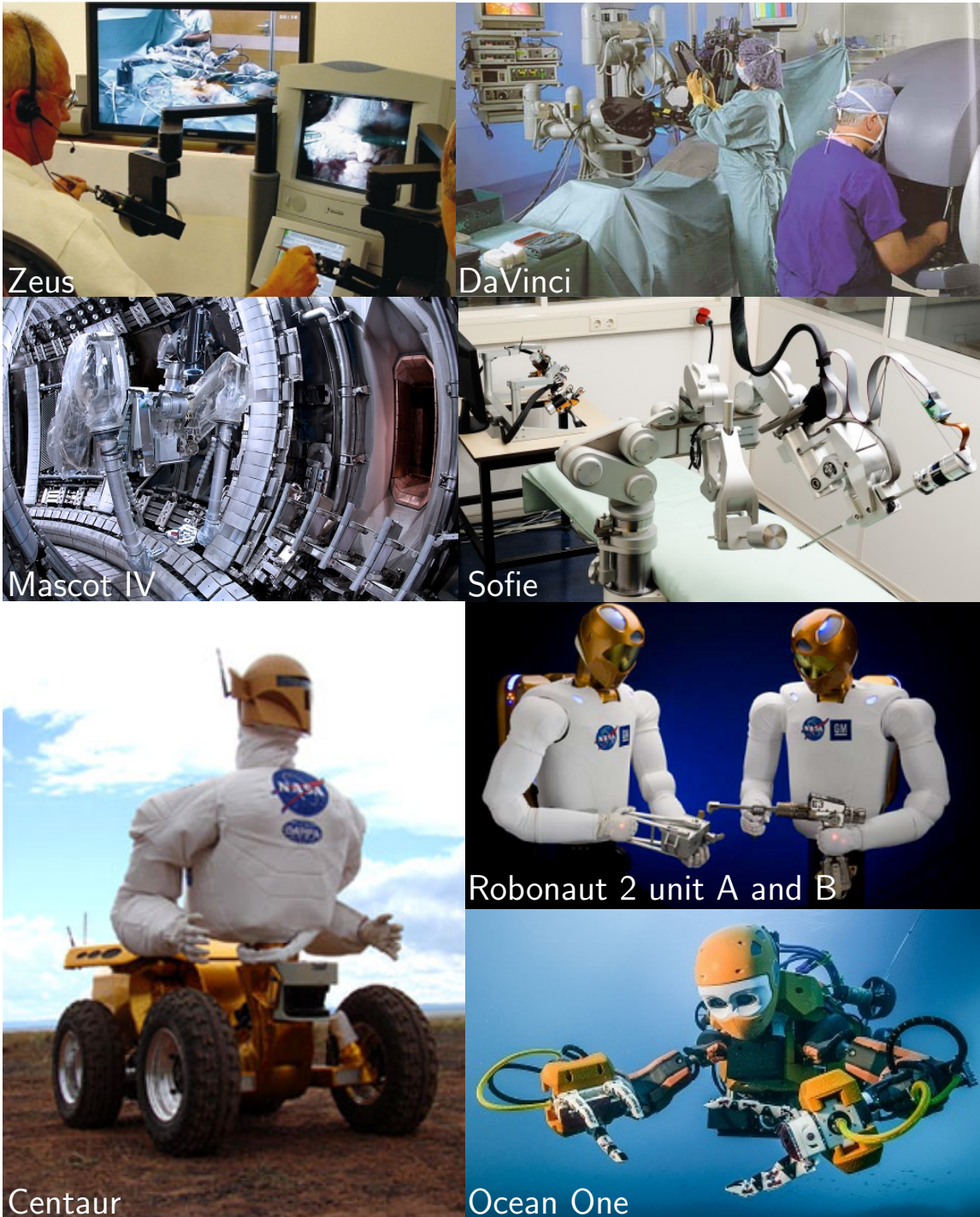
Figure 1.1: Examples of cooperative teleoperators: *Zeus* (source: Hoeckelmann et al. (2015)), *DaVinci* (source: http://www.teleroboticsurgeons.com/davinci.htm), *Mascot IV* (source: http://www.race.ukaea.uk/), *Sofie* (source: Eindhoven University of Technology), *Centaur* (source: Mehling et al. (2007), *Robonaut* (source: Diftler et al. (2011)), *Ocean One* (source: Stuart et al. (2017))

device that exchange motion information through the communication channel with a slave device located at the remote location that interact with the environment, this is called unilateral teleoperation. Unilateral telemanipulators (without force feedback or a local compliance control) means that the slave is strictly controlled by the master position signal, which results in a stiff system where position errors may result in undesired contact forces (Melchiorri (2003)).

The system is said to be controlled bilaterally if the slave possesses force sensors that transmit back to the master reaction forces from the environment. This forces are reflected to the operator by the haptic master device. Haptic devices recreate the sense of touch by applying forces, vibrations, or motions to the operator, here the haptic master displays force feedback from the slave's interaction with the environment. This bilateral coupling creates telepresence, which means that the information about the remote environment is displayed to the operator in a natural manner, which implies a feeling of presence (Aracil et al. (2007)).

1.3.1 Bilateral Teleoperator

Bilateral teleoperation systems can be divided into five subsystems, the human operator, the master device, the communication channel, the slave device and the environment, as can be seen in Fig.1.2. This operation is coordinated through local and remote controllers. For an overview of teleoperation in general the reader is referred to Niemeyer et al. (2016).
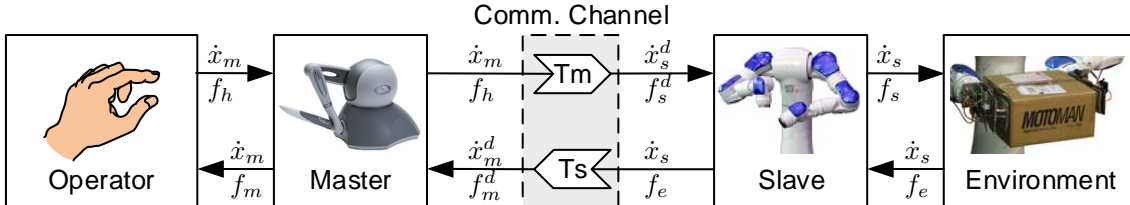
Figure 1.2: Representation of a Bilateral Teleoperated System

Robotic Manipulator

Consider a robotic manipulator with n joints, where the joint configuration is denoted by $q \in \mathbb{R}^n$. The pose of the end-effector is denoted by $x(q) \in SE(3)$, i.e. $x(q) = [p(q)^\mathsf{T} Q(q)^\mathsf{T}]^\mathsf{T}$, containing the translation $p \in \mathbb{R}^3$ of the coordinate frame $\mathbb{E}$ with respect to the inertial frame $\mathbb{E}_s$ and the orientation $Q \in SO(3)$ represented by a unit quaternion, i.e. $Q = [Q_s \ Q_v^\mathsf{T}]^\mathsf{T}$ (see Appendix C.2).

Let the differential direct kinematics be expressed by $v = [\dot{p}^\mathsf{T} \ \omega^\mathsf{T}]^\mathsf{T}$, where $\dot{p} \in \mathbb{R}^3$ is the linear velocity and $\omega \in \mathbb{R}^3$ is the angular velocity. Then the differential direct

kinematics can be expressed as

$$v = J_G(q)\,\dot{q},\tag{1.1}$$

where the matrix $J_G \in \mathbb{R}^{6\times n}$ is the geometric Jacobian.

Also, the wrench $h \in \mathbb{R}^n$ applied by the end-effector is given by $h = [f^\mathsf{T}\gamma^\mathsf{T}]$ where $f,\gamma \in \mathbb{R}^3$ denote the force and moments respectively. By invoking the principle of virtual work, a relationship dual to (1.1) can be derived

$$\tau = J_G^\mathsf{T}(q)\,h,\tag{1.2}$$

where $\tau \in \mathbb{R}^n$ is the vector of torques acting at the joints of the manipulator.

Master and Slave devices

These devices are considered to be robotic manipulators, serial or parallel, with sensors to measure positions and velocities and/or force **applied by the operator or** exerted by the environment. The master is controlled by the operator, its commands are computed by the master controller and sent through the communication channel to the slave controller that commands the slave to interact with the remote environment.

The dynamics of the master (m) and slave (s), as described by Siciliano et al. (2009) are represented by

$$M_m(q_m)\ddot{q}_m + C_m(q_m,\dot{q}_m)\dot{q}_m + g_m(q_m) = \tau_m + J_m(q_m)^\mathsf{T}f_h,\tag{1.3a}$$

$$M_s(q_s)\ddot{q}_s + C_s(q_s,\dot{q}_s)\dot{q}_s + g_s(q_s) = \tau_s - J_s(q_s)^\mathsf{T}f_e,\tag{1.3b}$$

where n_i are the number of joints of the manipulators with $i \in \{m,s\}$, $q_i \in \mathbb{R}^{n_i}$ are the joints configurations, $M_i \in \mathbb{R}^{n_i \times n_i}$ are the inertia matrices, $C_i \in \mathbb{R}^{n_i \times n_i}$ are the Coriolis matrices, $g_i \in \mathbb{R}^{n_i}$ are the gravity vectors, $J_i \in \mathbb{R}^{n_i}$ the manipulator's geometric Jacobian, and $\tau_i \in \mathbb{R}^{n_i}$ are the control torques given by $\tau_i = J_i(q_i)f_i$. Also, $f_h \in \mathbb{R}^{n_d}$ represents the wrench (force and torque) exerted by the operator on the master's end-effector and $f_e \in \mathbb{R}^{n_d}$ represents the wrench (force and torque) exerted by the slave's end-effector on the environment, where n_d is the denotes the operational space of the robot manipulators.

If the robotic manipulators are kinematically equivalent, they can be connected at a joint level, in this case we have

$$q_s^d = q_m + q_{off}, \quad q_m^d = q_s - q_{off}, \quad q_{off} = q_s - q_m,\tag{1.4}$$

where q_s^d, q_m^d refers to a desired joint configurations for the slave and master respec-

tively and q_{off} is a shared offset between them, if they share the same workspace at both sites $q_{off} = 0$.

If the robotic manipulators are not kinematically equivalent (different configuration and dimensions) the dissimilar robot end-effectors are connected at their tips, then (1.3a) and (1.3b) are transformed to the operational space representation, given by

$$\bar{M}_m(x_m)\ddot{x}_m + \bar{C}_m(x_m,\dot{x}_m)\dot{x}_m + \bar{g}_m(x_m) = f_m + f_h, \tag{1.5a}$$

$$\bar{M}_s(x_s)\ddot{x}_s + \bar{C}_s(x_s,\dot{x}_s)\dot{x}_s + \bar{g}_s(x_s) = f_s - f_e, \tag{1.5b}$$

with

$$\bar{M}_i(q_i) = J_i^{\dagger^\mathsf{T}} M_i(q_i) J_i^\dagger, \quad \bar{g}_i(q_i) = J_i^{\dagger^\mathsf{T}} g_i(q_i),$$
$$\bar{C}_i(q_i,\dot{q}_i) = J_i^{\dagger^\mathsf{T}} \left(M_i(q_i)\dot{J}_i^\dagger + C_i(q_i,\dot{q}_i) J_i^\dagger, \right),$$

where $\bar{M}_i \in \mathbb{R}^{n_d \times n_d}$, $\bar{C}_i \in \mathbb{R}^{n_d \times n_d}$, $\bar{G}_i \in \mathbb{R}^{n_d}$, are the equivalent matrices and vectors in the operational space and $x_i \in R^{n_d}$ denotes the end-effector pose, for details see Aldana et al. (2013).

Remote Environment

The interaction with the remote environment has a hybrid nature, the force exerted by the slave end-effector to the environment is nonzero when there is contact and zero when there is not. For simplicity, design and simulation of controllers for robotic telemanipulation are still tied to classical linear string-damper contact models of the environment.

In certain cases the linear theory is enough to describe the mechanical impedance of an object, then a simple model like Kelvin-Voight (Fig.1.3a) can be adopted. If the visco-elastic behavior of the material is remarkable the Zener (Fig.1.3b) model can be adopted, which is frequently adopted when instantaneous and delayed elasticities arise. When the material can not be represented linearly, nonlinear models like the Hunt-Crossley model can be considered (Fig.1.3c). For mode detail the reader is referred to Erickson et al. (2003), Biagiotti and Melchiorri (2007) and Ahmad et al. (2016).

Dynamic interaction between the slave robot and the environment may cause chattering instability. The switching transition between unconstrained and constrained motion was studied by Ni and Wang (2002), under the assumptions of negligible time delay and manipulators with linear decoupled dynamics.

(a) Kelvin-Voight model	(b) Zener model	(c) Hunt-Crossley model
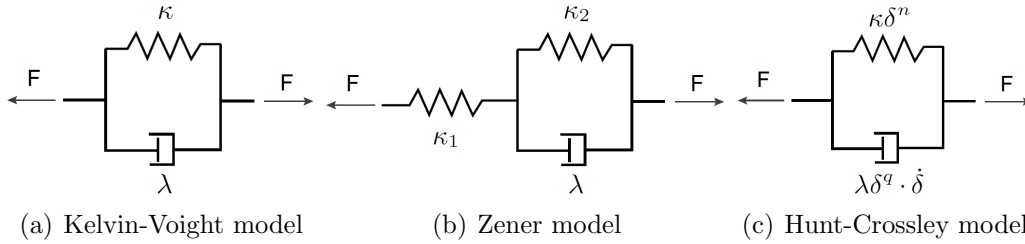
Figure 1.3: Model for the behavior of compliant materials.

Operator

A challenging problem of bilateral teleoperated system is to ensure the transparency and stability in the presence of time delays in the communication channels and uncertainty in the environment. It can be defined as the correspondence between the master and slave positions and forces (Yokokohji and Yoshikawa (1994)), or a match between the impedance perceived by the operator and the environment impedance (Lawrence (1993)). Transparency is a performance index of how well the operator perceives the interaction forces with the environment in terms of impedance and admittance. Perfect transparency is achieved when $f_e = -f_h$ and $\dot{x}_m = \dot{x}_s$ (Lawrence (1992)). Transparency gives the operator a feeling of telepresence and is the second major goal in teleoperation systems design, after stability.

Communication delays can occur not only due to the distance between the local and remote sites, but also because of the encoding and decoding process between the master and slave systems. In this context, transparency and stability problems have been studied by using, for instance, energy-based approaches (Stramigioli et al. (2010)), passivity-based schemes (Nuno et al. (2011b)), small gain theorems (Shahbazi et al. (2015)), Lyapunov-Krasovskii functional (Liu and Khong (2015)), and frequency domain analysis (Yang et al. (2016)). Particularly, the energy tanks approach (Franken et al. (2011)) separates the control architecture in two layers, one that rules the desired transparency and other that ensures the passivity of the teleoperated system. This allows that any controller designed to ensure transparency can be implemented in a passive manner.

The trade-off between transparency and robust stability (passivity) was studied by Lawrence (1993), who revealed that all four information channels (see Fig. 1.5) are necessary to achieve good transparency, and that transparency and passivity are conflicting objectives. This trade-off is due to the fact that delays in the communication channel tend to destroy passivity, which can be recovered by a suitable reformulation of the information transmitted (e.g. transmission of linear combinations of forces and velocities between master and slave), which degrades the transparency of the overall teleoperator.

Communication Channel

The information exchange between master and slave is transmitted through distance. Communication channels have bandwidth limitation and may present package loss or complete loss of communication during teleoperation.

A round trip delay (constant or variant) is introduced by the communication channel, a delay of T_m from master to slave and a delay of T_s from slave to master, such that it takes $T_m + T_s$ seconds until the operator knows the result of the previous command. Time delay could be *small* (few milliseconds), *medium* (tenth of millisecond) or *high* (some seconds) (Melchiorri (2003)). This phenomena affects the teleoperator performance and stability, and have been the focus of intensive research over the years.

1.3.2   Overview of Teleoperation Control

Typically the teleoperator exchange signals of force F, position P or velocity V or functions of those quantities. A large variety of control architectures have been proposed over the years. They have been classified by the kind of signals transmitted (e.g. $P - P$ architecture, just position signals), the number of signals transmitted (number of channels, e.g. 4-channel architecture).

Overviews of proposed control architectures for delayed teleoperation have appeared in numerous articles. Hashtrudi-Zaad and Salcudean (2001) categorizes manipulators as devices of the impedance or admittance type. Admittance relates a force input to a motion output (mobility when being pushed). Impedance relates a motion input to a force output (resistance against motion). Two-channel architectures were discussed.

A comparative study of the performance of teleoperation techniques based on passivity, parameter prediction or adaptation, compliance or variable structure was presented by P. Arcara (2002) and Melchiorri (2003). The performance was analyzed under five aspects: stability, inertia and damping, tracking, stiffness and drift. Under these criteria, it was determined by P. Arcara (2002) that the ideal telemanipulator should be stable for any time-delay, present negligible inertia, zero tracking error, display the same stiffness at the master side as the one perceived in the interaction at the slave side and no position drift.

A survey of schemes that consider online gained information about the environment, operator or task (EOT) explicitly taken into account in the control law was presented by Passenberg et al. (2010), they concluded that EOT schemes have the disadvantage of been mostly application-dependent in comparison with the application-independent classic control approaches.

A tutorial of passivity based controllers was presented by Nuno et al. (2011b),

it was divided in scattering based, damping injection and adaptive scheme, and only controllers that dealt with time-delay were considered. The passivity property implies that if energetic passivity of the closed-loop teleoperator can be ensured, its mechanical interaction with any passive environments and humans will be necessarily stable, regardless of how uncertain or complicated their dynamics are (Lee and Spong (2006)).

The survey presented by Hokayem and Spong (2006) considered schemes classified on whether they are passivity based or not, and the survey presented by Sun et al. (2014) on whether they are wave-variable based or not.

In the following, the principal architectures will be briefly addressed.

Position-Position (P-P)

This is a synchronization architecture, i.e. both manipulators are set to track each other. The environment is reflected to the operator by a stiff master-slave connection. The controllers (usually proportional-derivative) aim to achieve synchronization and can be implemented as,

$$f_{mc} = k_{pm}\left(x_s - x_m\right) + k_{dm}\left(\dot{x}_s - \dot{x}_m\right), \tag{1.6a}$$

$$f_{sc} = k_{ps}\left(x_m - x_s\right) + k_{ds}\left(\dot{x}_m - \dot{x}_s\right) \tag{1.6b}$$

where k_{pi} and k_{di} with $i \in \{m, s\}$ are positive gains.

This can be interpreted as a spring and damper between the tips of each robot (Niemeyer et al. (2016)). While in free-motion, the operator will feel the dynamic forces needed to move the slave. If the slave does not easily move under environment forces (i.e. not back-drivable), the environment force may be hidden from the operator, defeating the purpose of force feedback.

The presence of time delays in the teleoperated system leads to the generation of virtual energy in the communication channel. Considering time-delays in the system, the controlled signals are given by

$$f_{mc} = k_{pm}\left(x_s^{T_s} - x_m\right) + k_{dm}\left(\dot{x}_s^{T_s} - \dot{x}_m\right),$$
$$f_{sc} = k_{ps}\left(x_m^{T_m} - x_s\right) + k_{ds}\left(\dot{x}_m^{T_m} - \dot{x}_s\right),$$

where the $x_i^{T_i}$ and $\dot{x}_i^{T_i}$ with $i \in \{m, s\}$ indicates the time-delayed position and velocity, respectively. The time-delayed positions and velocities can be expressed as the actual positions with time-varying difference terms as in Franken et al. (2012),

given by

$$x_m^{T_m} = x_m + \Delta x_m, \qquad x_s^{T_i} = x_s + \Delta x_s,$$
$$\dot{x}_m^{T_m} = \dot{x}_m + \Delta \dot{x}_m, \qquad \dot{x}_s^{T_i} = \dot{x}_s + \Delta \dot{x}_s,$$

then the time-delayed control signals can be expressed as

$$f_{mc} = k_{pm}\left(x_s - x_m\right) + k_{dm}\left(\dot{x}_s - \dot{x}_m\right) + k_{pm}\Delta x_s + k_{dm}\Delta \dot{x}_s, \qquad (1.7a)$$
$$f_{sc} = k_{ps}\left(x_m - x_s\right) + k_{ds}\left(\dot{x}_m - \dot{x}_s\right) + k_{pm}\Delta x_s + k_{dm}\Delta \dot{x}_s,, \qquad (1.7b)$$

where the first term of (1.7) is equal to the control signals for the undelayed system (1.6) and the second term represents the additional component due to the influence of the time-delays.

Position-Force Control (P-F)

In this force-reflection architecture, a force sensor is placed at the tip of the slave end-effector such that the master reflects the measured force signal from the environment to the operator, while the operator sends position or velocity signals to the slave. This allows the operator to feel the environment forces acting on the slave's sensors, thus having a better sense of the environment. The system controllers are given by

$$f_m = f_e,$$
$$f_s = -K_p(x_s - x_{sd}) - K_v(\dot{x}_s - \dot{x}_{sd})$$

When the slave end-effector is not in contact with the environment (free motion) the system performs as unilateral teleoperation, and the stability is not affected by the delays (Heck et al. (2015)). Is when the slave sensors get in contact with the environment that the measured forces are reflected to the operator and bilateral teleoperation is achieved. When in contact with the environment the maximum admissible delay for which stability is achieved decreases as the control gains increase, therefore the gains have to be tuned as a trade-off between stability and performance requirements (P. Arcara (2002)). Therefore, contact stability may require a high level of damping. In order to avoid this, energy monitoring approaches can be adopted to guarantee stability (Heck et al. (2015)).

Scattering and wave variables

In the 80s, it was observed that a teleoperator can be modeled as a two-port network (Buzan and Sheridan (1989); Hannaford and Fiorini (1988)) for which analysis

tools were available. The behavior of the system then could be represented as a hybrid matrix $H(s)$ (Hannaford (1989)).

$$
\begin{bmatrix} f_m(s) \\ -\dot{x}_s(s) \end{bmatrix} = \underbrace{\begin{bmatrix} h_{11}(s) & h_{12}(s) \\ h_{21}(s) & h_{22}(s) \end{bmatrix}}_{H(s)} \begin{bmatrix} \dot{x}_m(s) \\ f_s(s) \end{bmatrix} \tag{1.9}
$$

where $H(s)$ in the hybrid matrix, and $f_m(s)$, $f_s(s)$, $\dot{x}_m(s)$ and $\dot{x}_s(s)$ are the Laplace transforms of $f_m(t)$, $f_s(t)$, $\dot{x}_m(t)$ and $\dot{x}_s(t)$, respectively. Then, the scattering variables were proposed by Anderson and Spong (1988, 1989) to render the communication channel and thus the system passive, they showed that a system is passive if and only if $\|S(j\omega)\|_\infty \leq 1$, where the scattering operator $S(s)$ is given by

$$
S(s) = \begin{bmatrix} 1 & 0 \\ 0 & 1 \end{bmatrix} (H(s) - I)(H(s) + I) \tag{1.10}
$$

where I is the identity matrix. This formulation allows to develop control laws that guarantee passivity.

A similar formulation called wave variable transformation was introduced by Niemeyer and Slotine (1991). Wave variables (Fig. 1.4) are used for describing the transfer of energy between the master and the slave (Ferre et al. (2007)).
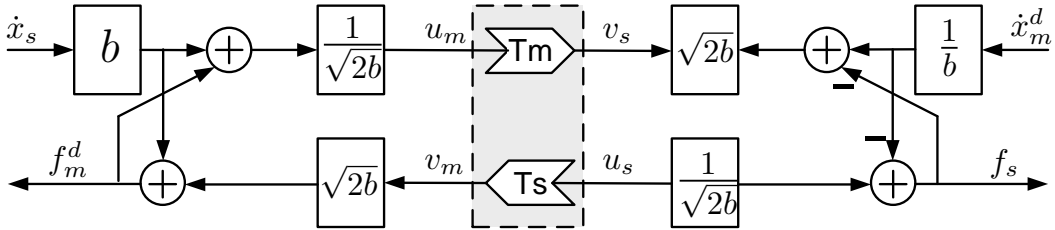
Figure 1.4: Wave variables

The basic idea of the wave variables approach is to transform the effort f_m, f_s and flow $\dot{x}_m, \dot{x}_s$ variables by a linear transformation into wave variables as follows

$$
u_m = \frac{1}{\sqrt{2b}}(f_m + b\dot{x}_m), \qquad\qquad u_s = \frac{1}{\sqrt{2b}}(f_s + b\dot{x}_s),
$$
$$
w_m = \frac{1}{\sqrt{2b}}(f_m - b\dot{x}_m), \qquad\qquad w_s = \frac{1}{\sqrt{2b}}(f_s - b\dot{x}_s),
$$

where b is the characteristic wave impedance given by positive constant or a symmetric positive definite matrix and assumes the role of a tuning parameter. An increase on b results in a smaller position drift but at expense of performance (due to the extra damping).

Passivity of the wave variables is by their construction robust to constant time delays (G.Niemeyer and Slotine (2004)). A wave variable approach for variable time delays was proposed by Yokokohji et al. (1999) at expense of the passivity.

A major drawback may occur due to inaccurate integration. The velocity information is extracted from the communicated scattering variables, then integrated to recover the position information, if the integration becomes inaccurate then the master/slave position may drift (Lee and Spong (2006)). This leads to drift in the position synchronization and distortion on the reflected force.

There are alternatives to cope with this: Impedance matching which consists in matching the characteristic impedance with the rest of the system (Hokayem and Spong (2006); Niemeyer and Slotine (1991)). Wave filtering which consists in inserting a filter into the wave transmission path, this does not affect passivity but may increase inertia and reduce stiffness, thus reducing performance (G.Niemeyer and Slotine (2004)).

A scheme that includes a modified Smith Predictor, a Kalman filter and an energy regulator was used by Munir and Book (2002) to improve the teleoperator performance. The behavior of traditional wave variable controllers under variable wave impedance was investigated by Tanner and Niemeyer (2004). The proposed system provides a controller that feels light in free motion and stiff on contact with environment.

An approach based on the generalized scattering transformation was proposed by Vittorias and Hirche (2010) which consists in the use of approximate knowledge of the damping properties of the human arm, the controlled manipulators and/or the environment for stabilizing control design of a teleoperation system with communication unreliability, thus improving performance.

4-channel architecture

This architecture captures in its generality a large variety of bilateral control schemes. This general teleoperator architecture proposed by Lawrence (1992) presents control loops establishing communication links between master and slave, where they exchange velocities and forces.

Fig. 1.5 shows a block diagram of the teleoperator system, where Z_h and Z_e are the impedance of the operator and the remote task, Z_m and Z_s are the impedance of the master and the slave, C_m and C_s are the master and slave controllers and C_1, C_2, C_3 and C_4, represent the communication blocks.

The dynamics of the system is given by the hybrid matrix formulation (Hannaford
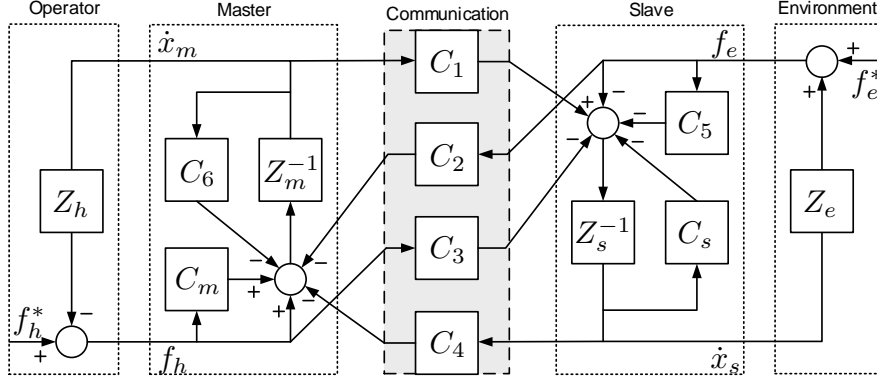
Figure 1.5: 4-channel bilateral teleoperation system (from Aziminejad et al. (2008))

(1989)) in the Laplace domain given by (1.9) where

$$h_{11} = (Z_m + C_m)D(Z_s + C_s - C_3C_4) + C_4,$$
$$h_{12} = -(Z_m + C_m)D(I - C_3C_2) - C_2,$$
$$h_{21} = D(Z_s + C_s - C_3C_4),$$
$$h_{22} = -D(I - C_3C_2),$$

where $D = (C_1 + C_3Z_m + C_3C_m)^{-1}$.

This architecture can represent all teleoperation structures through appropriate selection of subsystem dynamics parameters C_1 to C_6 (Lawrence (1992, 1993)). Ideal transparency can be achieved if the parameters follow the following conditions

$$C_1 = Z_s + C_s, \quad C_2 = 1 + C_6, \quad C_3 = 1 + C_5, \quad C_4 = -(Z_m + C_m),$$

the first and fourth conditions ensure that the master and slave dynamics get cancelled using inverse dynamics while the second and fourth ensure that the net effect of f_h and f_e is the same for the master and the slave. This requires exact knowledge about the master and slave dynamics and exact measurement of acceleration and force (Willaert et al. (2014)).

Synchronization and Damping Injection

Several strategies that do not require scattering transformation to achieve synchronization have been proposed in the literature. Most of these strategies achieve stability and asymptotic convergence to zero of position errors under free-motion ($f_e = 0$ and $f_h = 0$) and considering passive operator and environment.

Lee and Spong (2006) proposed a passivity based method for teleoperation considering damping injection. It uses P+d (proportional plus damping) control or PD+d control (proportional derivative plus damping) to connect the master and

slave via spring and damper over the delay communication channel. This method has the advantage of this method is the explicit position feedback through the delayed P control action. The stability of the method was proved by Nuno et al. (2008) under certain assumptions like passive operator, passive environment, free motion ($f_h = f_e = 0$) and gravity compensation. Nuno et al. (2009b) extended the method to variable time delays.

A dynamic adaptive control law that state synchronize a teleoperated system considering constant time-delays was proposed by Chopra et al. (2008). It was later proved by Nuno et al. (2010b) to be only applicable to systems without gravity, where the previous dynamic adaptive controller that uses position and velocities errors with constant time delay was proposed. A similar dynamic adaptive controller was proposed by Nuno et al. (2010a) for constant time-delays which requires acceleration measurements.

The master and slave PD+d controllers are typically given by

$$\tau_m = k_{pm}\left(q_s^{T_s} - q_m\right) + k_{dm}\left(\dot{q}_s^{T_s} - \dot{q}_m\right) - b_m\dot{q}_m,$$
$$\tau_s = k_{ps}\left(q_m^{T_m} - q_s\right) + k_{ds}\left(\dot{q}_m^{T_m} - \dot{q}_s\right) - b_s\dot{q}_s.$$

where $q_i^{T_i} := q_i(t - T_i)$ where $i \in \{m, s\}$. Note that setting $k_{dm} = k_{ds} = 0$ gives a P+d controller.

A common Lyapunov-Krasovskii function for damping injection schemes was presented by Nuno et al. (2011b) and is given by

$$V = V_1 + V_2 + V_3,$$
$$V_1 = \frac{\beta_m}{2}\dot{q}_m^\mathsf{T} M_m(q_m)\dot{q}_m + \frac{\beta_s}{2}\dot{q}_s^\mathsf{T} M_s(q_s)\dot{q}_s,$$
$$V_2 = \beta_m E_h + \beta_s E_e,$$
$$V_3 = \frac{K_l}{2}|q_m - q_s|^2 + \frac{K_d \beta_r}{2}\int_{t-T_m(t)}^{t}|\dot{q}|^2 d\theta + \frac{K_d}{2}\int_{t-T_s(t)}^{t}|\dot{q}_s|^2 d\theta.$$

where for PD+d controllers $K_l, K_d \in \mathbb{R}^+$, for P+d controllers $K_l \in \mathbb{R}^+$ and $K_d = 0$, and for passive output interconnection (a special case of PD+d controllers (Chopra and Spong (2007))) $K_d \in \mathbb{R}^+$ and $K_l = 0$, and $E_h = -\int_0^t \dot{q}_m^\mathsf{T}\tau_h d\theta + \kappa_m \geq 0$ and $E_e = -\int_0^t \dot{q}_s^\mathsf{T}\tau_e d\theta + \kappa_s \geq 0, \forall t \geq 0$ represent the operator and environment which are assumed to form a velocity to force passive map.

Several damping injection P+d and PD+d controllers have been proposed in the literature. Nuno et al. (2008) proved the stable behavior of nonlinear teleoperators with PD-like schemes for constant delays under the assumption that

$$b_m b_s > T^2 k_{pm} k_{ps}.$$

These results were extended to variable time delays by Nuno et al. (2009a) and Nuno et al. (2009b) under the assumption that

$$4b_m b_s > \left(\bar{T}_m^2 + \bar{T}_s^2 \right) k_{pm} k_{ps}$$

where $\bar{T}_m$ and $\bar{T}_s$ are upper bounds for the time-delays.

It was then extended by Nuno et al. (2011a) considering bounded operator and environment forces and filtered errors to avoid the need of velocity measurements, where position synchronization and velocity synchronization were achieved. Also velocity measurements were avoided for the implementation of the controller by Sarras et al. (2012) using an Immersion and Invariance (I&I) observer where two modifications in the observer design were proposed and by Aldana et al. (2013) using a first order filter where the controller was proposed for the operational space.

A dynamic adaptive controller with damping injection for constant time-delays was proposed by Nuno et al. (2010a) and extended with a different Lyapunov function by Nuno et al. (2014a) with which sufficient conditions for asymptotic convergence are derived.

Synchronization robust against variable time delays of manipulators considering flexible joints was proposed by Nuno et al. (2012b) where it was assumed the absence of gravity. Later, an scheme that considers gravity compensation was proposed by Nuno et al. (2013b) and extended considering a dynamic adaptive controller for variable time delays by Nuno et al. (2014b).

Position/Force-Force Control

This strategy is an extension of the P-F architecture where the operator transmits force to the slave. It is a simple way to potentially improve the system performance and stability. Its advantages have been discussed in Hashtrudi-Zaad and Salcudean (2002). It has better transparency and larger tunning flexibility than the P-F approach (Willaert et al. (2010)).

Compared with the P-F architecture, the introduction of one more channel can enhance system stability as well as stability/transparency trade-off (Albakri et al. (2013)), this was experimentally confirmed by Sherman et al. (2000) by comparing 2-channel P-P, P-F and 3-channel P-PF architectures.

A proportional position error and force feedback with damping injection was proposed by Nuno et al. (2008), where bounded position and velocity errors is achieved and asymptotic synchronization is proved under free motion ($f_h = f_e = 0$).

A general analysis of performance and stability robustness of 3-channel architectures was presented by Albakri et al. (2013) using Llewellyn's absolute stability conditions (Llewellyn (1952),Adams and Hannaford (1999)) and the notion of Z_{width}

to evaluate transparency (Colgate and Brown (1994)).

Time Domain Passivity Control

The Time Domain Passivity Control (TDPC) approach to maintain the passivity of a system was proposed by Hannaford and Ryu (2001) and applied by Ryu et al. (2004) to bilateral teleoperation, there the energy in the system was computed with Passivity Observer (PO) and the energy of the system was dissipated using a time varying element called Passivity Controller (PC). Essentially the PO measures the system active behavior and the PC injects variable damping.

The main advantage of this approach is that the damping injection only happens when the passivity is near to get lost, then the system does not require constant damping to guarantee passivity.

Extensions to consider time delays was proposed by Artigas et al. (2007) where the strategy considers backward (BPC) and forward (FPC) passivity controllers, and by Ryu and Preusche (2007) where the input and the output energy was separated at each master and slave port and bounding each output energy of one port to the input energy at the other port.

An upgrade of the work presented by Ryu and Preusche (2007) was proposed by Ryu et al. (2010) where a detailed complete framework and more rigorous passivity analysis is included. The TDPC was recently applied in the MM-SS scheme proposed by Panzirsch et al. (2015) where two masters manipulate objects via one slave and a virtual gripping point.

Energy storage tanks

The use of energy storage tanks allows to obtain the highest possible transparency allowed by the passivity constraint. Several recent works have considered the use of energy tanks to keep systems passive. Among them, Ferraguti et al. (2013) presented an impedance control strategy that reproduces variable stiffness preserving passivity, Tadele et al. (2014) proposed a variable impedance controller for domestic robots, Schindlbeck and Haddadin (2015) presented an impedance controller for rigid and flexible joint robots, Dietrich et al. (2016) proposed a hierarchy-based approach for kinematically redundant manipulators and which was extended by Dietrich et al. (2017) for arbitrary priority levels, and Salvietti et al. (2017) proposed a multicontact bilateral teleoperation scheme.

Energy tank applied for teleoperation were introduced by Franken et al. (2011, 2009) to represent the energy available for the controllers, considering a two-layer architecture which allows the combination of passivity and transparency.

The lower layer called Passivity Layer (PL) enforces passivity of the system and

the top layer called Transparency Layer (TL), where any bilateral controller can be implemented in a passive manner, achieves the desired performance. The tanks act as an energy budget that powers the controlled movements. When the tanks are empty the respective control signals are cancelled to recover passivity. Both tanks are refilled with energy extracted from the operator by the injected damping from the tank Level Controller (LC). The energy provided by the operator is distributed between both tanks. The main difference with the TDPC approach is the explicit use of energy tanks.

Franken et al. (2012) found a build-up effect in the energy stored when P-P controller is implemented, which prevents the PL from stabilizing the system. This is because the injected energy far exceeds the energy required due to the delay. The problem was solved by removing the excess energy by limiting the energy stored in the tank. This approach was extended by Ferraguti et al. (2015) for the case when the system transits from autonomous to teleoperated mode.

An alternative two-layer control architecture was proposed by Heck et al. (2015) and by Heck (2011) for bilateral teleoperation with constant time delays. It considers an outer layer called Performance Layer (PeL) where any controller can be implemented and an inner layer called Passivity Layer (PaL) that modifies the output of the PeL to render the teleoperator passive. The PaL follows a principle of energy duplication, i.e. the slave and master controllers represent a duplicate of the operator environment. There the control signal provided by the PeL in each side is saturated by means of a constant that depends on the energy stored in the respective tank.

1.4 Cooperative Control

This work relates to the control of dual- or multi-arm robots performing cooperative tasks. Cooperative control of multiple robots has been widely studied in the literature and many approaches have been proposed for real-world applications that a single manipulator cannot perform, such as object handling and assembly, large and heavy load transportation. A survey that summarizes recent developments on control, modeling and planning of dual-arm or multi-arm manipulators was presented by Smith et al. (2012) and Caccavale and Uchiyama (2016). Few studies have considered the control design for bilateral teleoperation of multiple cooperative robots using adaptive and passivity-based techniques.

Several of the motion and force control of multi-arm schemes that have been presented in the literature are hereafter briefly discussed.

1.4.1 Cooperative Task Space

Uchiyama and Dauchez (1988) proposed a non-master/slave scheme for coordination of dual-arm manipulators called *Symmetric Formulation*, the cooperative tasks are described in terms of forces and velocities at the *virtual sticks* attached to the manipulators end-effectors. A major problem of this approach is that the task-space variables deriving from the kinetostatic mapping are often unsuitable for the description of the cooperative task (Caccavale et al. (1999)).

An alternative formulation called *cooperative task space* proposed by Chiacchio et al. (1996) directly defines the task variables in terms of the *absolute* and *relative* motion of the cooperative system. Consider a system of two manipulators, for each manipulator (i=1,2) let $p_i \in \mathbb{R}^3$ denote the position vector, $R_i \in \mathbb{R}^{3\times3}$ the orientation matrix and Q_i the unit quaternion corresponding to R_i (see the Appendix C).

The *cooperative task space* formulation is given by

$$p_a = \frac{p_1 + p_2}{2}, \qquad\qquad p_r = p_2 - p_1, \qquad\qquad (1.13a)$$

$$R_a = R_1 R\left(r, \vartheta/2\right), \qquad\qquad R_r = R\left(r, \vartheta\right) = R_1^{\mathsf{T}} R_2, \qquad\qquad (1.13b)$$

where the vector r and the angle ϑ realize the rotation described by R_r. Then, the *cooperative task space* is described by the absolute position p_a, the relative position p_r, the absolute rotation R_a and the relative rotation R_r, as can be seen in Figure 1.6 and Figure 1.7.
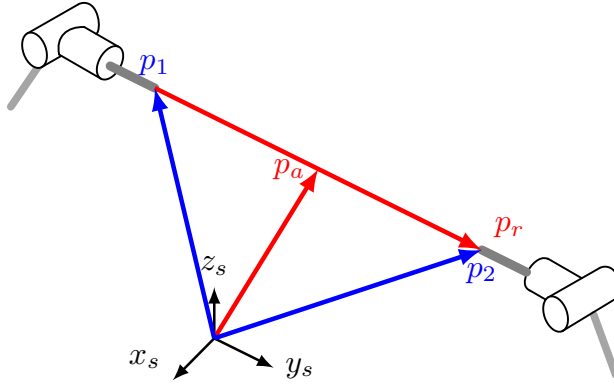
Figure 1.6: Cooperative Task Space: Absolute, Relative and End-effector position vector

In this context, Caccavale et al. (2000) presented a representation of the orientation in the cooperative task space using quaternions, given by

$$Q_a = Q_1 * Q_r^{1/2}, \qquad Q_r = Q\left(r, \vartheta\right) = Q_1^{-1} * Q_2, \qquad\qquad (1.14)$$

where $Q_r^{1/2} = Q\left(r, \vartheta/2\right) = exp\left\{\frac{1}{2}\log Q_r\right\}$, Q_a is the absolute quaternion and Q_r is the relative quaternion.
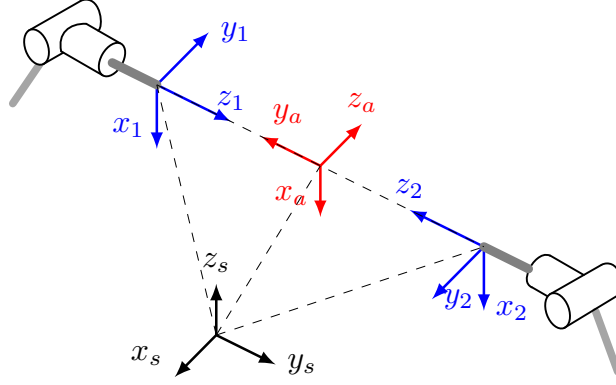
Figure 1.7: Cooperative Task Space: Absolute, Relative and End-effector Frame Orientation

Once the desired motion of the system are given in terms of cooperative task-space variables these can be transformed into the corresponding ones at the end effectors. This was considered for two manipulators by Caccavale et al. (2000) who proposed the generation of reference trajectories given by

$$p_1^d = p_a^d - \frac{1}{2}\,p_r^d, \qquad\qquad p_2^d = p_a^d + \frac{1}{2}\,p_r^d, \qquad\qquad (1.15a)$$

$$R_1^d = R_a^d\,R^{\mathsf{T}}\left(r^d, \vartheta_r^d/2\right), \qquad\qquad R_2^d = R\left(r^d, \vartheta_r^d\right) = R_1^d\,R_r^d, \qquad\qquad (1.15b)$$

the equivalent orientation expressed in quaternions is given by

$$Q_1^d = Q_a^d * Q\left(-r^d, \vartheta_r^d/2\right), \qquad Q_2^d = Q_1^d * Q\left(r^d, \vartheta_r^d\right), \qquad\qquad (1.16)$$

Adorno et al. (2010) proposed an alternative representation considering dual quaternions and defined the *cooperative dual task space*. Later, Adorno (2012) proposed a generalization for more than two manipulators considering *cooperative dual task space* and presented a unified formulation and a decentralized control scheme.

The inverse kinematics problem for a two-manipulator system was stated by Chiacchio et al. (1996) as that to compute the joint variable trajectories corresponding to given coordinated motion trajectories for the absolute and relative task variables. The joint velocity solution can be given by

$$\dot{q} = J^{-1}(q)\left(v^d + Ke\right) \qquad\qquad (1.17)$$

with

$$q = \begin{bmatrix} q_1 \\ q_2 \end{bmatrix}, \quad e = \begin{bmatrix} e_a \\ e_r \end{bmatrix}, \quad J = \begin{bmatrix} J_a \\ J_r \end{bmatrix}, \qquad\qquad (1.18)$$

where q_1, q_2 are the joint vectors of the manipulators, v^d is the desired task velocity,

e_a is the absolute error and e_r is the relative error. The absolute Jacobian J_a and the relative Jacobian J_r are given by

$$J_a = \begin{bmatrix} \frac{1}{2}J_1 & \frac{1}{2}J_2 \end{bmatrix}, \quad J_r = \begin{bmatrix} -J_1 & J_2 \end{bmatrix}. \tag{1.19}$$

Several works consider the cooperative task-space formulation for fixed-grasp dual arm manipulation problems and propose control laws based on PD with gravity compensation. Two basic approaches have been addressed:

- Use inverse kinematic algorithms to compute the desired joint values that correspond to the cooperative task and substituting them within a joint space PD control scheme (Caccavale et al. (1999)).

- Use the cooperative task-space formulation to compute the desired pose of each manipulator based on the desired absolute and relative pose and substitute them within the robot's operational space PD controllers (Caccavale et al. (2000)).

Cooperative manipulators can be often viewed as closed-chain mechanisms and are often related to parallel manipulators. Freitas et al. (2011) explored this feature and parallel systems were modeled and kinematically controlled.

1.4.2 Cooperative position-force control

Here the position and force control loops are decoupled and treated independently. The control signal τ_m to the manipulators is then given by two contributions

$$\tau_m = \tau_p + \tau_h, \tag{1.20}$$

where τ_p is the signal for the position control and τ_h the signal for the internal force control.

PD force/motion control

A Lyapunov-based approach proposed by Wen and Kreutz-Delgado (1992) pursue to define force/position model-based PD-type control laws, where three different control structures based on the choice of variables used in the control design were obtained, named full dynamics, arms-as-actuator and feedback linearization. That approach was used by Montemayor and Wen (2004) considering delay in the force measurements.

Tinos et al. (2006) considered this approach for a cooperative underactuated system where end-effectors with passive joints rigidly connected to an undeformable

object. They also presented a method to measure the load capacity of cooperative systems with passive joints.

A telerobotic framework for human-directed dual-arm manipulation using visual servoing was proposed by Kruse et al. (2015) (which is an extension of the work presented by Kruse et al. (2013)). There a dual-arm robot manipulates a held object through human gestures, the force control method proposed by Wen and Kreutz-Delgado (1992) using force sensors in the end-effectors of the robot and a visual servoing algorithm based on ALVAR [1] tags using a Microsoft Kinect sensor to interpret the user's gestures and convert them into desired poses for the task.

Hybrid position-force control

The hybrid position/force control, which is based on the decomposition of the object motion and the internal forces space, was extended for cooperative manipulators by Hayati (1986). The command signal τ_m to the actuators of the two arms (see 1.20) is given by

$$\tau_p = K_p J_G^{-1} G_x(s) S B(x_o^d - x_o),$$
$$\tau_h = K_f J_G^{-1} G_f(s)(I - S) B(h_o^d - h_o),$$

where x_o is the operational space vector, h_o is the generalized forces vector, K_p, K_f are positive gains, J_G is the Jacobian matrix, G_x, G_f are the position and force control laws and I is the identity matrix. S is the selection matrix which is diagonal, its entries take the values of 1 and 0. It selects the position-controlled and the force-controlled variables. A diagram of the control scheme is shown in Fig. 1.8.
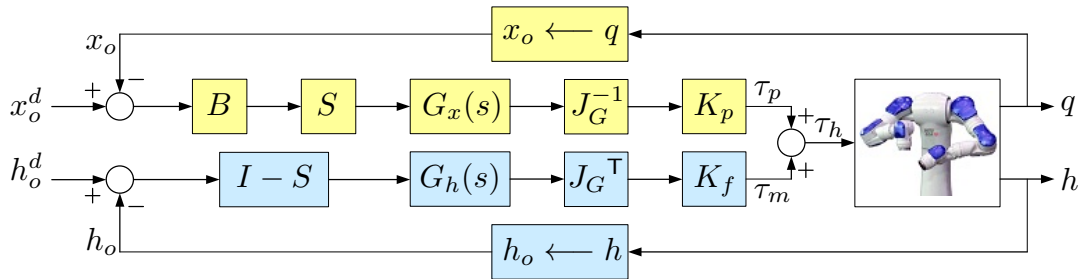
Figure 1.8: Hybrid position/force control scheme (Uchiyama and Dauchez (1988)).

Uchiyama et al. (1987) proposed a non-master/slave hybrid position/force control scheme in which the workspace position is given as the combination of the absolute and relative pose between the hands (Uchiyama and Dauchez (1988)). Later Uchiyama and Dauchez (1988) formalized this results and proposed the symmetric

---

[1]ALVAR: A library for virtual and augmented reality [Online], http://alvar.erve.vtt.fi/

formulation (to control dual-arm manipulators) in a hybrid position/force coordinated control scheme. This scheme was implemented using two PUMA's 560 robotic manipulators by Dauchez et al. (1990) and Dauchez et al. (1991).

Recently, Faria (2016) proposed a method of hybrid position-force control that uses the image-based identification method proposed by Faria et al. (2015) to estimate the pose of an object for its manipulation. There the force applied by the manipulators on the object was indirectly estimated using joint torque sensor measurements.

1.4.3   Impedance control

It uses the impedance concept proposed by Hogan (1985). The impedance control method simultaneously controls the motion along every direction in order to achieve a desired dynamic interaction between the manipulator and the environment. Control schemes for cooperative manipulators have been proposed for the control of object-environment interaction forces (Schneider and R. H. Cannon (1992)) or control of internal forces (Bonitz and Hsia (1996)).

Caccavale and Villani (1999) combine the external and internal impedance control strategies, the first in the object level the later in the end-effector level to reduce the internal forces applied to the object. Caccavale et al. (2008) present an scheme that allows individual activation/deactivation of external and internal impedance, such that the operator can choose to keep one or both of the impedance controllers.

In the work of Heck et al. (2013) the architecture for internal force-based impedance control of cooperative manipulators of Bonitz and Hsia (1996) was combined with the architecture of Caccavale et al. (2008) and an extension of the impedance controller of Schneider and R. H. Cannon (1992) to control motion and internal and external contact forces for the cooperative manipulation of a common object.

Impedance-based control scheme for cooperative control of dual-arms was proposed in Erhart et al. (2013) where uncertainties in the object and manipulator were modeled and evaluated by means of an internal force analysis.

1.4.4   Adaptive Control

The adaptive control scheme proposed by Jean and Fu (1993), where the manipulators end-effectors were rigidly attached to the manipulated object, was extended for teleoperated systems by Aldana et al. (2012) using the dynamic adaptive teleoperated controller proposed by Nuno et al. (2010b).

Kinematic and dynamic adaptive control laws were proposed by Liu and Khong

(2015) for a teleoperated SM/SS scheme position synchronization scheme that requires measurement of joint velocities.

An extension of the passivity analysis of Wang and Xie (2009) and the kinematic adaptive control of Cheah et al. (2006a,b) was presented by Wang (2013), where an adaptive task-space controlled synchronization scheme for networked robotic agents with kinematic and dynamic uncertainties was proposed.

In Erhart and Hirche (2013) an adaptive force/velocity control scheme for planar cooperative manipulation tasks of translation and rotation is proposed, it considers the direct kinematics of the manipulators uncertain (while the differential kinematic is known).

The adaptive teleoperated cooperative control scheme presented by Mohajerpoor et al. (2013) considers velocity synchronization with damping injection, and robot dynamic and object kinematic uncertainty for constant time delays.

1.4.5 Formation control

Formation control is intrinsically related to the coordination control of multi-agents systems and the key idea is to steer the overall system to track a predefined path while keep some particular geometric patterns through the information exchanged between two or more agents (Sieber et al. (2013)).

A formation control strategy of multiple agents without explicit communication is proposed by Bai et al. (2011); Bai and Wen (2010) to manipulate a flexible object, where the contact forces between the agents and the object are modeled as the gradient of nonlinear potentials and the deformations are assumed to be so small that the object can be considered a rigid body. It was later use in a teleoperation scheme by Ribeiro (2013); Ribeiro et al. (2014).

1.4.6 Acceleration and Jerk Measurement

Many interaction and motion control schemes designed for single arm or multiple arms found in the control literature require accurate measurement of the time-derivative of a given variable, such as image velocity, Cartesian velocity, force, or acceleration (Kruse et al. (2015); Mendoza et al. (2016); Wang and Xie (2009)).

However, this assumption can be a very restrictive condition from the practical point of view since those variables may be contaminated by sensor noise and time delays. In this context, adaptive control strategies can be proposed to avoid the need of measuring the time-derivative of the image velocity for visual servoing systems using filtered versions of the desired joint velocity and the output tracking errors (Leite and Lizarralde (2016); Lizarralde et al. (2013)).

1.5   Contribution

This work is an extension of the formation-based control presented by Bai and Wen (2010), which proposes a decentralized force control of cooperative manipulators. This in turn was extended by Ribeiro et al. (2014) where the formation-based control approach was applied as a Velocity/Force-Force (V/F-F) telemanipulation scheme using energy tanks strategy to passify the communication channel and guarantee passivity of the overall system.

Here, it is considered that the robotic manipulators at the slave side have kinematical and dynamical uncertainties. Then, the contributions can be summarized as follows:

- The proposal of a cooperative kinematic control law which uses a composite adaptive control law to estimate the kinematic parameters in a load transportation task.

- By means of a cascade interconnection, the proposal of a composite cooperative adaptive dynamic control law that estimates the kinematic and dynamic uncertain parameters of the manipulators in a load transportation task.

- The application of the proposed V/F-F scheme to teleoperate dual-arm manipulators in a load transportation task.

The comparison between our work and similar ones proposed in the literature is presented:

- In Table 1.1 comparing it with the works of Stramigioli et al. with focus on their work on passivity using Energy Tanks and Hirche et al. with focus on their work on cooperative control with load distribution.

- In Table 1.2 comparing it with the works of Wen et al. with focus on their work on cooperative control based in formation control and visual servoing and Basanez et al. with focus on their work on bilateral teleoperation using synchronization schemes.

- In Table 1.3 comparing it with the works of various authors that consider many teleoperation approaches teleoperation and adaptation of uncertain parameters.

The codes of all the references of the tables is presented in Table 1.4 except for reference c_2 which corresponds to the article called *Passivity-Based Adaptive Bilateral Teleoperation Control for Uncertain Manipulators without Jerk Measurements*

by Yanque et al. (see Yanque et al. (2016)), submitted to the *International Journal OF Adaptive Control and Signal Processing*, currently in revision.

In this context the work of Yanque et al. is the only one that considers cooperative control based on formation control with adaptation of kinematic and dynamic uncertainties in the context of teleoperation.

Table 1.1: Comparison with recent works of Stramigioli et al. and Hirche et al.

Authors		Stramigioli et al.				Hirche et al.				Yanque et al.	
References		c_3	c_4	c_5	c_6	c_7	c_8	c_9	c_{10}	c_1	c_2
Cooperative						o	o	o	o	o	o
Teleoperation		o	o							o	o
Energy Tanks		o	o	o	o					o	o
Load Distribution			o			o	o	o	o		
Control	Impedance-based		o	o			o		o		
	Adaptive Kinematics					o				o	o
	Formation Control				o		o			o	o
	Adaptive Dynamics									o	o
	Others	o	o								
Time Delays	Constant Time Delays										
	Variable Time Delays	o								o	o
Validation	Numerical Simulation									o	o
	Experimental Tests	o				o	o	o	o	o	o

Table 1.2: Comparison with recent works of Wen et al. and Basanez et al.

Authors		Wen et al.		Basanez et al.					Yanque et al.	
References		c_{11}	c_{12}	c_{13}	c_{14}	c_{15}	c_{16}	c_{17}	c_1	c_2
Cooperative		o	o						o	o
Teleoperated	Single Master / Single Slave			o	o		o			
	Single Master / Multi Slave					o			o	o
	Multi Master / Single Slave		o							
Control	Synchronizing Controller			o		o				
	Adaptive Dynamics			o			o		o	o
	Formation Control	o							o	o
	Others		o							
Time Delays	Constant Time Delays			o						
	Variable Time Delays							o	o	o
Validation	Numerical Simulation			o				o	o	o
	Experimental Tests	o	o				o		o	o

1.6   Outline of the Thesis

This work is organized as follows:

- Chapter 2: The general structure of the bilaterally teleoperated adaptive cooperative control scheme is presented. The Transparency Layer (TL) and Passivity Layer (PL) are defined. The scheme to enforce passivity of the teleoperated system using Energy Tanks is presented. A simulation of a simple teleoperated system that shows the effects of time delays and the action of the energy tanks is included.

Table 1.3: Comparison with recent works of various authors

Authors		Various Authors								
References		c_{18}	c_{19}	c_{20}	c_{21}	c_{22}	c_{23}	c_{24}	c_1	c_2
	Cooperative		○						○	○
Teleoperated	Single Master / Single Slave				○		○	○		
	Single Master / Multi Slave	○		○					○	○
	Multi Master / Single Slave					○				
Control	Impedance Based				○	○				
	Synchronizing Controller	○								
	Adaptive Kinematics	○	○				○		○	○
	Adaptive Dynamics	○			○		○		○	○
Time Delays	Constant Time Delays	○						○		
	Variable Time Delays				○		○		○	○
Validation	Numerical Simulation			○			○		○	○
	Experimental Tests		○			○	○		○	○

Table 1.4: References of Table 1.1, Table 1.2 and Table 1.3.

Code	Reference	Code	Reference
c_1	Yanque et al. (2016)	c_3	Franken et al. (2011)
c_4	Ferraguti et al. (2015)	c_5	Schindlbeck and Haddadin (2015)
c_6	Dietrich et al. (2016)	c_7	Erhart and Hirche (2013)
c_8	Sieber et al. (2015)	c_9	Bais et al. (2015)
c_{10}	Erhart and Hirche (2016)	c_{11}	Bai and Wen (2010)
c_{12}	Kruse et al. (2015)	c_{13}	Nuno et al. (2010b)
c_{14}	Nuno et al. (2011b)	c_{15}	Aldana et al. (2012)
c_{16}	Nuno et al. (2012a)	c_{17}	Nuno et al. (2013a)
c_{11}	Mohajerpoor et al. (2013)	c_{12}	Aghili (2013)
c_{13}	Heck et al. (2013)	c_{14}	Hua et al. (2015)
c_{15}	Shahbazi et al. (2015)	c_{16}	Liu and Khong (2015)
c_{17}	Li and Kawashima (2016)		

- Chapter 3: A control strategy for cooperative manipulators based on the formation control approach is presented. Operational space and dynamic adaptive control laws are proposed for cooperative manipulators with uncertainties in their kinematic and dynamic parameters.

- Chapter 4: Simulations and experiments of cooperative control are presented.

- Chapter 5: Presents the principal conclusions about the topics addressed in this work and a discussion about perspectives for future works.

Chapter 2

Telemanipulation Architecture

Here we present a control architecture for telemanipulation of an object using two or more robotics slave arms. It consists of a V/F-F teleoperation strategy (the master sends velocity (V) and force (F) commands to the slaves and the slaves send back force (F) information to the master) with a two-layer approach that guarantees stable bilateral telemanipulation in the presence of time-varying destabilizing factors such as communication delays. The architecture is composed of a top layer that enforces transparency and a lower layer that enforces passivity. From this approach the strategies to ensure transparency and passivity can be designed in an independent manner. The objective is to control the velocity and grasp force of an object performing translation motion, while it is grasped by slave robots located in a remote environment using master robots in the local environment.

2.1 Passivity

As the teleoperation architecture presented in this work is closely related to passivity, here a brief revision of passivity concepts taken from (Khalil (2002), Cap. 6) is addressed.

Passivity is an input-output property of dynamical systems that has its origins in network theory and relates to the exchange of energy between interconnected systems (Hokayem and Spong (2006)). A system is passive if the energy absorbed by the network over any period of time is greater and or equal to the increase of the energy stored in the network over the same period.

2.1.1 State Models and $\mathcal{L}_2$ and Lyapunov Stability

Consider a dynamical system represented by the state model

$$\dot{x} = f(x, u), \qquad y = h(x, u), \tag{2.1}$$

where $f : \mathbb{R}^n \times \mathbb{R}^p \to \mathbb{R}^n$ is locally Lipschitz, $h : \mathbb{R}^n \times \mathbb{R}^p \to \mathbb{R}^p$ is continuous, $f(0,0) = 0$ and $h(0,0) = 0$. The system (2.1) is said to be passive if there exists a continuously differentiable positive semidefinite function $V(x)$ called storage function such that

$$u^\mathsf{T} y \leq \dot{V} = \frac{\partial V}{\partial x} f(x, u), \qquad \forall (x, u) \in \mathbb{R}^n \times \mathbb{R}^p, \tag{2.2}$$

also, is said to be output strictly passive if $u^\mathsf{T} y \geq \dot{V} + y^\mathsf{T} \rho(y) > 0, \forall y \neq 0$.

Lemma 1 *(Lemma 6.6 of (Khalil (2002))) If the system (2.1) is passive with a positive definite storage function $V(x)$, then the origin of $\dot{x} = f(x, 0)$ is stable.* □

    Proof: See Khalil (2002) p. 242.

Lemma 2 *(Lemma 6.7 of (Khalil (2002))) Consider the system (2.1). The origin of $\dot{x} = f(x, 0)$ is asymptotically stable if the system is strictly passive or output strictly passive and zero-state observable.* □

    Proof: See Khalil (2002) p. 243.

2.1.2 Feedback Systems

Consider the feedback connection of Fig. 2.1 where H_1 and H_2 are time-invariant dynamical systems given by

$$\dot{x}_i = f_i(x_i, e_i), \tag{2.3a}$$

$$y_i = h_i(x_i, e_i), \tag{2.3b}$$

and the closed-loop state model takes the form

$$\dot{x} = f(x, u), \tag{2.4a}$$

$$y = h(x, u). \tag{2.4b}$$
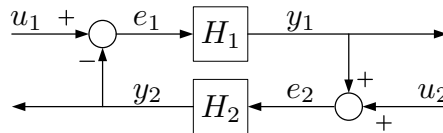
Figure 2.1: Feedback connection.

Theorem 1 *(Theorem 6.3 of (Khalil (2002))) Consider the feedback connection of two time-invariant dynamical systems of the form (2.3). The origin of the closed-loop system (2.4b) (when $u = 0$) is asymptotically stable if*

- *both feedback components are strictly passive,*

- *both feedback components are output strictly passive and zero-state observable, or*

- *one component is strictly passive and the other one is output stricktly passive and zero-state observable.*

Furthermore, if the storage function for each component is radially unbounded, the origin is globally asymptotically stable. □

Proof: See Khalil (2002) p. 250.

2.2   Transparency Layer (TL)

Transparency is a performance measure of how well the system is able to convey to the human operator the perception of direct interaction with the environment (Franken et al. (2011)). It is considered a human operator in a local environment manipulating a virtual object with a master robot, which is a haptic device capable of measuring motions and reflecting forces to the operator (Niemeyer et al. (2016)). This provides the desired velocity and force closure constraints to the slave robots in a remote environment which are grasping an actual object. The interaction forces between the slaves and the object are transmitted back to the operator through the master by imposing the reflected force upon him.

2.2.1   Local environment

The operator operates a master device that sends velocity and force signals to the slaves which reflects the environment measured force signal to the operator. In this work a master haptic device is considered, such that the motion of the master is imposed directly by the operator and the desired grasping force (that the operator sends to the slaves) is set to be a function of the master position.

Consider that the master dynamical system is given by

$$M_m(q_m)\ddot{q}_m + C_m(q_m, \dot{q}_m)\dot{q}_m + g_m(q_m) = \tau_m + \tau_h, \tag{2.5}$$

where $q_m \in \mathbb{R}^{n_m}$ is the vector of joint configurations, n_m is the number of joints, $M_m \in \mathbb{R}^{n_m \times n_m}$ is the inertia matrix, $C_m \in \mathbb{R}^{n_m \times n_m}$ is the Coriolis matrix and $g_m \in \mathbb{R}^{n_m}$ is the gravity matrix. $\tau_m, \tau_h \in \mathbb{R}^{n_m}$ are the master and operator torque. During the teleoperation, the master sends a velocity signal $\dot{p}_m$ and a force signal f_h to the slaves, and the master controller computes τ_m using the force signal f_m^d received from the slave.

Consider that the operator makes the master end-effector follow a trajectory along a virtual plane while applying force perpendicularly to this plane as in Fig. 2.2. The operator desired grasping force f_h can be defined as a function of the penetra-
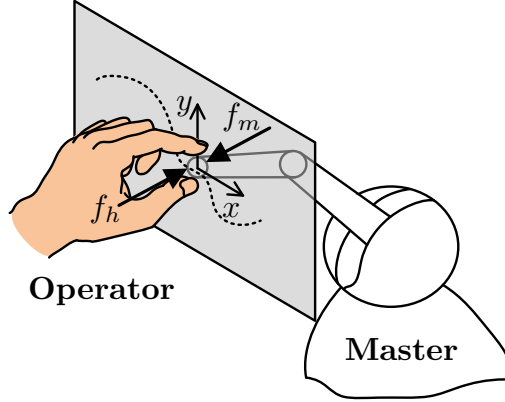
Figure 2.2: Manipulation of a deformable virtual object.

tion of the master end-effector in the virtual plane (e.g. a spring). The reflected reaction force f_e (from the slave) is applied perpendicularly to the virtual plane by the master robot. Then, the master manipulator τ_m is given by (including a gravity compensation)

$$\tau_m = J_m^\mathsf{T}(q_m) f_e \ \vec{v}_m + g_m(q_m), \tag{2.6}$$

where $J_m(q_m) \in \mathbb{R}^{3 \times n_m}$ is the position part of the manipulator Jacobian, f_e is the environment force received from the slaves and $\vec{v}_m \in \mathbb{R}^3$ is the unit vector perpendicular to the virtual plane.

2.2.2 Remote environment

An object is being grasped by the slave end-effectors in the remote environment, as shown in Fig 2.3, where $m_o g$ is the force due to the objects weight (m_o is the object mass and g is the standard gravity), f_{1z}^d, f_{2z}^d are the forces applied by the manipulators that cancel the objects weight, f_{1x}^d, f_{2x}^d are the squeezing forces applied and n_1, n_2 are the normal forces.

It is considered that the coefficient of friction of the objects surface is high enough and the normal forces are high enough that the object does not slip the grasp.

The slave sensors send the measured contact force f_e to the master and the slave controllers receive the velocity $\dot{p}_o^d$ and force f^d signals to compute the slave control signal τ_i. This is detailed in Section 3.
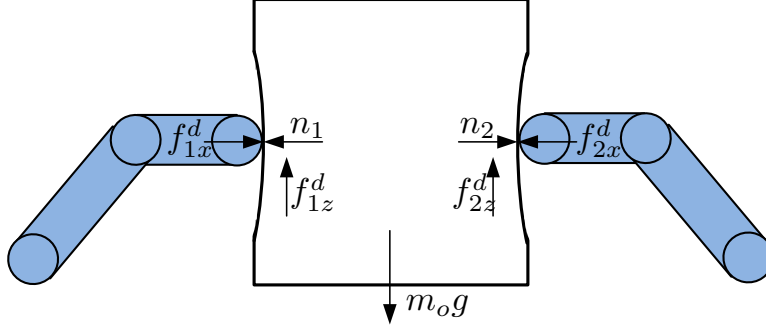
Figure 2.3: Two arms holding a deformable object

2.3 Passivity Layer (PL)

Passivity of a system is a sufficient condition to guarantee its stability. A system is considered to be passive if the energy that can be extracted from it is bounded by the sum of the injected and initial stored energy. Any proper combination of passive systems will be passive (Franken et al. (2011))

The total energy of the system $E_T(t)$ at instant t is given by

$$E_T(t) = E_m(t) + E_c(t) + E_s(t) \tag{2.7}$$

where $E_m(t)$, $E_s(t)$, and $E_c(t)$ represents the energy present at the master side, at the slave side, and in the communication channel, respectively.

The passivity condition for the system can be expressed as

$$E_T(t) \geq 0 \,, \tag{2.8}$$

assuming that initial stored energy is zero.

Physical energy exchange takes place between operator and master, and between environment and the slave. The requirement necessary to ensure a passive interconnection of the entire system with the physical world is

$$\dot{E}_T(t) \leq P_m(t) + P_s(t) \,, \tag{2.9}$$

where $P_m(t)$ and $P_s(t)$ are, respectively, the power flowing from the master and slave robot into the master and slave controller, and $\dot{E}_T(t)$ is the rate of change of the energy balance of the system. Equations (2.8) and (2.9) ensures passivity of the system and a passive connection of the system with the physical world, respectively.

In Section 2.4, a strategy that saturates the control signals provided by the TL to enforce passivity of the teleoperated system using energy tanks will be addressed. Fig. 2.4 shows a diagram of the proposed architecture.
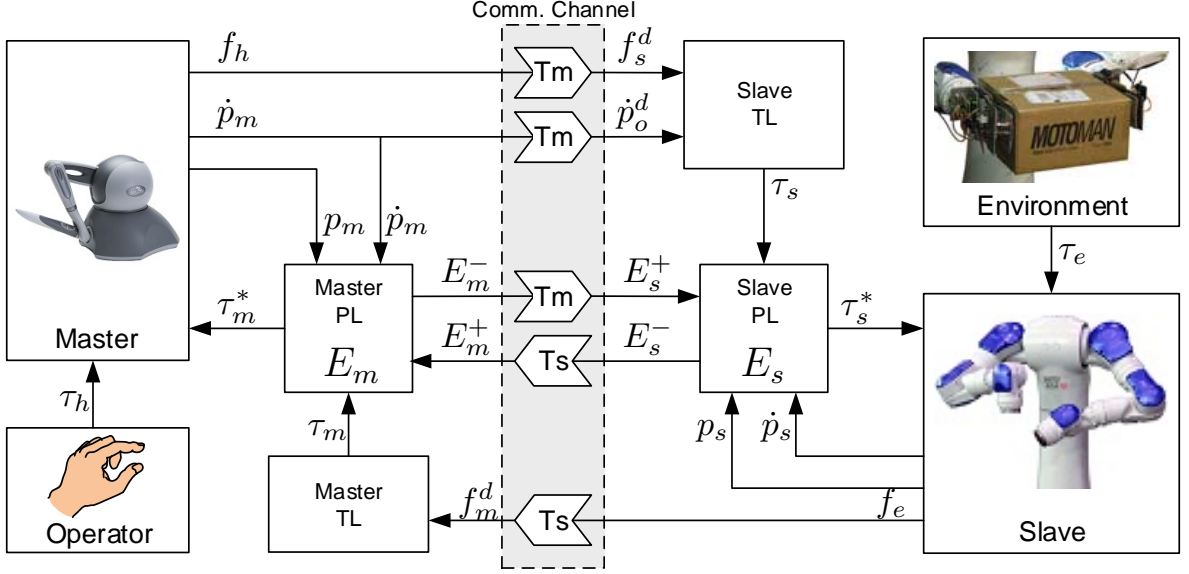
Figure 2.4: Telemanipulation architecture

2.4 Passivity enforcement using Energy Tanks

Here, the approach presented by Franken et al. (2011) using energy tanks which monitors the energy flow in the system is implemented to guarantee that no virtual energy is created and, thus guaranteeing stability. It is designed to enforce passivity by saturating the commands generated by the Transparency layer (TL) when necessary. With this approach, any controller can be implemented in a passive manner given arbitrary time delays. Hereafter the subscript $j \in \{m, s\}$ refer to either master m or slave s. Consider that the energy exchanged with the physical world ΔE_j is given by

$$\Delta E_j(k) = f_j \left(\overline{k}\right)^\mathsf{T} \left[p_j(k) - p_j(k-1)\right], \tag{2.10}$$

where $f_j(\overline{k})$ is the force exerted during the sample period (considered constant), p_j is the end-effector position, k is the sample instant and $\overline{k}$ is the interval between $k-1$ and k.

Alternatively, the energy exchange can be given by

$$\Delta E_j(k) = \tau_j \left(\overline{k}\right)^\mathsf{T} \left[q_j(k) - q_j(k-1)\right], \tag{2.11}$$

where $\tau_j(\overline{k})$ is the torque exerted during the sample period (considered constant) and q_j is the manipulator joint position vector.

Then the energy level in the tank $E_j(k)$ is given by

$$E_j(k) = E_j(\overline{k}) + E_j^+(k) - \Delta E_j \tag{2.12}$$

where $E_j(\overline{k})$ is the energy before operations and $E_j^+(k)$ the received energy. Finally, the energy left on the tank and available during the next sample period $E_j(\overline{k+1})$ is given by

$$E_j(\overline{k+1}) = E_j(k) - E_j^-(k), \tag{2.13}$$

where $E_j^-(k) = \beta E_j(k)$ is the energy send and $\beta \in [0,1]$.

Remark 1 *In this case, to compute the energy that one tank sends to the other (E_j^-) it was considered the Simple Energy Transfer Protocol (SETP) proposed in Franken et al. (2011), given by $\beta \in [0,1]$ which guarantees that in free motion $(f_h = f_e = 0)$ the energy level in both tanks tend to be equal as $t \to \infty$.*

Remark 2 *In the slave side it is considered one energy tank for all the slaves because they are all grasping the same object exerting almost the same force during movement. If not, individual slave tanks and an energy transfer protocol between them should be considered.*

2.4.1 Master Tank Level Controller

A tank level controller (LC) is considered at the master side to monitor the level of the energy tank $E_m(k)$ with respect to a desired level E_d. When the energy level is below the desired level the LC extracts energy from the user to refill the tank. This is done in the master side by applying an additional force f_{LC} in the opposite direction of the master movement given by

$$f_{LC} = \begin{cases} 0 & \text{if } E_m(k) > E_d, \\ -\alpha \left[E_d - E_m(k) \right] \dot{p}_m & \text{otherwise.} \end{cases} \tag{2.14}$$

where the constant $\alpha > 0$ tunes the rate at which energy is extracted and E_d is the desired energy level.

Remark 3 *The value of α can be selected considering the maximum force that the master manipulator can exert to oppose the operator movement. Also, if the desired level E_d is too high it might take too much time to fill the tank at the beginning of the movement.*

2.4.2 Saturation of controlled torque

In order to maintain passivity, the controlled torque $\tau_j(k)$ computed by the TL is limited by the PL by means of saturation functions. The fundamental function considered is given by

$$\tau_{j1}(k) = \begin{cases} 0 & \text{if } E_j(\overline{k+1}) \leq 0, \\ k_s \tau_j(k) & \text{otherwise.} \end{cases} \tag{2.15a}$$

$$k_s = \begin{cases} \frac{E_j(k+1)}{E_d} & \text{if } E(k+1) \in [0, E_d], \\ 1 & \text{otherwise.} \end{cases} \tag{2.15b}$$

where k_s allows a gradual reduction of the controlled torque to prevent chattering. This function considers the critical case, where the control signal is turn to zero due to loss of passivity.

Remark 4 *Note that (2.15a) is the critical case when passivity is lost and the controlled torque turns to zero. This means that the applied controlled torque is actually the gravity compensation, such that the end-effectors do not apply force to the object but try to stay in their last positions.*

A limit to the torque exerted by the manipulator $\tau_{j,lim}$ can be considered, then a second saturation function can be given by $\tau_{j2}(k) = \tau_{j,lim}$. Other functions can be considered as well.

The maximum allowable torque is given by

$$\hat{\tau}_j(k) = \min[\tau_{j1}(k), \tau_{j2}(k)], \tag{2.16}$$

then the torque computed by the PL is given by

$$\hat{\tau}_j^*(k) = \text{sgn}(\tau_j(k))\min\left(|\tau_j(k)|, \hat{\tau}_j(k)\right). \tag{2.17}$$

where τ_m is given in (2.6) and τ_s in (3.40). The saturated torques τ_j^* are given by

$$\tau_m^*(\overline{k+1}) = \hat{\tau}_m^*(k) + \tau_{LC}(k), \qquad \tau_s^*(\overline{k+1}) = \hat{\tau}_s^*(k). \tag{2.18}$$

where $\tau_{LC} = J_i^\mathsf{T} f_{LC}$.

2.5 Behavior of the Energy Tanks

To clarify the behavior of the energy tanks three typical cases of teleoperation can be analyzed. In all cases both tanks are constantly losing energy in the form of ΔE_m and ΔE_s, when energy is available.

(a) First Case, beginning of the teleoperation.

(b) Second Case, synchronization.

(c) Third Case, tank losing passivity.
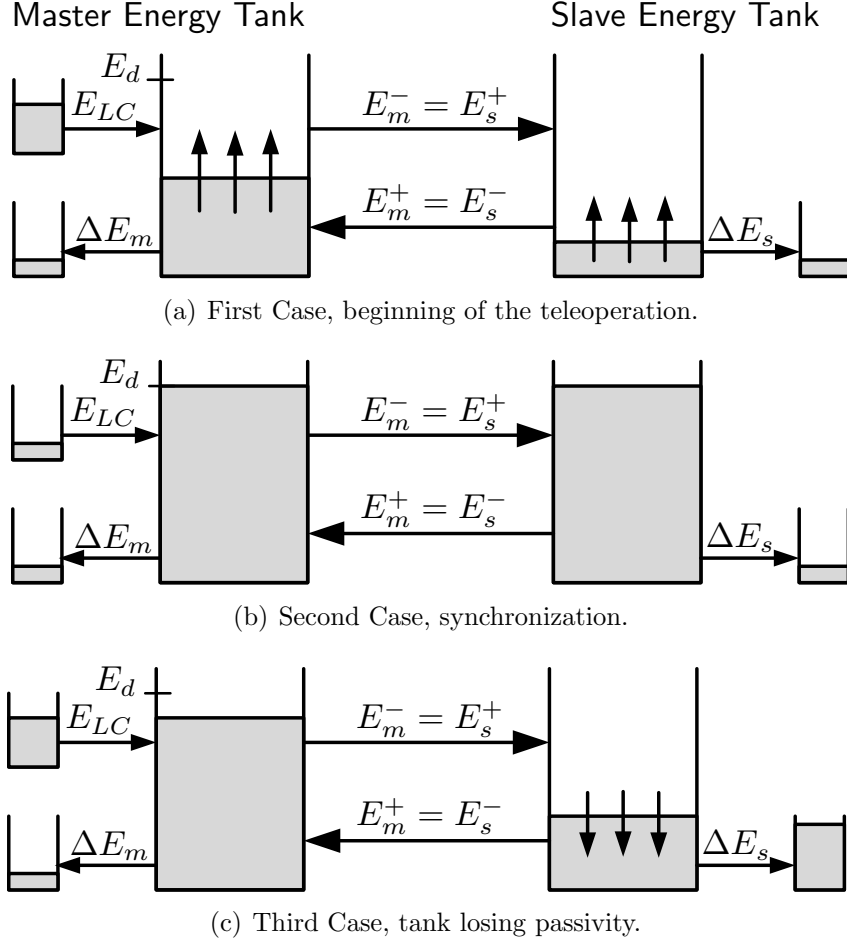
Figure 2.5: Typical Cases of Teleoperation.

First case, the beginning of the teleoperation (Fig. 2.5(a)). The tank level controller (LC) injects damping to the master in order to extract energy from the operator E_{LC} to replenish the master energy tank. This allows it to send energy E_m^- to the slave energy tank. The energy available in the slave energy tank allows movement of the slave end-effector and also allows the slave tank to send energy to the master tank E_s^-.

Second case, tanks are close to the desired energy level E_d (Fig. 2.5(b)). This is when the energy levels of the tanks have synchronized, the tank level controller (LC) is still injecting damping but at a lower rate, to maintain the same energy level in both tanks.

Third case, represents an energy tank (slave tank in this case) losing passivity (Fig. 2.5(c)). Here it is considered that the slave uses more energy than available (higher rate of ΔE_s) and is losing passivity. This leads to an increment of the damping from the tank level controller (LC) to extract more energy from the operator E_{LC}. Eventually, if the tank gets depleted ($E_s < 0$), the fundamental saturation function acts (2.15) keeping the system passive.

2.6 Conclusions

The architecture of the proposed Single Master Multi Slave (SM-MS) teleoperated system was presented, the set up at the master side as well as details of how the force signals received from the slaves are reflected to the master are explained. Also, the teleoperated system was shown in Fig. 2.4 where the context of the action of the energy tank approach is *hopefully* clarified.

A bilateral telemanipulation framework that enforces passivity based on a variation of the Time Domain Passivity Control (TDPC) approach that uses the concept of Energy Tanks to storage energy in order to ration out damping to keep the overall system passivity was revised.

This scheme considers the gradual injection of damping as a function of the energy of the system in order keep passivity while maintaining transparency, this is important because prevents the excessive injection of damping that leads to sluggishness in the system.

It was clarified that in the critical case when passivity is lost the saturated control signal should turn to the gravity vector instead of zero torque, such that the robotic manipulators do not apply forces but try to keep their positions.

A simple example consisting of a one-dimensional bilateral teleoperated system implemented with energy tanks was analyzed. Four cases were tested with and without time delays and energy tanks action.

Chapter 3

Passivity-Based Adaptive Control

Here, the cooperative control strategy for the slaves manipulators is based on the formation control formalism proposed in Bai and Wen (2010) for groups of agents undergoing pure translational motion. The proposed control strategy can be considered as a decentralized control scheme, which considers elastic deformations on the object such that only forces − instead of forces and moments − are transmitted. Then, the tracking problem for a given desired velocity is assumed to be subject to the constraints imposed by the force closure.

Consider the grasping and manipulation problem of a deformable object performed by n robot manipulators. Let $p_{ci} \in \mathbb{R}^3$ be the position of the contact point c_i, for the i-th robot end-effector, without object deformation. Let $p_o \in \mathbb{R}^3$ be the position of a fixed point $\mathbb{O}$ of the object (e.g., the center of mass of the object) with the coordinated frame $\mathbb{E}_o$ attached to the object with origin in $\mathbb{O}$ and $p_i \in \mathbb{R}^3$ be the position of the i-th robot end-effector, considering object deformation. Notice that all position vectors are expressed with respect to the inertial frame $\mathbb{E}_s$, as shown in Fig. 3.1.
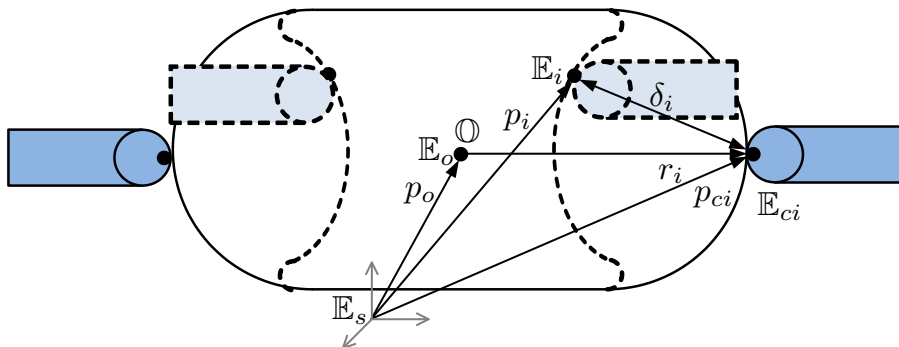
Figure 3.1: End-effectors manipulating a deformable object.

Considering that the object orientation is denoted by the rotation matrix $R_o \in$

$SO(3)$, the position vector p_{ci} and its time-derivative $\dot{p}_{ci}$ are given respectively by

$$p_{ci} = p_o + R_o\, r_i\,, \qquad\qquad \dot{p}_{ci} = \dot{p}_o + \dot{R}_o\, r_i\,, \qquad\qquad (3.1)$$

where the constant vector $r_i \in \mathbb{R}^3$ is given by $r_i = p_{ci} - p_o$. Assuming that the object orientation is constant, implies that $\dot{R}_o = 0$ and, consequently,

$$\dot{p}_{ci} = \dot{p}_o\,. \qquad\qquad (3.2)$$

In this context, the object deformation vector $\delta_i \in \mathbb{R}^3$ can be expressed by

$$\delta_i = p_i - p_{ci}\,, \qquad\qquad (3.3)$$

which generates a reaction force vector $f_i \in \mathbb{R}^3$ along the end-effector orientation given by the unit vector $\vec{d}_i \in \mathbb{R}^3$.

The reaction force f_i could be modeled as the gradient of a positive-definite potential function of deformation given by

$$f_i = \nabla P(\delta_i)\,. \qquad\qquad (3.4)$$

In this case, when $\delta_i = 0$ the i-th robot end-effector is not deforming the object and, thus, no reaction force is generated satisfying the condition

$$P(\delta_i) = 0\,, \qquad \nabla P(\delta_i) = 0 \quad \Leftrightarrow \quad \delta_i = 0\,. \qquad\qquad (3.5)$$

It is assumed that

$$\nabla^2 P(\delta_i^d) > 0\,, \qquad\qquad (3.6)$$

where δ_i^d is the desired deformation. This is satisfied by linear spring-force models. This assumption is used to propose the positive definite storage function in the next section. The object motion dynamics, which is restricted to purely translational motion, can be modeled by

$$m_o\, \ddot{p}_o = \sum_{i=1}^{n} f_i\,, \qquad\qquad (3.7)$$

where m_o is the mass of the object and f_i is the contact force between the i-th robot end-effector and the manipulated object.

3.1 Robot Kinematics

Here, we consider the kinematic model of the robot manipulator. Consider that the position vector of the i-th robot end-effector $p_i \in \mathbb{R}^3$ can be obtained from the forward kinematics map as

$$p_i = k_i(q_i) = Z_i(q_i)\,b_i\,, \tag{3.8}$$

where $q_i \in \mathbb{R}^{n_i}$ is the vector of joints angles, n_i is the number of joints of the i-th robot manipulator, and $k_i(\cdot)$ is in general a nonlinear function. Notice that, the right-hand side of (3.8) can be linearly parameterized by $Z_i(q_i)\,b_i$, where $Z_i(q_i) \in \mathbb{R}^{3 \times \ell_i}$ is the forward kinematics regressor matrix, $b_i \in \mathbb{R}^{\ell_i}$ denotes the constant kinematic parameters vector and ℓ_i is the number of kinematic parameters (Leite et al. (2011)).

The end-effector velocity vector $\dot{p}_i \in \mathbb{R}^3$ can be related to the joint velocity vector $\dot{q}_i \in \mathbb{R}^{n_i}$ by the following differential kinematics equation:

$$\dot{p}_i = J_i(q_i)\,\dot{q}_i = W_i(q_i, \dot{q}_i)\,b_i\,, \tag{3.9}$$

where $J_i(q_i) \in \mathbb{R}^{3 \times n_i}$ is the position part of the manipulator Jacobian. Notice that, the right-hand side of (3.9) can also be linearly parameterized by $W_i(q_i, \dot{q}_i)\,b_i$, where $W_i \in \mathbb{R}^{3 \times \ell_i}$ is the differential kinematics regressor matrix. It is worth mentioning that the kinematic model (3.9) also has the following property, which will be useful for the purpose of control design and stability analysis for robot manipulators with *revolute joints*.

(P1) The Jacobian matrix $J_i(q_i)$ is bounded for all possible values of q_i, that is:

$$||J_i(q_i)||_\infty \leq c_0\,, \qquad \forall q_i \in [0, 2\pi]\,,$$

where $c_0 \in \mathbb{R}$ is a known positive constant, because $J_i(\cdot)$ depends on $q_i(t)$ as the argument of bounded trigonometric functions (Kelly et al. (2005)).

The control design is based on the kinematic control approach at the velocity level due to its simplicity of implementation and satisfactory performance when the given task is carried out with low velocities and slow accelerations. In this context, if the robot manipulator has limited performance in terms of required velocity/acceleration and high-gear reduction ratios, we assume that $u_i \triangleq \dot{q}_i$, where $u_i \in \mathbb{R}^{n_i}$ is the velocity control signal applied to the motor drive of the joints of the i-th robot manipulator (Caccavale and Uchiyama (2016)). Then, considering the kinematic control approach we obtain the following decentralized open loop control system:

$$\dot{p}_i = J(q_i)\,u_i\,. \tag{3.10}$$

40

3.1.1 Uncertain Kinematics

Here, we consider that the forward kinematics and the differential kinematics models are both uncertain. The uncertainties in robot kinematics may arise, for example, (i) when its end-effector is handling different objects with uncertain dimensions to use as a tool or (ii) when the end-effector is replaced by tools with different dimensions which are more suitable to carry out a particular task (Siciliano et al. (2009)). Therefore, it is clear that the existence of uncertainties in the kinematic model is a relevant problem in robotics and can be considered separately from the problem of uncertainties in the dynamic model (Leite and Lizarralde (2016)).

In this work, it is considered that the only source of parametric uncertainty is due to the geometric parameters of the robotic manipulator, given by the Denavit-Hartenberg parameters a_i e d_i for $i = 1, 2, ..., n$ (Siciliano et al. (2009)). This means that the uncertainties related to the measurement error of the joint transducer (i.e. joint offsets) are not considered. Then, be analyzing the structure of the direct kinematic equation of the manipulator, it can be verified that only the position coordinates depend on the manipulator geometric parameters, therefore, they can be affected by the kinematic uncertainties. As a consequence, only the manipulator position Jacobian is affected by the presence of kinematic uncertainties (Leite (2011)).

Then, considering the presence of parametric uncertainty in the robot kinematic model (3.8), the estimated or predicted position vector $\hat{p}_i \in \mathbb{R}^3$ can be expressed as

$$\hat{p}_i = \hat{k}_i(q_i) = Z_i(q_i)\,\hat{b}_i\,, \tag{3.11}$$

where $\hat{k}_i$ is the approximate forward kinematics map and $\hat{b}_i \in \mathbb{R}^{\ell_i}$ denotes a set of estimated kinematic parameters. It is well-known from Slotine and Li (1991) that the linear parameterization models (3.8) and (3.11) can be used for online parameter estimation, provided that p_i and Z_i can be measured from the system signals.

Now, considering the presence of parametric uncertainty in the robot kinematic model (3.9), the estimated or predicted velocity vector of the i-th robot end-effector $\dot{\hat{p}}_i \in \mathbb{R}^3$ can be expressed as

$$\dot{\hat{p}}_i = \hat{J}_i(q_i)\,\dot{q}_i = W_i(q_i, \dot{q}_i)\,\hat{b}_i\,, \tag{3.12}$$

where $\hat{J}_i \in \mathbb{R}^{3 \times n_i}$ is the position part of the approximate manipulator Jacobian.

3.1.2 Parameter Adaptation

Uncertainty in the kinematic parameters may cause inaccuracy or instability during control operation. This uncertainty can be gradually reduced by an adaptation

law (Slotine and Li (1991), p.312). For updating the estimated kinematic parameter $\hat{b}_i$ we consider the following gradient-type adaptive law

$$\dot{\hat{b}}_i = -\Gamma_k \left(W_i^\mathsf{T}(q_i, \dot{q}_i) \, \tilde{f}_i \right) , \qquad\qquad \Gamma_k = \Gamma_k^\mathsf{T} > 0 , \qquad\qquad (3.13)$$

where Γ_k is the kinematic adaptive gain matrix and $\tilde{f}_i \in \mathbb{R}^3$ is the force error given by $\tilde{f}_i = f_i - f_i^d$.

Notice that the design of the adaptive kinematic scheme would require the measurement of the contact force vector f_i, the joint position vector q_i and joint velocity vector $\dot{q}_i$, of the i-th robot manipulator.

From a practical point of view, these assumptions imposed on the adaptive kinematic scheme are reasonable and acceptable, since we are designing a hybrid position-force control for cooperative robotic systems.

3.1.3 Composite Adaptation

A composite adaptation law considers the prediction error as an additional source of information for the parameter adaptation. This can improve the performance of the adaptive controller (Slotine and Li (1991), p.382).

Let $\epsilon_i \in \mathbb{R}^3$ be the prediction error defined by $\epsilon_i := p_i - \hat{p}_i$. From the linear parameterization models (3.8) and (3.11), the prediction error ϵ_i can be expressed as

$$\epsilon_i = p_i - Z_i(q_i) \, \hat{b} = Z_i(q_i) \, \tilde{b}_i . \qquad\qquad (3.14)$$

where $\tilde{b}_i = b_i - \hat{b}_i$ is the parameter estimation error.

Then, for updating the estimated kinematic parameter $\hat{b}_i$ we consider the following *composite* gradient-type adaptive law

$$\dot{\hat{b}}_i = -\Gamma_k \left(W_i^\mathsf{T}(q_i, \dot{q}_i) \, \tilde{f}_i + Z_i^\mathsf{T}(q_i) \, \epsilon_i \right) , \qquad\qquad \Gamma_k = \Gamma_k^\mathsf{T} > 0 . \qquad\qquad (3.15)$$

Compared with the adaptive kinematic scheme, the design of the composite adaptive kinematic scheme would also require the measurement of the end-effector position vector p_i of the i-th robot manipulator.

It is worth noting that, the proposed adaptive scheme consists of using a composite gradient-type adaptation law based on the prediction error obtained *directly* from the end-effector position vector. Instead, the adaptive scheme presented by Leite and Lizarralde (2016); Lizarralde et al. (2013); Yanque et al. (2016) employ a *standard* gradient-type adaptation based on the prediction error obtained from the *filtered* end-effector position.

Remark 5 *The composite adaptation law based on the prediction error $\epsilon_i(t)$ and force error $\tilde{f}_i(t)$ not only ensures the global stability of the adaptive kinematic control system, but also leads to fast and smooth parameter convergence and, consequently, smaller tracking errors (Slotine and Li (1991)).*

Remark 6 *It is worth noting that the practical implementation of the proposed composite adaptive cooperative kinematic control scheme depends on the measurement of the position vector p_i. In this context, we assume that the position of the robot end-effector can be measured from a position sensing device such as laser trackers or cameras.*

3.2   Kinematic control approach

Now, to achieve the goal of moving an object while a firm grasp is maintained in the presence of kinematic uncertainties, we propose an adaptive cooperative control scheme at the kinematic level for uncertain robot manipulators. The decentralized cooperative control signal is given by

$$u_i = \hat{J}_i^{\dagger}(q_i)\,(v_i + w_1)\,, \tag{3.16}$$

where $\hat{J}_i^{\dagger} = \hat{J}_i^{\mathsf{T}}(\hat{J}_i\,\hat{J}_i^{\mathsf{T}})^{-1}$ is the pseudo-inverse Jacobian matrix and v_i is the Cartesian control signal to be designed and $w_1 \in \mathbb{R}^3$ is a vanishing input signal. It is worth noting that, the control signal (3.16) locally minimizes the norm of the joint velocities, provided that $v_i(t)$ does not lead the i-th robot arm to *singular configurations*, where the Jacobian matrix $J_i(q_i)$ has deficient rank. The failure of this last condition is a fairly open-problem in robotics and other correlated areas, and has been widely discussed in the control literature.

Then, substituting (3.16) into (3.10) we obtain the following open-loop dynamics in the Cartesian space (see A.1):

$$\dot{p}_i = v_i + w_1 + \varepsilon_i\,, \tag{3.17}$$

where $\varepsilon_i \in \mathbb{R}^3$ is a vanishing perturbation term due to the uncertain kinematics given by :

$$\varepsilon_i = W_i(q_i, \beta_i)\,\tilde{b}_i\,. \qquad \beta_i = \hat{J}_i^{\dagger}(q_i)(v_i + \omega_1), \tag{3.18}$$

where β_i is obtained in Appendix A.1.

3.3 Operational Space Control System

The control goal of the cooperative robotic system is to allow the object grasped by the i-th robot end-effector tracks a desired velocity $\dot{p}_o^d(t)$, while the current contact force f_i is regulated to a desired value f_i^d. To achieve this aim, an operational space control signal $v_i \in \mathbb{R}^3$ is proposed as follows

$$v_i = \dot{p}_o^d - K_v \, \tilde{f}_{if} \,, \tag{3.19}$$

where $K_v = K_v^\mathsf{T} > 0$ is the control gain matrix, $\tilde{f}_i \in \mathbb{R}^3$ is the force error vector defined as $\tilde{f}_i = f_i - f_i^d$ and the filtered force error dynamics $\tilde{f}_{if} \in \mathbb{R}^3$ is governed by

$$\dot{\tilde{f}}_{if} = -\lambda_k \, \tilde{f}_{if} + \lambda_k \, \tilde{f}_i \,, \tag{3.20}$$

where $\lambda_k > 0$ is the cutoff frequency in radians per second.

Since the grasped object will eventually move with a desired time-varying velocity $\dot{p}_o^d(t)$, the end-effectors of the robot manipulators are subject to the following dynamic constraint:

$$m_o \, \ddot{p}_o^d = \sum_{i=1}^{n} f_i^d \,, \tag{3.21}$$

where f_i^d should be chosen so that the contact forces f_i for $i = 1, 2, \ldots, n$ satisfy the desired properties, such as *force closure grasp*. This requires the previous knowledge of the object geometry and the suitable grasping points for handling the object.

Notice that, from (3.4) the reaction force f_i depends on the object deformation δ_i. Therefore, if δ_i can be regulated to some desired value δ_i^d, f_i would also be maintained accordingly. To this end, we assume that the reaction force f_i^d is modeled by a linear spring-force model. Thus, achieving a desired contact force f_i^d is equivalent to driving the deformation from a current value δ_i to a desired value δ_i^d. Then, the deformation error $\tilde{\delta}_i$ can be simply defined as

$$\tilde{\delta}_i = \delta_i - \delta_i^d \,. \tag{3.22}$$

This is similar to the *formation control problem*, where the relative positions between agents are driven to some desired values (Bai and Wen (2010)). Defining the object velocity error vector $\dot{\tilde{p}}_o$ as:

$$\dot{\tilde{p}}_o = \dot{p}_o - \dot{p}_o^d \,, \tag{3.23}$$

and considering the object dynamics (3.7) as well as the dynamic constraint (3.21),

44

the object velocity error dynamics is governed by:

$$m_o \ddot{\tilde{p}}_o = \sum_{i=1}^{n} \tilde{f}_i \,. \tag{3.24}$$

Considering (3.2), taking the time-derivative of (3.3), and using (3.17) and (3.23), we see that the object deformation error dynamics can be given by:

$$\dot{\tilde{\delta}}_i = -\dot{\tilde{p}}_o - \dot{p}_o^d + v_i + w_1 + W(q_i, \beta_i)\,\tilde{b}_i \,. \tag{3.25}$$

Finally, considering (3.19), the closed-loop error system yields:

$$\dot{\tilde{\delta}}_i = -\dot{\tilde{p}}_o - K_v\,\tilde{f}_{if} + w_1 + W(q_i, \beta_i)\,\tilde{b}_i \,. \tag{3.26}$$

Therefore, controlling the contact forces f_i (i.e, the object deformations δ_i) between the robot end-effectors and the object as well as the object velocity simultaneously, makes it possible to maintain a firm grasp of the object during the manipulation task.

The algorithm of the cooperative kinematic control is presented in Table 3.1.

Table 3.1: Algorithm of the Cooperative Kinematic Control

Cooperative System	$f_i = \nabla P(\delta_i) \quad \dot{p}_i = J(q_i)\,u_i$
Object Restriction	$m_o\,\ddot{p}_o = \sum_{i=1}^{n} f_i$
Velocity Control Signal	$u_i = \hat{J}_i^{\dagger}(q_i)\,(v_i + w_1)$
Operational Space Control Law	$v_i = \dot{p}_o^d - K_v\,\tilde{f}_{if}$
Filtered Force	$\dot{\tilde{f}}_{if} = -\lambda_k\,\tilde{f}_{if} + \lambda_k\,\tilde{f}_i$
Linear Parameterization	$\dot{\hat{p}}_i = \hat{J}_i(q_i)\,\dot{q}_i = W_i(q_i, \dot{q}_i)\,\hat{b}_i$
Prediction Error	$\epsilon_i = p_i - Z_i(q_i)\,\hat{b} = Z_i(q_i)\,\tilde{b}_i$
Composite	$\dot{\hat{b}}_i = -\Gamma_k\left(W_i^{\mathsf{T}}(q_i, \dot{q}_i)\,\tilde{f}_i + Z_i^{\mathsf{T}}(q_i)\,\epsilon_i\right)$
Adaptation Law	$\Gamma_k = \Gamma_k^{\mathsf{T}} > 0$

The block diagram of the proposed adaptive kinematic control is presented in Fig. 3.2.

Now, we can state the following theorem:

Theorem 2 *Consider a cooperative robotic system modeled by (3.4) and (3.10) manipulating a deformable object satisfying (3.7), with velocity control signal (3.16) and the operational space control law (3.19) based on the filtered force (3.20). Consider the kinematic adaptive scheme based on the linear parameterization models (3.11) and (3.12), the prediction error (3.14) and the composite adaptation law (3.15). Assume that the desired velocity $\dot{p}_o^d$ is uniformly bounded and the desired grasping*
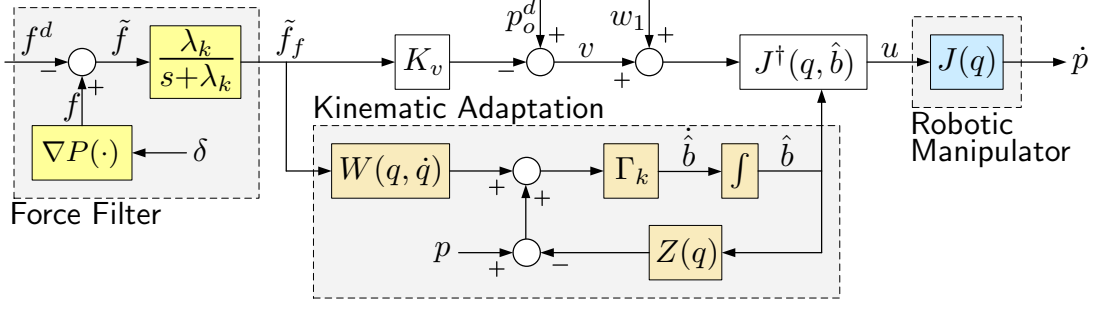
Figure 3.2: Adaptive kinematic control block diagram

force f_i^d is uniformly bounded and satisfies (3.21). In addition, assume that the end-effector position p_i and the regressor matrices Z_i and W_i are measured from the system signals. Then, the map $w_1 \mapsto \tilde{f}_i$ is output strictly passive with positive definite storage function:

$$2V_k(\tilde{f}_{if}, \tilde{\delta}_i, \dot{\tilde{p}}_o, \tilde{b}_i) = m_o \dot{\tilde{p}}_o^\mathsf{T} \dot{\tilde{p}}_o + \sum_{i=1}^{n} \left[2\Delta_i + \lambda_l \tilde{f}_{if}^\mathsf{T} \tilde{f}_{if} + \tilde{b}_i^\mathsf{T} \Gamma_k^{-1} \tilde{b}_i \right], \qquad (3.27)$$

with $\Delta_i = P(\delta_i) - P(\delta_i^d) - f_i^{d\mathsf{T}} \tilde{\delta}_i$. Moreover, for $w_1 = 0$, the following properties hold: (i) all system signals are uniformly bounded; (ii) $\lim_{t \to \infty} \tilde{f}_{if}(t) = 0$, $\lim_{t \to \infty} \tilde{f}_i(t) = 0$, $\lim_{t \to \infty} \tilde{\delta}_i(t) = 0$, $\lim_{t \to \infty} \epsilon_i(t) = 0$, $\lim_{t \to \infty} \dot{\tilde{p}}_o(t) = 0$.

Proof 1 The time-derivative of the potential function (3.4) of the deformation and the desired deformation is given by

$$\dot{P}(\delta_i) = \nabla P(\delta_i) \dot{\delta}_i = f_i^\mathsf{T} \dot{\delta}_i, \qquad \dot{P}(\delta_i^d) = \nabla P(\delta_i^d) \dot{\delta}_i^d = f_i^{d\mathsf{T}} \dot{\delta}_i^d, \qquad (3.28)$$

then, considering constant desired force f_i^d, the time-derivative of Δ_i from (3.27) is given by

$$\begin{aligned}
\dot{\Delta}_i &= f_i^\mathsf{T} \dot{\delta}_i - f_i^{d\mathsf{T}} \dot{\delta}_i^d - f_i^{d\mathsf{T}} \dot{\tilde{\delta}}_i \\
&= f_i^\mathsf{T} \dot{\delta}_i - f_i^{d\mathsf{T}} \dot{\delta}_i^d - f_i^{d\mathsf{T}} \dot{\delta}_i + f_i^{d\mathsf{T}} \dot{\delta}_i^d \\
&= f_i^\mathsf{T} \dot{\delta}_i - f_i^{d\mathsf{T}} \dot{\delta}_i, \\
&= \tilde{f}_i^\mathsf{T} \dot{\delta}_i,
\end{aligned}$$

The time-derivative of the storage function V_k in (3.27) is given by:

$$\dot{V}_k(\tilde{f}_{if}, \tilde{\delta}_i, \dot{\tilde{p}}_o, \tilde{b}_i) = \sum_{i=1}^{n} \left(\tilde{f}_i^\mathsf{T} \dot{\tilde{\delta}}_i + \lambda_l \tilde{f}_{if}^\mathsf{T} \dot{\tilde{f}}_{if} + \tilde{b}_i^\mathsf{T} \Gamma_k^{-1} \dot{\tilde{b}}_i \right) + m_o \dot{\tilde{p}}_o^\mathsf{T} \ddot{\tilde{p}}_o, \qquad (3.29)$$

and, then, using the object velocity error dynamics (3.7) and the object deformation

error dynamics (3.26) we obtain:

$$\dot{V}_k(\tilde{f}_{if}, \tilde{\delta}_i, \dot{\tilde{p}}_o, \tilde{b}_i) = \sum_{i=1}^{n} \left(-\tilde{f}_i^\mathsf{T} K_v \tilde{f}_{if} - \lambda_l \lambda_k \tilde{f}_{if}^\mathsf{T} \tilde{f}_{if} + \lambda_l \lambda_k \tilde{f}_{if}^\mathsf{T} \tilde{f}_i + \tilde{f}_i^\mathsf{T} w_1 \right)$$
$$+ \sum_{i=1}^{n} \left[\tilde{f}_i^\mathsf{T} W_i(q_i, \dot{q}_i) \tilde{b}_i + \tilde{b}_i^\mathsf{T} \Gamma_k^{-1} \dot{\tilde{b}}_i \right] .$$

Finally, taking $K_v = \lambda_l \lambda_k I$ and using the composite gradient-type adaptation law (3.14) with (3.15) yields:

$$\dot{V}_k(\tilde{f}_{if}, \tilde{\delta}_i, \dot{\tilde{p}}_o, \tilde{b}_i) = \sum_{i=1}^{n} \left[-\tilde{f}_{if}^\mathsf{T} K_v \tilde{f}_{if} - \tilde{b}_i^\mathsf{T} Z_i(q_i)^\mathsf{T} Z_i(q_i) \tilde{b}_i + \tilde{f}_i^\mathsf{T} w_1 \right] , \qquad (3.30)$$

which defines an output strictly passive map $w_1 \mapsto \tilde{f}_i$. Thus, for $w_1 = 0$, we have that $\dot{V}_k \le 0$. Because V_k is a positive definite function with non-positive time-derivative, we have that $V_k \in \mathcal{L}_\infty$ which implies that $\tilde{f}_{if}, \tilde{\delta}_i, \dot{\tilde{p}}_o, \tilde{b}_i \in \mathcal{L}_\infty$ and, thus, the equilibrium state is uniformly stable. Because $V_k \ge 0$ and $\dot{V}_k \le 0$, $\lim_{t \to \infty} V_k(t)$ exists. For the time-derivative of V_k for $w_1 = 0$ we have $\int_0^t \dot{V}_k(t')dt' = V_0 - V_\infty$ where $V_0 = V_k(0)$, which implies that $\tilde{f}_{if}, \epsilon_i \in \mathcal{L}_2$. Since the signals $\dot{p}_o^d$, f_i^d and δ_i^d are assumed to be uniformly bounded, from (3.22) and (3.23) we have $\dot{p}_o, \delta_i \in \mathcal{L}_\infty$ and consequently from (3.4) implies that $f_i \in \mathcal{L}_\infty$. From (3.20), since $\tilde{f}_{fi} \in \mathcal{L}_\infty$ we conclude that $\tilde{f}_i \in \mathcal{L}_\infty$ and, thus, $\dot{\tilde{f}}_{if} \in \mathcal{L}_\infty$. Considering $q_i, \dot{q}_i \in \mathcal{L}_\infty$ then it follows that $Z_i, W_i \in \mathcal{L}_\infty$ and, thus, from (3.14) implies that $\epsilon_i, \dot{\epsilon}_i \in \mathcal{L}_\infty$. Consequently, from (3.15), we conclude that $\dot{\tilde{b}}_i \in \mathcal{L}_\infty \cap \mathcal{L}_2$. Therefore, using Barbalat's lemma Khalil (2002) and because $\epsilon_i, \tilde{f}_{if} \in \mathcal{L}_2$ and $\dot{\epsilon}_i, \dot{\tilde{f}}_{if} \in \mathcal{L}_\infty$ implies that $\lim_{t \to \infty} \epsilon_i(t) = 0$ and $\lim_{t \to \infty} \tilde{f}_{if}(t) = 0$. From (3.20) implies that $\lim_{t \to \infty} \tilde{f}_i(t) = 0$ and, thus $\lim_{t \to \infty} \tilde{\delta}_i(t) = 0$. Consequently, from (3.26) we have $\lim_{t \to \infty} \dot{\tilde{p}}_o(t) = 0$, which demonstrates the stability and the convergence properties of the adaptive kinematic control.

<div style="text-align:right">□</div>

Remark 7 *An alternative and simpler solution consist of using only the force tracking error $\tilde{f}_i$ in the gradient-type adaptation law given by (3.13) in Theorem 2 (instead of the composite adaptation law given by (3.15)), without resorting to the prediction error ϵ_i. In that case, the proof has a similar development with the same storage function where its time-derivative is given by*

$$\dot{V}_k(\tilde{f}_{if}, \tilde{\delta}_i, \dot{\tilde{p}}_o, \tilde{b}_i) = \sum_{i=1}^{n} \left[-\tilde{f}_{if}^\mathsf{T} K_v \tilde{f}_{if} + \tilde{f}_i^\mathsf{T} w_1 \right] . \qquad (3.31)$$

3.4 Robot Dynamics

Here, we consider the cooperative control problem for robot manipulators with *nonnegligible* dynamics. A natural extension of the proposed kinematics-based controller considering the robot dynamics is presented. The dynamic model of a rigid robot manipulator is given by:

$$M_i(q_i)\,\ddot{q}_i + C_i(q_i, \dot{q}_i)\,\dot{q}_i + g_i(q_i) = \tau_i - J_i^{\mathsf{T}}(q_i)\,f_i\,, \tag{3.32}$$

where $\tau_i \in \mathbb{R}^{n_i}$ is the vector of generalized torques, $M_i(q_i) \in \mathbb{R}^{n_i \times n_i}$ is the manipulator inertia matrix, $C_i(q_i, \dot{q}_i) \in \mathbb{R}^{n_i \times n_i}$ is the Coriolis matrix for the manipulator where the term $C_i(q_i, \dot{q}_i)\,\dot{q}_i \in \mathbb{R}^{n_i}$ is the torque vector due to the Coriolis and centrifugal forces, and $g_i(q_i) \in \mathbb{R}^{n_i}$ includes gravity terms and other forces acting at the joints of the i-th robot manipulator. Notice that other actuation torques such as those due to the viscous and Coulomb friction forces could also be included in the robot dynamics.

It is well known that the left-hand side of (3.32) can be linearly parameterized by $Y_i(q_i, \dot{q}_i, \ddot{q}_i)\,a_i$, where $Y_i \in \mathbb{R}^{n_i \times m_i}$ is the dynamic regressor matrix, $a_i \in \mathbb{R}^{m_i}$ denotes the constant dynamic parameters and m_i is the number of dynamic parameters (Siciliano et al. (2009), p. 338). Then equation (3.32) can be rewritten as

$$Y_i(q_i, \dot{q}_i, \ddot{q}_i)\,a_i = \tau_i - J_i^{\mathsf{T}}(q_i)\,f_i\,, \tag{3.33}$$

It is worth mentioning that a particular choice for the elements of the Coriolis matrix can be obtained from Christoffel's symbols, which provide notable algebraic properties for the robot dynamic model (3.32), that we will use in the sequel for the purpose of control design and stability analysis. Thus, we consider the following properties of matrices $M_i(q_i)$ and $C_i(q_i, \dot{q}_i)$:

(P2) $M_i(q_i)$ is symmetric, positive definite and bounded matrix for all $q_i \in \mathbb{R}^{n_i}$, i.e., there exist a known positive constant $c_1 \in \mathbb{R}$ such that

$$M_i = M_i^{\mathsf{T}} > 0, \qquad ||M_i||_\infty \le c_1\,.$$

(P3) For a particular choice of the matrix $C_i(q_i, \dot{q}_i)$, the following relation holds

$$\xi^{\mathsf{T}}\left(\dot{M}_i - 2C_i\right)\xi = 0\,, \qquad \forall \xi \in \mathbb{R}^{n_i}\,.$$

It is worth mentioning that, based on the linear parameterization property applied to (3.9), the product between the transpose Jacobian matrix $J_i^{\mathsf{T}}(q_i)$ and the

contact force vector f_i can also be linearly parameterized as:

$$\tau_{i,ext} = J_i^{\mathsf{T}}(q_i)\, f_i = F_i(q_i, f_i)\, b_i\,, \tag{3.34}$$

where $F_i \in \mathbb{R}^{n_i \times \ell_i}$ is the kinetic regressor matrix. In what follows, we will use the above relationship for designing the dynamic control law for the cooperative robotic system.

Here, the key idea is to employ the *cascade control strategy* (Guenther and Hsu (1993)) to tackle the hybrid velocity and force control problem for cooperative robot manipulators in the presence of parametric uncertainties in the robot kinematics and dynamics. The application of the cascade framework to the case of cooperative robots is a contribution of this work and is analogous to the case of visual servoing considered by (Hsu et al. (2007); Leite and Lizarralde (2016); Lizarralde et al. (2013)). The cascade control strategy can be designed by cascading the kinematic control scheme with the dynamic control scheme according to the following steps. First, we assume that there exists a dynamic control law

$$\tau_i = h_i(q_i, \dot{q}_i, q_i^d, \dot{q}_i^d, \ddot{q}_i^d) + J_i^{\mathsf{T}}(q_i)\, f_i\,, \tag{3.35}$$

which guarantees the control goal is attended, i.e.,

$$q_i \rightarrow q_i^d(t)\,, \qquad \tilde{q}_i := q_i - q_i^d \rightarrow 0\,, \tag{3.36}$$

where $q_i^d \in \mathbb{R}^{n_i}$ denotes the desired trajectory assigned in joint space and assumed to be uniformly bounded, and $\tilde{q}_i$ the joint position error vector.

Now, let us suppose that it is possible to define the desired trajectory q_i^d and its time-derivatives $\dot{q}_i^d$, $\ddot{q}_i^d$ in terms of a control signal v_i such that we have $\dot{p}_i = v_i$ except for a vanishing term in the right-hand side, that is,

$$\dot{p}_i = v_i + J_i(q_i)\, L(s)\, \tilde{q}_i\,, \tag{3.37}$$

where $L(\cdot)$ denotes a linear operator, possibly noncausal, with s being the differential operator. Therefore, we can conclude that the Cartesian control signal (3.16), designed to the kinematic control case, could be applied to (3.37) and the stability property of the closed-loop control system still remains.

In order to carry out the stability analysis of the proposed cooperative control scheme, we employ the passivity framework, which establishes simple rules to describe the feedback connection of time-invariant dynamical systems based on the Lyapunov formalism (Khalil (2002)). Actually, we can show that the cooperative control scheme based on the kinematic control approach has passivity properties,

which allows for ensuring the closed-loop stability when it is connected in cascade with a dynamic control scheme with similar passivity properties (Hsu et al. (2007); Leite and Lizarralde (2016); Lizarralde et al. (2013)). For passive interconnected control systems with external disturbances, the following general result can be stated:

Theorem 3 *(Hsu et al. (2007)) Consider the interconnected systems, where Σ_1 is the driven system and Σ_2 is the driving system, described by:*

$$\Sigma_1: \quad \dot{x}_1 = \eta_1(x,t) + \xi(x,t)\,y_2 + \zeta(x,t)\,, \qquad\qquad y_1 = \varphi_1(x_1)\,,$$
$$\Sigma_2: \quad \dot{x}_2 = \eta_2(x,t) + w_2\,, \qquad\qquad\qquad\qquad\quad y_2 = \varphi_2(x_2)\,,$$

as seen in Fig. 3.3, where $x = [x_1\ x_2]^{\mathsf{T}}$, η_1, η_2 are piecewise continuous functions in time t and locally Lipschitz in x for all $t > 0$. $x \in \mathcal{D}$, where $\mathcal{D} \subset \mathbb{R}^n$ is a domain
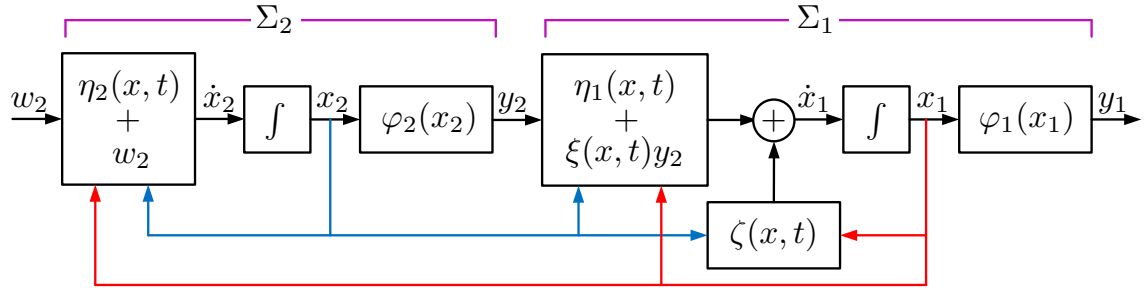
Figure 3.3: Interconected system in cascade

that contains the origin $x = 0$; φ_1, φ_2, ξ are continuous functions, ζ is a vanishing perturbation term and w_2 is an external input. Suppose that $\|\zeta(x,t)\| \leq \gamma\|x\|\|$, $\forall\, t \geq 0$, $\forall\, x \in \mathcal{D}$, where γ is a non-negative constant. Assume that $\|\xi(x,t)\| \leq c$, $\forall x,t$ and for some $c > 0$. If system Σ_1 is output strictly passive from $y_2 \to y_1$ with positive definite storage function $V_1(x_1)$ such that

$$\dot{V}_1 \leq -\lambda_1\|y_1\|^2 + c_1\,y_2^{\mathsf{T}}y_1\,, \qquad \lambda_1 > 0\,,$$

and system Σ_2 is output strictly passive from $w_2 \mapsto y_2$ with positive definite storage function $V_2(x_2)$ such that

$$\dot{V}_2 \leq -\lambda_2\|y_2\|^2 + c_2\,w_2^{\mathsf{T}}y_2\,, \qquad \lambda_2 > 0\,.$$

Then, for $w_2 = 0$, the following properties hold: (i) $x_1, x_2 \in \mathcal{L}_\infty$; (ii) $\lim_{t\to\infty}y_1(t)=0$, $\lim_{t\to\infty}y_2(t)=0$;

Proof 2 *Please see the Appendix B.1.*

50

3.4.1 Adaptive Robot Control

Now, let us consider the existence of parametric uncertainties in the robot dynamic model (3.32). In this context, we will show that the control design for the cooperative robotic system can be derived by simply cascading the proposed adaptive kinematic control scheme with the Slotine-Li adaptive scheme (Slotine and Li (1988)). First, let us consider the following signals defined in the joint space as:

$$\dot{q}_i^r = \dot{q}_i^d - \lambda_d\,\tilde{q}_i\,, \qquad \sigma_i = \dot{q}_i - \dot{q}_i^r = \dot{\tilde{q}}_i + \lambda_d\,\tilde{q}_i\,, \qquad (3.38)$$

where $q_i^r \in \mathbb{R}^{n_i}$ is the velocity reference signal, $\sigma_i \in \mathbb{R}^{n_i}$ is a measure of the tracking accuracy, and $\lambda_d > 0$ is a constant parameter.

Here, we assume that the dynamic model (3.32) subject to parametric uncertainties can be expressed in terms of the dynamic regressor matrix $Y(q_i, \dot{q}_i, \dot{q}_i^r, \ddot{q}_i^r)$ according to

$$\hat{M}_i(q_i)\,\ddot{q}_i^r + \hat{C}_i(q_i,\dot{q}_i)\,\dot{q}_i^r + \hat{g}_i(q_i) = Y(q_i, \dot{q}_i, \dot{q}_i^r, \ddot{q}_i^r)\,\hat{a}_i\,, \qquad (3.39)$$

where $\hat{a}_i \in \mathbb{R}^{m_i}$ is a set of estimated dynamic parameters to be adapted online and $\hat{M}_i, \hat{C}_i, \hat{g}_i$ denote the corresponding approximated terms of the robot dynamic model. A dynamic control law for the i-th robot end-effector can be given by

$$\tau_i = Y_i(q_i, \dot{q}_i, \dot{q}_i^r, \ddot{q}_i^r)\,\hat{a}_i - K_d\,\sigma_i - F_i(q_i, f_i)\,\hat{b}_i + w_2\,, \qquad (3.40)$$

where $K_d \in \mathbb{R}^{n_i \times n_i}$ is a positive definite gain matrix and $w_2 \in \mathbb{R}^{n_i}$ is a fictitious external input, which drives the closed-loop system.

Then, from the robot dynamic model (3.32), the velocity signals (3.38) and the dynamic control law (3.40), the closed-loop error dynamics can be written as

$$M_i(q_i)\,\dot{\sigma}_i + [\,C_i(q_i,\dot{q}_i) + K_d\,]\,\sigma_i = Y_i(q_i, \dot{q}_i, \dot{q}_i^r, \ddot{q}_i^r)\,\tilde{a}_i + F_i(q_i, f_i)\,\tilde{b}_i + w_2\,, \qquad (3.41)$$

where $\tilde{b}_i = \hat{b}_i - b_i$ is the i-th kinematic parameter error vector and $\tilde{a}_i = \hat{a}_i - a_i$ is the i-th dynamic parameter error vector.

The vector of estimated kinematic parameters $\hat{b}_i$ can be updated by using the following composite gradient-type adaptive law:

$$\dot{\hat{b}}_i = -\Gamma_k(Z_i^\mathsf{T}\,\epsilon_i + F_i^\mathsf{T}\,\sigma_i)\,, \qquad \Gamma_k = \Gamma_k^\mathsf{T} > 0\,, \qquad (3.42)$$

whereas the vector of estimated dynamic parameters $\hat{a}_i$ can be updated by using the

following standard gradient-type adaptive law:

$$\dot{\hat{a}}_i = -\Gamma_d Y_i^{\mathsf{T}} \sigma_i \,, \qquad\qquad \Gamma_d = \Gamma_d^{\mathsf{T}} > 0 \,, \qquad\qquad (3.43)$$

where Γ_k is the kinematic adaptation gain matrix and Γ_d is the dynamic adaptation gain matrix.

The algorithm of the cooperative kinematic control is presented in Table 3.2.

Table 3.2: Algorithm of the Cooperative Dynamic Control

Robot Dynamic Model	$M_i(q_i)\,\ddot{q}_i + C_i(q_i,\dot{q}_i)\,\dot{q}_i + g_i(q_i) = \tau_i - J_i^{\mathsf{T}}(q_i)\,f_i$
Dynamic Control Law	$\tau_i = Y_i(q_i,\dot{q}_i,\dot{q}_i^r,\ddot{q}_i^r)\,\hat{a}_i - K_d\,\sigma_i - F_i(q_i,f_i)\,\hat{b}_i + w_2$
Dynamic Adaptation Law	$\dot{\hat{a}}_i = -\Gamma_d Y_i^{\mathsf{T}} \sigma_i \,, \qquad \Gamma_d = \Gamma_d^{\mathsf{T}} > 0$
Parameterization Model	$\hat{p}_i = \hat{k}_i(q_i) = Z_i(q_i)\,\hat{b}_i$ $\tau_{i,ext} = J_i^{\mathsf{T}}(q_i)\,f_i = F_i(q_i,f_i)\,b_i$
Prediction Error	$\epsilon_i = p_i - Z_i(q_i)\,\hat{b} = Z_i(q_i)\,\tilde{b}_i$
Composite Adaptation Law	$\dot{\hat{b}}_i = -\Gamma_k(Z_i^{\mathsf{T}}\,\epsilon_i + F_i^{\mathsf{T}}\,\sigma_i)\,, \qquad \Gamma_k = \Gamma_k^{\mathsf{T}} > 0$

The block diagram of the proposed adaptive kinematic and dynamic control is presented in Fig. 3.4. The stability analysis and passivity properties of the closed-
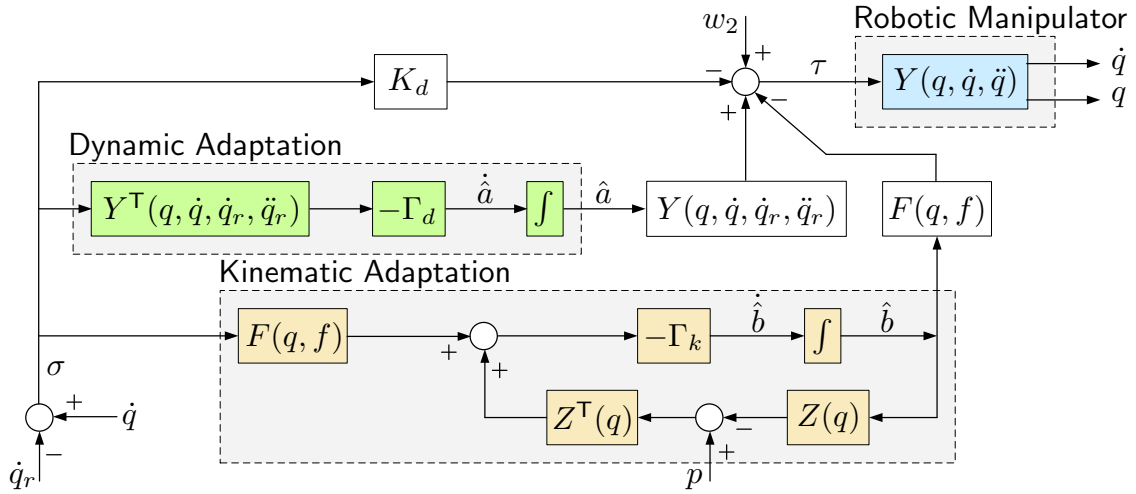
Figure 3.4: Adaptive kinematic and dynamic control block diagram

loop dynamic system (3.41) can be established in the following theorem:

Theorem 4 *Consider the robot dynamic model (3.32), the dynamic control law (3.40) with the dynamic adaptation law (3.43). Now, consider the linear parameterization models (3.11) and (3.34), with the prediction error (3.14) and the composite adaptation law (3.42). Assume that the end-effector position p_i and the regressor matrices Y_i, Z_i and F_i are measured from system signals. Then, the map $w_2 \mapsto \sigma_i$*

is output strictly passive with positive definite storage function

$$2V_d(\sigma_i, \tilde{a}_i, \tilde{b}_i) = \sum_{i=1}^{n} \left(\sigma_i^{\mathsf{T}} M_i(q_i) \, \sigma_i + \tilde{a}_i^{\mathsf{T}} \Gamma_d^{-1} \tilde{a}_i + \tilde{b}_i^{\mathsf{T}} \Gamma_k^{-1} \tilde{b}_i \right) . \qquad (3.44)$$

Moreover, for $w_2 = 0$, the following properties hold: (i) All system signals are uniformly bounded; (ii) $\lim_{t\to\infty}\epsilon_i(t) = 0$, $\lim_{t\to\infty}\sigma_i(t) = 0$, which implies that $\lim_{t\to\infty}\tilde{q}_i(t) = 0$, $\lim_{t\to\infty}\dot{\tilde{q}}_i(t) = 0$.

Proof 3 *The time-derivative of the storage function V_d in (3.44) is given by:*

$$\dot{V}_d(\sigma_i, \tilde{a}_i, \tilde{b}_i) = \sum_{i=1}^{n} \left(\sigma_i^{\mathsf{T}} M_i \, \sigma_i + \frac{1}{2} \sigma_i^{\mathsf{T}} \dot{M}_i \sigma_i + \tilde{a}_i^{\mathsf{T}} \Gamma_d^{-1} \dot{\tilde{a}}_i + \tilde{b}_i^{\mathsf{T}} \Gamma_k^{-1} \dot{\tilde{b}}_i \right) , \qquad (3.45)$$

and, then, using the closed-lopp error dynamics (3.41) we obtain:

$$\begin{aligned}
\dot{V}_d(\sigma_i, \tilde{a}_i, \tilde{b}_i) &= \sum_{i=1}^{n} \left[-\sigma_i^{\mathsf{T}} K_d \sigma_i + \sigma_i^{\mathsf{T}} Y(q_i, \dot{q}_i, \dot{q}_i^r, \ddot{q}_i^r)\tilde{a}_i + \sigma_i^{\mathsf{T}} F(q_i, f_i)\, \tilde{b}_i \right] \\
&\quad + \sum_{i=1}^{n} \left[\tilde{a}_i^{\mathsf{T}} \Gamma_d^{-1} \dot{\tilde{a}}_i + \tilde{b}_i^{\mathsf{T}} \Gamma_k^{-1} \dot{\tilde{b}}_i + \sigma_i^{\mathsf{T}} w_2 \right] ,
\end{aligned}$$

Finally, using the gradient-type adaptation laws (3.42) and (3.43) yields:

$$\dot{V}_d(\sigma_i, \tilde{a}_i, \tilde{b}_i) = \sum_{i=1}^{n} \left[-\sigma_i^{\mathsf{T}} K_d \sigma_i - \tilde{b}_i^{\mathsf{T}} Z_i(q_i)^{\mathsf{T}} Z_i(q_i)\, \tilde{b}_i + \sigma_i^{\mathsf{T}} w_2 \right] , \qquad (3.46)$$

which defines an output strictly passive map from $w_2 \mapsto \sigma_i$. Thus, for $w_2 = 0$, we have that $\dot{V}_d \leq 0$. Because V_d is a positive definite function with non-positive time-derivative, we have that $V_d \in \mathcal{L}_\infty$ which implies that $\sigma_i, \tilde{a}_i, \tilde{b}_i \in \mathcal{L}_\infty$ and, thus, the equilibrium state is uniformly stable. Because $V_d \geq 0$ and $\dot{V}_d \leq 0$, $\lim_{t\to\infty}V_d(t)$ exists. For the time-derivative of V_d for $w_2 = 0$ we have $\int_0^t \dot{V}_d(t')dt' = V_0 - V_\infty$ where $V_0 = V_d(0)$, which implies that $\sigma_i, \epsilon_i \in \mathcal{L}_2$. Considering $q_i, \dot{q}_i \in \mathcal{L}_\infty$ then it follows that $Z_i, W_i \in \mathcal{L}_\infty$ and, thus, from (3.14) implies that $\epsilon_i, \dot{\epsilon}_i \in \mathcal{L}_\infty$. Since the signals $q_i^d, \dot{q}_i^d$ are previously assumed to be uniformly bounded and $\sigma_i \in \mathcal{L}_\infty$, from the velocity signals (3.38), we conclude that $\tilde{q}_i, \dot{\tilde{q}}_i \in \mathcal{L}_\infty$, which implies that $q_i, \dot{q}_i, \dot{q}_i^r, \ddot{q}_i^r \in \mathcal{L}_\infty$ and, consequently, $Y_i \in \mathcal{L}_\infty$. Thus, from the kinematic and dynamic adaptation laws, (3.42) and (3.43), we have that $\tilde{b}_i, \tilde{a}_i \in \mathcal{L}_\infty \cap \mathcal{L}_2$ and, consequently, from the closed-loop error dynamics (3.41), implies that $\dot{\sigma}_i, \dot{\epsilon}_i \in \mathcal{L}_\infty$. Therefore, using Barbalat's lemma Khalil (2002) and because $\sigma_i, \epsilon_i \in \mathcal{L}_2$ and $\dot{\sigma}_i, \dot{\epsilon}_i \in \mathcal{L}_\infty$, implies that $\lim_{t\to\infty}\epsilon_i(t) = 0$ and $\lim_{t\to\infty}\sigma_i(t) = 0$ and, consequently, $\lim_{t\to\infty}\tilde{q}_i(t) = 0$ and $\lim_{t\to\infty}\dot{\tilde{q}}_i(t) = 0$, which demonstrates the global stability of the closed-loop dynamic control system.

□

Remark 8 *It is worth noting that (i) considering the q_i, $\dot{q}_i$ and f_i measurable, all signals necessary to compute the regressor matrices Z_i, W_i, F_i and Y_i are available and (ii) the convergence of the estimated parameters $\hat{a}_i$ and $\hat{b}_i$ to the real values depends on the level of excitation of the regressor matrices Z_i, W_i, F_i and Y_i, respectively.*

3.4.2 Cascade Control

Now, we are able to apply the cascade control strategy previously presented to generate the reference signals $q_i^d, \dot{q}_i^d, \ddot{q}_i^d$ for the robot dynamic control (3.40) (See Fig.3.5).
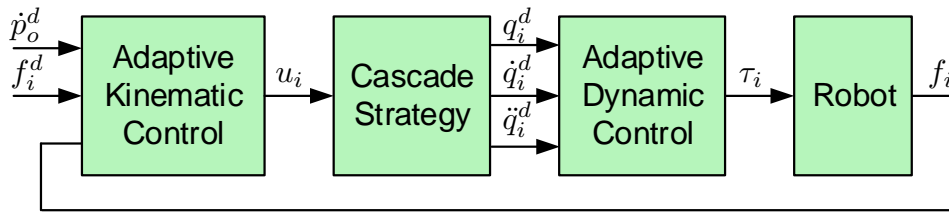

Figure 3.5: Cascade Control Strategy

Following the cascade framework and using the velocity signals (3.38), we can define

$$\dot{q}_i^r = \hat{J}_i^{\dagger}(q_i)\, v_i \,, \tag{3.47}$$

so that the Cartesian motion of the i-th robot end-effector is governed by

$$\dot{p}_i = v_i + \hat{J}_i(q_i)\, \sigma_i + W_i(q_i, \beta_i)\, \tilde{b}_i \,, \tag{3.48}$$

where $\sigma_i \in \mathbb{R}^{n_i}$ is a vanishing term from Theorem 4 (it converges asymptotically to zero), and $W_i(q_i, \dot{q}_i)\, \tilde{b}_i$ is a kinematic perturbation term, which arises because of the uncertain robot kinematics.

Then, the cascade control strategy can be implemented by simply setting:

$$\dot{q}_i^d = \dot{q}_i^r + \lambda_d\, \tilde{q}_i \,, \qquad\qquad \ddot{q}_i^d = \ddot{q}_i^r + \lambda_d\, \dot{\tilde{q}}_i \,. \tag{3.49}$$

noting that, $\ddot{q}_i^d$ depends on $\ddot{q}_i^r$ which in turn from (3.47) depends on the time-derivative of v_i. Since v_i, in (3.19), is defined in term of the filtered force error (3.20), the control law (3.40) does not depends on measuring the time-derivative of the force $\dot{f}_i$, which requires the time-derivative of the acceleration usually referred

as *jerk*. [1] Thus, the proposed control law is performed without jerk measurements.

Now, we consider the passivity properties of the adaptive dynamic control system, stated by Theorem 4, and the adaptive kinematic control system, stated by Theorem 2. Thus, we can apply Theorem 3 to analyze the stability properties of the overall closed-loop system, where the cascaded subsystems Σ_1 and Σ_2 are identified by the corresponding states as

$$\Sigma_1: \quad x_1^\mathsf{T} = \begin{bmatrix} \tilde{f}_i^\mathsf{T} & \tilde{f}_{if}^\mathsf{T} & \tilde{\delta}_i^\mathsf{T} & \dot{\tilde{p}}_o^\mathsf{T} \end{bmatrix}, \quad y_1 = \tilde{f}_i, \tag{3.50}$$

$$\Sigma_2: \quad x_2^\mathsf{T} = \begin{bmatrix} \tilde{q}_i^\mathsf{T} & \dot{\tilde{q}}_i^\mathsf{T} & \tilde{a}_i^\mathsf{T} & \tilde{b}_i^\mathsf{T} \end{bmatrix}, \quad y_2 = \begin{bmatrix} \sigma_i^\mathsf{T} & \epsilon_i^\mathsf{T} \end{bmatrix}^\mathsf{T}. \tag{3.51}$$

with a combined kinematic adaptation law (from (3.15) (3.42))

$$\dot{\tilde{b}}_i = -\Gamma_k \left(Z_i^\mathsf{T} \epsilon_i + F_i^\mathsf{T} \sigma_i + W_i^\mathsf{T} \tilde{f}_i \right), \qquad \Gamma_k = \Gamma_k^\mathsf{T} > 0,$$

and the storage functions $V_1(x_1)$ and $V_2(x_2)$ are defined as

$$2V_1(x_1) = m_o \dot{\tilde{p}}_o^\mathsf{T} \dot{\tilde{p}}_o + \sum_{i=1}^{n} 2\Delta_i + \lambda_l \tilde{f}_{if}^\mathsf{T} \tilde{f}_{if}, \tag{3.52}$$

$$2V_2(x_2) = \sum_{i=1}^{n} \sigma_i^\mathsf{T} M_i(q_i) \sigma_i + \tilde{a}_i^\mathsf{T} \Gamma_d^{-1} \tilde{a}_i + \tilde{b}_i^\mathsf{T} \Gamma_k^{-1} \tilde{b}_i. \tag{3.53}$$

Then, from Theorem 3, we can conclude that (i) all signals of the interconnected system are bounded; (ii) $\lim_{t\to\infty} \sigma_i(t) = 0$, $\lim_{t\to\infty} \epsilon_i = 0$, $\lim_{t\to\infty} \tilde{f}_i = 0$, $\lim_{t\to\infty} \tilde{\delta}_i = 0$ and $\lim_{t\to\infty} \dot{\tilde{p}}_o = 0$.

3.5   Conclusions

A cooperative controller which achieves convergence to the desired velocity and force regulation considering the uncertain kinematics and dynamics was proposed using a formation-control framework. The force closure is implemented on a kinematic level to guarantee a firm grasp of the object.

From a cascade control strategy, the adaptive kinematic controller is combined to the adaptive dynamic controller, ensuring the overall stability of the interconnected systems thanks to the inherent passivity properties of the cooperative robotic system. It is remarkable that the need of measuring the time-derivative of the force error was avoided by considering the filtered force error in the Cartesian control law.

The proposed composite gradient-type adaptive control laws were summarized

---

[1] The time-derivative of acceleration is called *jerk*, and generally to mention a change in contact force f_i with respect to time t, it is used the term *yank* (Jazar (2011)). Under certain assumptions (e.g. constant body mass), $\dot{f}_i$ is proportional to the jerk.

in Theorem 2 for the Cartesian control approach and in Theorem 4 for the dynamic control approach, then the passivity properties and stability of the proposed theorems were proved using a positive definite storage functions.

Chapter 4

Simulations and Experiments

In this chapter, several simulations and experiments are presented to illustrate the teleoperation scheme adopted, the cooperative control schemes mentioned in Section 1.4.1 and the teleoperated adaptive cooperative control scheme proposed in chapters 2 and 3.

For the simulations and experiments of bimanual manipulation the robotic manipulator considered is the Motoman DIA 10, a description and its direct and differential kinematics is presented in Appendix D.

4.1   Simulations

In this section several simulations of bimanual manipulation are presented. First some preliminary results of cooperative control of robotic manipulators considering the *cooperative task space approach* (Chiacchio et al. (1996)) to manipulate an object in planar movement and considering the *symmetric formulation* (Uchiyama and Dauchez (1988)) to manipulate a pizza palette.

Then, a simulation of the teleoperation of one degree of freedom robotic manipulators is presented using the two layer approach. And finally, a simulation of object manipulation using the proposed formation control based adaptive cooperative teleoperated scheme.

In all simulations it is consider that the inertial frame $\mathbb{E}_s$ (the origin of the coordinate system) is located at the base of the Motoman.

4.1.1   Cooperative Control: Object Manipulation - Planar

In this simulation the cooperative control of two planar 3 joint robotic manipulators is presented. The control objective is to manipulate a held object and make it follow a circular trajectory in the X-Y plane while rotating around the Z axis.

The Motoman model is used considering several joints in fixed positions in order have two planar manipulators to only actuate the joints q_3, q_5, q_7 for the right planar manipulator and the joints q_{10}, q_{12}, q_{14} for the left planar manipulator, then the planar joint vector for the two arm system q_p is given by

$$q_p = \begin{bmatrix} \overbrace{q_3 \quad q_5 \quad q_7}^{\text{Right Planar Arm}} & \overbrace{q_{10} \quad q_{12} \quad q_{14}}^{\text{Left Planar Arm}} \end{bmatrix}^\mathsf{T}. \tag{4.1}$$

Consider a time-varying desired absolute and relative planar positions $p_a^d, p_r^d \in \mathbb{R}^2$ and orientations $\phi_a^d, \phi_r^d \in \mathbb{R}$, given by

$$p_a^d = r_c \begin{bmatrix} \cos \frac{\pi t}{8} \\ \sin \frac{\pi t}{8} \end{bmatrix} + p_a^o, \qquad\qquad p_r^d = l_c \begin{bmatrix} \cos \phi_a \\ \sin \phi_a \end{bmatrix}, \tag{4.2a}$$

$$\phi_a^d = \frac{\pi}{8} \sin \frac{\pi t}{8} + \phi_a^o, \qquad\qquad \phi_r^d = \pi \tag{4.2b}$$

where p_a^d describes a circular trajectory of radius $r_c = 0.1m$, p_r^d describes a variable orientation where the distance between the end-effectors is kept constant at $l_c = 0.25m$. The initial desired position $p_a^o \in \mathbb{R}^2$ and orientation $\phi_a^o \in \mathbb{R}$ are given by

$$p_a^o = \begin{bmatrix} 0 & 0.4 \end{bmatrix}^\mathsf{T} \qquad \phi_a^o = \frac{\pi}{2}. \tag{4.3}$$

The planar absolute and relative desired planar poses $x_a^d, x_r^d \in \mathbb{R}^3$ are given by

$$x_a^d = \begin{bmatrix} p_a^d \\ \phi_a^d \end{bmatrix}, \qquad x_r^d = \begin{bmatrix} p_r^d \\ \phi_r^d \end{bmatrix}, \tag{4.4}$$

then the poses of the end-effectors in operational space x_{Rp}, x_{Lp} (as well as their respective desired values x_{Rp}^d, x_{Lp}^d) can be computed with (1.15a) and are given by

$$x_{Rp} = \begin{bmatrix} p_{Rp} \\ \phi_{Rp} \end{bmatrix}, \qquad x_{Lp} = \begin{bmatrix} p_{Lp} \\ \phi_{Lp} \end{bmatrix}, \tag{4.5}$$

where $p_{Rp}, p_{Lp} \in \mathbb{R}^2$ and $\phi_{Rp}, \phi_{Lp} \in \mathbb{R}$ are the position and orientation of the right and left planar manipulators, respectively. The pose representation is greatly simplified by the fact that the orientation can be represented by an scalar.

The control law is given by

$$\dot{q}_p = J_p^{-1} v_p, \tag{4.6}$$

where $J_p = diag\{J_R, J_L\}$, $J_R, J_L \in \mathbb{R}^{3 \times 3}$ are the Jacobians of the planar manipula-

tors, $v = \begin{bmatrix} v_R & v_L \end{bmatrix}$, $v_R, v_L \in \mathbb{R}^3$ is the Cartesian control signal given by

$$v_R = \dot{x}_{Rp}^d - K\tilde{x}_{Rp}, \qquad v_L = \dot{x}_{Lp}^d - K\tilde{x}_{Lp}, \qquad (4.7)$$

where $\tilde{x}_{Rp}, \tilde{x}_{Lp} \in \mathbb{R}^3$ are the pose errors and $K_p \in R^3$ is the planar control gain.

The simulation results are presented in Fig. 4.1 for the position and orientation errors and in Fig. 4.2 for the velocities and positions of the joints.
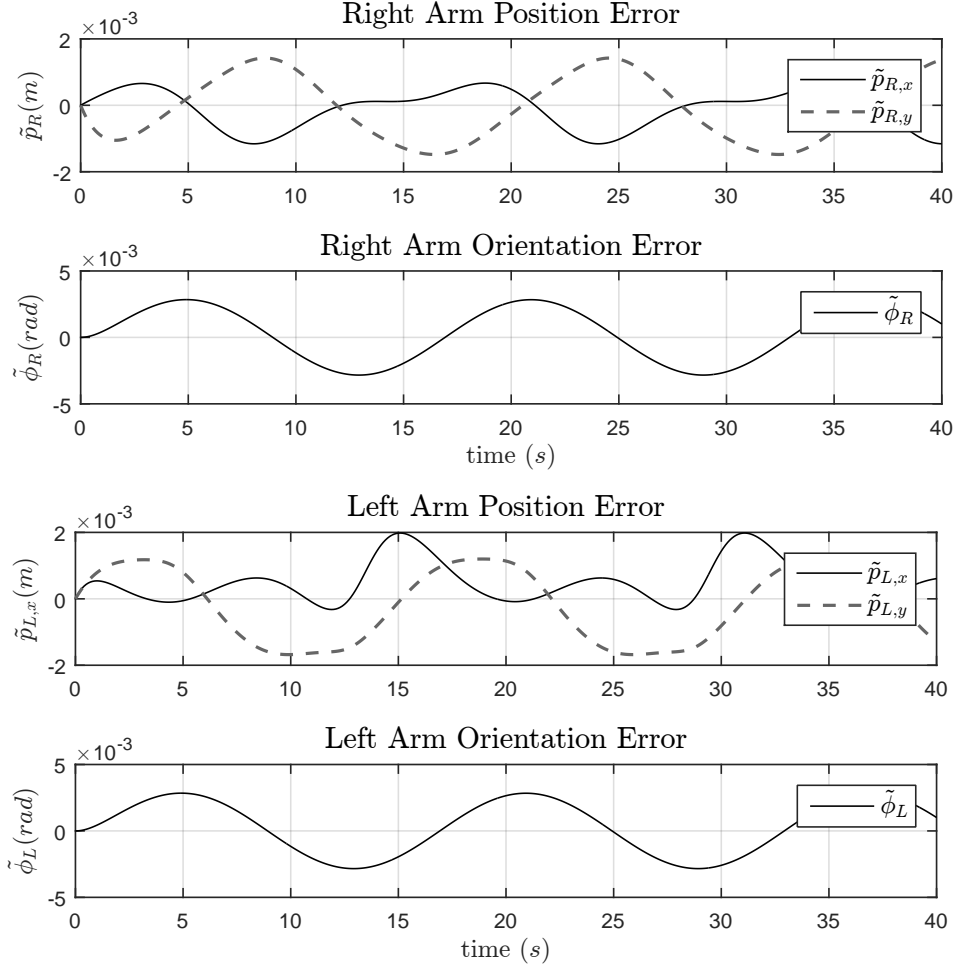

Figure 4.1: Position and Orientation Errors.

The simulation considered a time of 40s with an integration step of 0.1s and a planar control gain of 1. The position and orientation errors showed in Fig. 4.1 where less than $\pm 2 \times 10^{-3} m$ and $\pm 5 \times 10^{-3} rad$, respectively. It should be noted that the selected initial absolute position of the effectors coincides with the initial absolute position of the trajectory, such that the initial pose error was zero.
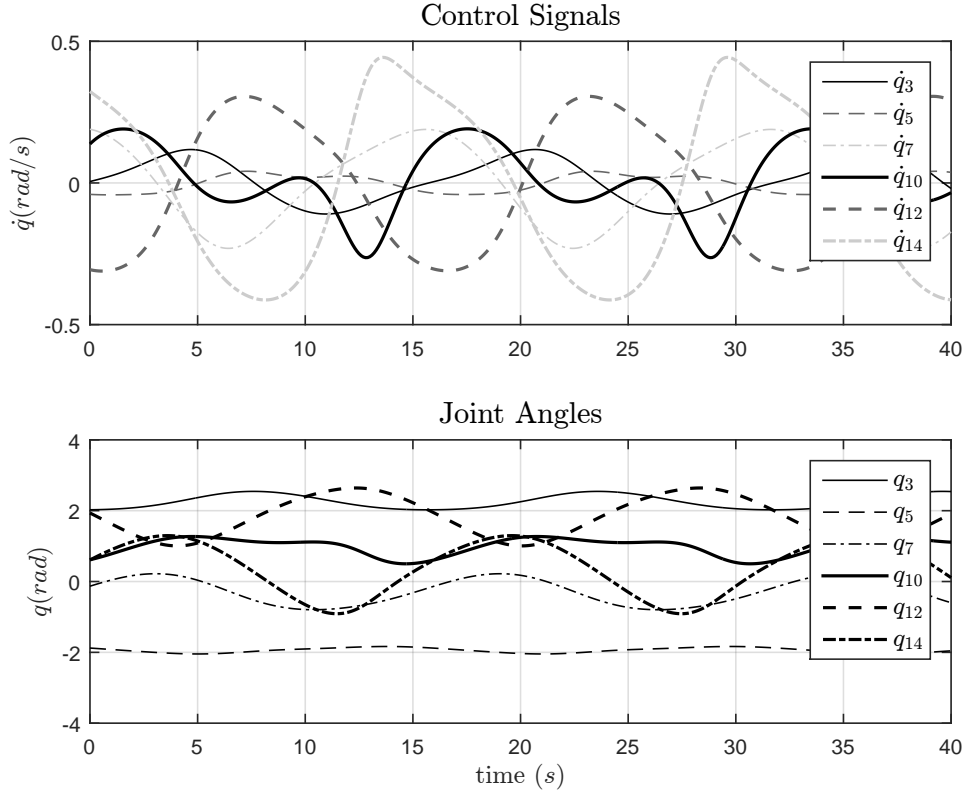
Figure 4.2: Velocities and Positions of the Joints.

4.1.2 Cooperative Control: Palette Manipulation

This simulation is inspired by one of the tasks studied in the RoDyMan Project (RObotic DYnamic MANipulation)[1] (Fig. 4.3), which consist on a unified network for robotic dynamic manipulation of deformable objects (Petit et al. (2017); Satici et al. (2016)).

In this case, the task is the manipulation of a pizza palette by a bimanual robotic manipulator with the symmetric formulation (Caccavale and Uchiyama (2016)) which considers *virtual sticks* fixed to the end-effectors such that the kinematic controller controls the pose of the tips of the virtual sticks (tovs) is addressed.

The task considers both arms grasping a palette with grippers, the left arm has a firm grasp on the palette while the right arm holds it loosely. In its initial pose both arms have the same orientation facing to the front of the Motoman, the center of movement is located between the end-effectors at their initial position.

For this task it is considered that the virtual sticks have not the same orientation of their end-effectors, instead they are rotated $\pi/2\,rad$, such that they face each other. Figure 4.4(a) shows the initial configuration of the robotic manipulator, where the left and right end-effector and virtual stick have green and red colors,
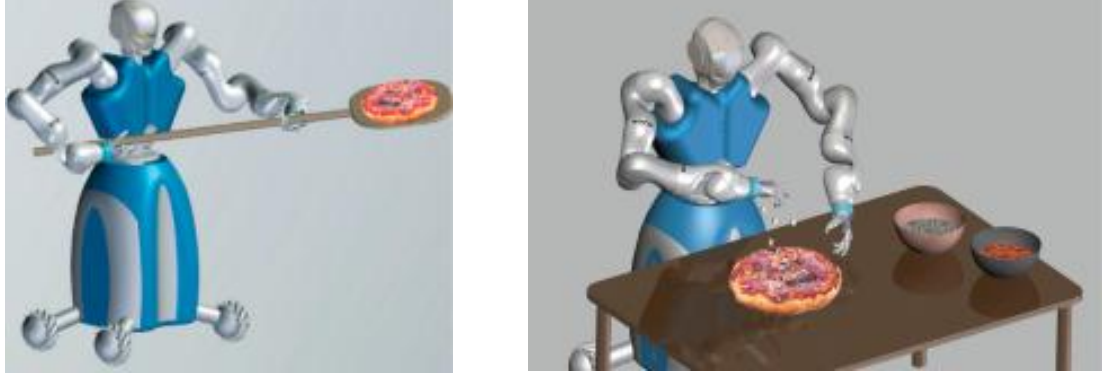
---

[1]http://www.rodyman.eu/

Figure 4.3: RoDyMan (RObotic DYnamic MANipulation) Project

respectively.

The task can be divided in three sub-tasks that considers the control of:

- The absolute position of the end-effectors (Fig. 4.4(b)); by making the absolute position of the tovs p_a follow a trajectory given by

$$p_a^d = \begin{bmatrix} 0.6 \\ 0 \\ 1.3 \end{bmatrix} + 0.1 \sin \frac{\pi t}{6} \begin{bmatrix} 1 \\ 1 \\ 1 \end{bmatrix}. \tag{4.8}$$

- The relative position between end-effectors (Fig. 4.4(c)); by considering a time varying length of the virtual stick of the right end-effector l_R, i.e.,

$$l_R = 0.4 \left(1 - \left\| \sin \frac{\pi t}{2} \right\| \right) \tag{4.9}$$

then, the virtual sticks vectors of both arms r_L, r_R are given by

$$r_L = 0.4 \ R_{vL} \ \vec{z}, \qquad r_R = l_R \ R_{vR} \ \vec{z}. \tag{4.10}$$

where R_{vL}, R_{vR} are the rotation matrices that correspond to the quaternions Q_{vL}, Q_{vR}, given by

$$Q_{vL} = Q_L * Q \left(\frac{\pi}{2}, \vec{x} \right), \qquad Q_{vR} = Q_R * Q \left(-\frac{\pi}{2}, \vec{x} \right). \tag{4.11}$$

- Rotation of the palette around its axis (Fig. 4.4(d)); by considering that the desired orientation of the left end-effector is given by the desired absolute orientation, and the desired orientation of the right end-effector by the product

of the desired absolute and the desired relative orientation, i.e.,

$$Q_a^d = Q\left(\frac{\pi}{8}\sin\frac{\pi t}{8}, -\vec{x}\right) * Q\left(\frac{\pi}{2}, \vec{y}\right), \qquad (4.12a)$$

$$Q_r^d = Q\left(\frac{\pi}{8}\sin\frac{\pi t}{8}, \vec{y}\right) \qquad (4.12b)$$

$$Q_L^d = Q_a^d, \qquad Q_R^d = Q_a^d * Q_r^d. \qquad (4.12c)$$

(a) Initial position.

(b) Movement of the palette.

(c) Relative position of the end-effectors.
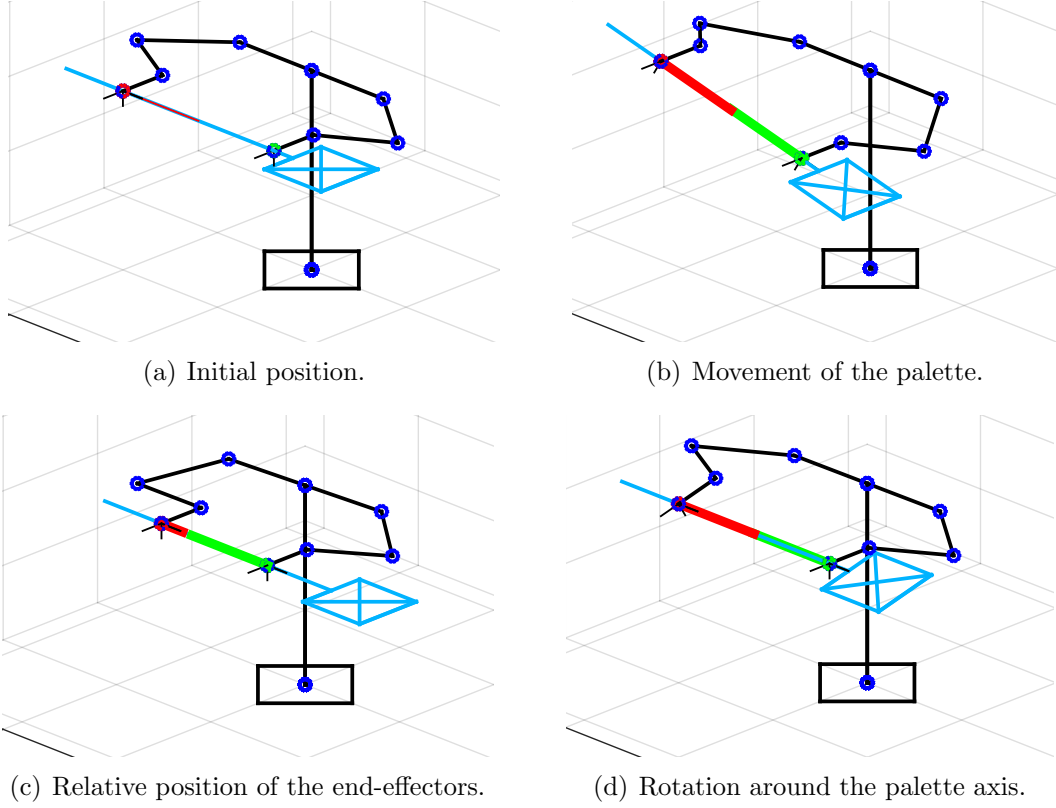
(d) Rotation around the palette axis.

Figure 4.4: Movements performed to manipulate the palette.

The position error of the tovs $\tilde{p}_{sL}, \tilde{p}_{sR} \in \mathbb{R}^3$ are given by

$$\tilde{p}_{sL} = p_{sL} - p_{sL}^d, \qquad \tilde{p}_{sR} = p_{sR} - p_{sR}^d, \qquad (4.13)$$

with

$$\begin{aligned} p_{sL} &= p_L + r_L, \\ p_{sR} &= p_R + r_R, \end{aligned} \qquad \begin{bmatrix} p_{sL}^d \\ p_{sR}^d \end{bmatrix} = \begin{bmatrix} I/2 & I/2 \\ I & -I \end{bmatrix} \begin{bmatrix} p_a^d \\ p_r^d \end{bmatrix}, \qquad (4.14)$$

where $I \in \mathbb{R}^{3\times 3}$ is the identity matrix and $p_{sL}, p_{sR} \in \mathbb{R}^3$ is the position of the tovs and p_a^d, p_r^d are the absolute and relative desired positions of the tovs. Notice that in the symmetric formulation the control objective considers that the tovs of both end-effectors have the same positions, then $\dot{p}_a^d = \dot{p}_L^d = \dot{p}_R^d$ and $\dot{p}_r^d = \begin{bmatrix} 0 & 0 & 0 \end{bmatrix}^\mathsf{T}$.

The orientation error $\tilde{Q}_{v,L}, \tilde{Q}_{v,R} \in \mathbb{R}^3$ is given by the vector part of $\tilde{Q}_L, \tilde{Q}_R$, which are given by

$$\tilde{Q}_L = Q_L * \left(Q_L^d\right)^{-1}, \qquad \tilde{Q}_R = Q_R * \left(Q_R^d\right)^{-1}, \tag{4.15}$$

The kinematic cooperative control law is given by

$$\dot{q}_M = J_M^\dagger \begin{bmatrix} v_R \\ v_R \end{bmatrix} \tag{4.16}$$

where

$$v_R = \begin{bmatrix} I & O \\ S(r_R) & I \end{bmatrix} \begin{bmatrix} \dot{p}_R^d + K_p \tilde{p}_{sR} \\ \omega_R^d + K_o \tilde{Q}_{v,R} \end{bmatrix} \qquad v_L = \begin{bmatrix} I & O \\ S(r_L) & I \end{bmatrix} \begin{bmatrix} \dot{p}_L^d + K_p \tilde{p}_{sL} \\ \omega_L^d + K_o \tilde{Q}_{v,L} \end{bmatrix}, \tag{4.17}$$

where $K_p, K_o \in \mathbb{R}^3$ are the position and orientation gain matrices.

The position and orientation errors are presented in Fig. 4.5 and the control signals, joints angles and manipulability of each arm in Fig. 4.6.
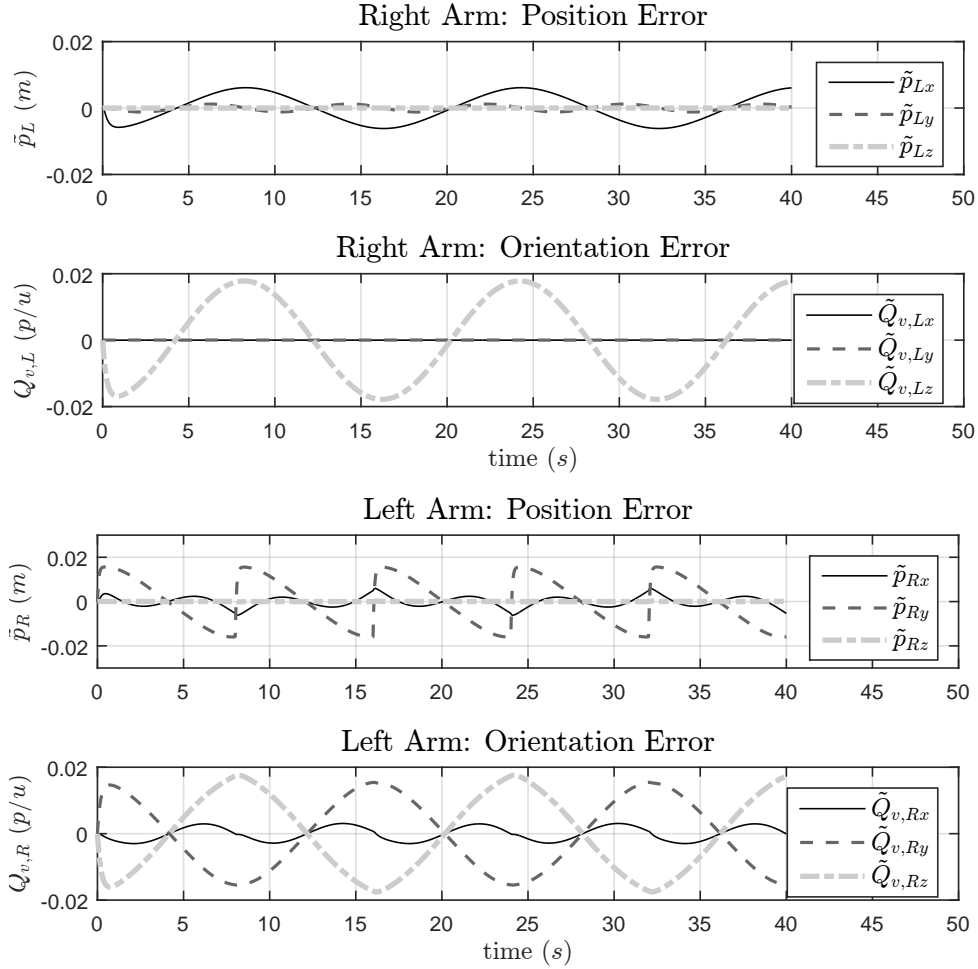

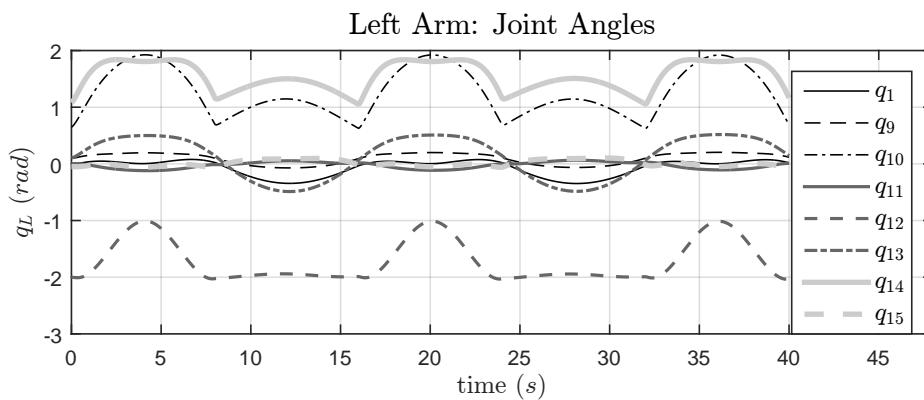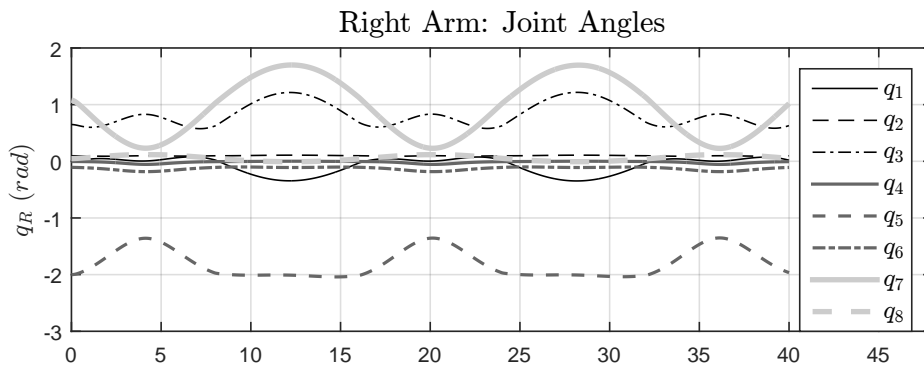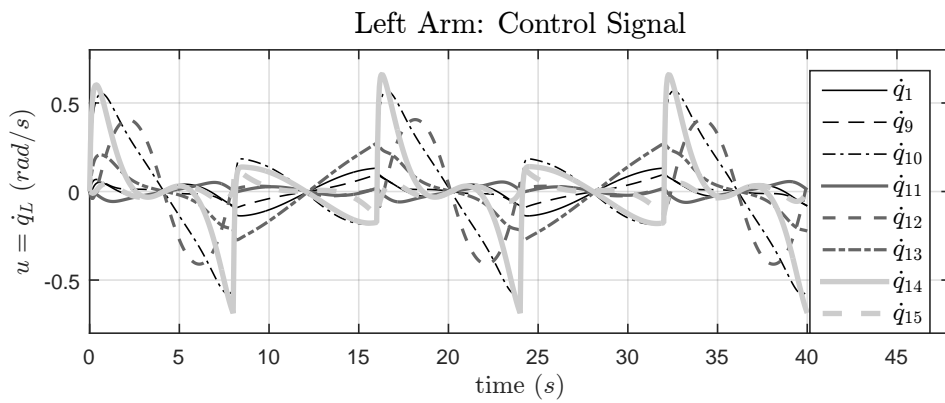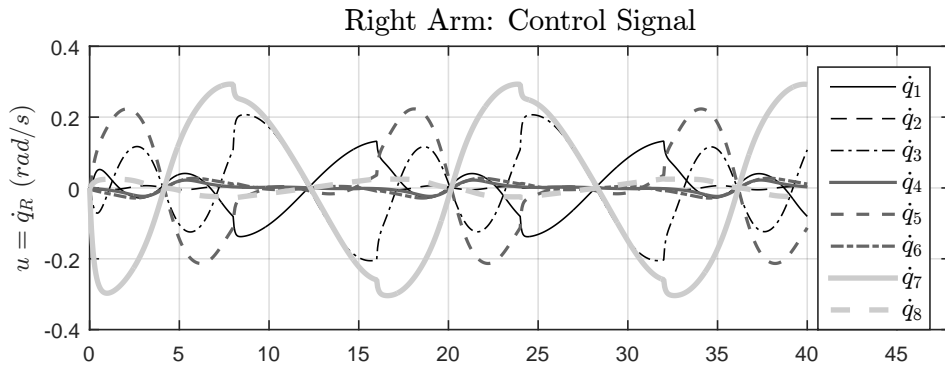Figure 4.5: Position and Orientation Errors and Manipulability.

Figure 4.6: Velocities and Positions of the Joints.

4.1.3 Teleoperation of two one-degree-of-freedom manipulators using Energy Tanks

To illustrate the teleoperation strategy of passivation via energy tanks, a simple example (based on Franken et al. (2009)) is presented. This simulation shows how the passivation via energy tanks contributes to stabilize the teleoperated system and reduces significantly the oscillations due to the switching between non-contact and contact with the environment.

The teleoperation system consist on two identical one-degree-of-freedom (1-DOF) manipulators, one master and one slave. The control objective consist on making the slave touch a wall (in the remote site) in such a way that the operator exerts a constant force to the master, which is *in contact* with a virtual wall. This force exerted by the operator is cancelled by the force reflected by the master, which has the same magnitude as the contact force measured by the force sensor. This allows the operator to feel as if he were in contact to the actual wall through the master.

Model of the Teleoperated System

It consist on a Master and Slave one-dimensional systems, given by

$$m_t \ddot{p}_m + b_t \dot{p}_m = f_h + f_m, \tag{4.18a}$$

$$m_t \ddot{p}_s + b_t \dot{p}_s = f_s + f_e, \tag{4.18b}$$

where p_m, p_s are the positions (in m), m_t is the mass (in kg), b_t is the damping coefficient (in kg/s), f_m, f_s are the manipulator forces, f_h is the operator force and f_e is the environment force (in N). No scaling in the signals is considered.

The Master and Slave controllers are given by

$$f_m = f_e^{T_s}, \tag{4.19a}$$

$$f_s = -k_p \left(p_s - p_m^{T_m} \right) - k_v \dot{p}_s, \tag{4.19b}$$

where $f_e^{T_s}$ is the environment force *measured* by the slave force sensors with a time delay of T_s (from the slave to the master), $p_m^{T_m}$ is the master position with a time delay of T_m (from master to slave) and k_p, k_s are positive constants. Here a P-F architecture was selected, which is a simpler force reflecting scheme than the V/F-F developed in the previous chapter.

The operator behavior is modeled be means of a controller set to move the master towards a virtual wall, pushing the virtual wall at a distance p_m^d (at the master side),

given by

$$f_h = -k_h \left(p_m - p_m^d \right) - b_h \dot{p}_m, \qquad (4.20)$$

where k_h, b_h are the proportional and derivative gains.

The environment force appears when a wall located at a distance p_{sw} (at the slave side) is pushed by the slave, is given by

$$f_e = -k_e p_u - b_e |p_u| \dot{p}_u, \qquad p_u = \begin{cases} 0, & \text{if } p_s < p_{sw} \\ p_s - p_{sw}, & \text{otherwise.} \end{cases} \qquad (4.21)$$

Notice that it is considered that the actual wall presents elastic deformation, meaning that the slave end-effector can cause an elastic deformation by pushing the wall.

Schematic of the Simulation

A schematic of the simulation is presented in Fig. 4.7. There the master and slave end-effectors are represented by a circle with letters M and S, respectively. Both move in horizontal directions towards a virtual and actual wall, respectively.

(a) Master gets in contact with the wall.

(b) Master losses contact with the virtual wall.

(c) Slave losses contact with the actual wall.

(d) Control objective achieved.
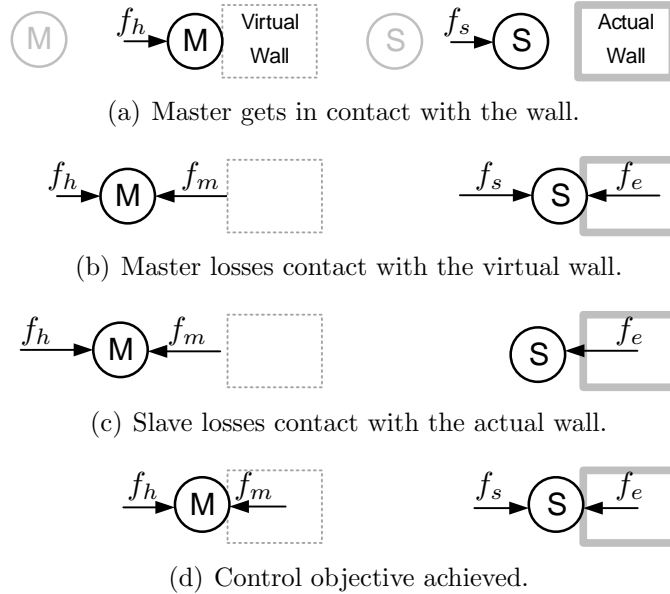
Figure 4.7: Schematic of the simulation.

Figure 4.7(a) illustrates the beginning of the simulation when the master gets in contact with the virtual wall. Initially the master and slave are separated the same distance from their respective walls. Due to the time-delay the slave controller, which always tries to match the master position, receives the signal to dislocate with a delay.

Figure 4.7(b) shows when the master receives the reflected force from the slave and recoils from the virtual wall. At that moment the slave is still exerting force on the actual wall because it has not receive the dislocation command due to the time-delay. Instants later (Fig. 4.7(c)), the slave controller receives the signal of the recoiled master and also recoils from the actual wall, losing contact with it.

Figure 4.7(d) shows the system when the control objective is achieved, this happens when the operator exerts a constant force on the master, which reflects to the operator the force measured by the slave, which is exerting a constant force on the wall.

Simulation Results

For the simulations it is considered that the operator objective is to penetrate the *virtual wall* (located at p_{ws}). The parameters of the teleoperated system are given in Table 4.1.

Table 4.1: Parameters of the teleoperated system

Manipulators		Controllers	
$m_t = 1$	$b_t = 1$	$k_p = 1$	$k_v = 10$
Operator		Environment	
$k_h = 5$	$b_h = 1$	$k_e = 25$	$b_e = 10$
$p_m^d = 0.20$		$p_{ws} = 0.15$	
Energy Tanks			
$\beta_m = 0.01$	$\beta_s = 0.02$	$f_{lm} = 5$	$f_{ls} = 5$
$\alpha = 50$		$H_d = 0.1$	

Notice that the desired position of the master p_m^d is located $0.05m$ inside the *virtual wall* (located at p_{ws}). This is to make the operator exert a constant force towards the *actual wall*.

For this simulations have been considered 4 cases, in all cases the operator is set to try to take the master to the position p_m^d, given that the *actual wall* at the slave side is located at p_{ws} the master will feel the reaction force from the environment, transmitted through the communication channel and reflected to the operator by the master. The simulation time of all cases is $20s$ with variable time step.

Case 1: Showed in Fig. 4.8, where the teleoperator presents no time delays and the passivation provided by the energy tanks is active. It can be seen that the operator gets constantly repealed without achieving a force equilibrium during the simulation time.

Case 2: Showed in Fig. 4.9, where the teleoperator presents no time delays and the passivation provided by the energy tanks is active. The saturated controlled forces are represented by f_m^*, f_s^* in the master and slave side, respectively. It can

be see that the saturated force in the master side acts at the very beginning of the simulation to replenish the master energy tank by injecting damping to he system It can be seen that the damping action of the passivation stabilizes the system.

Note that neither the operator reach its desired position ($p_m^d = 0.20$), nor the wall repeals totally the slave, both reach a force equilibrium of $|f_h| = |f_s|$, the master at $p_m = 0.166m$ and the slave at $p_s = 0.157m$. Albeit a higher proportional gain could result in a higher penetration from the master.

Case 3: Showed in Fig. 4.10, where the teleoperator presents no time delays and the passivation provided by the energy tanks is active.

It can be seen that the presence of time delays lead to higher oscilations in the system, as expected.

Case 4: Showed in Fig. 4.11, where the teleoperator presents no time delays and the passivation provided by the energy tanks is active.

Again, the passivation attenuates the oscillation even in the presence of time delays and stabilizes the system.
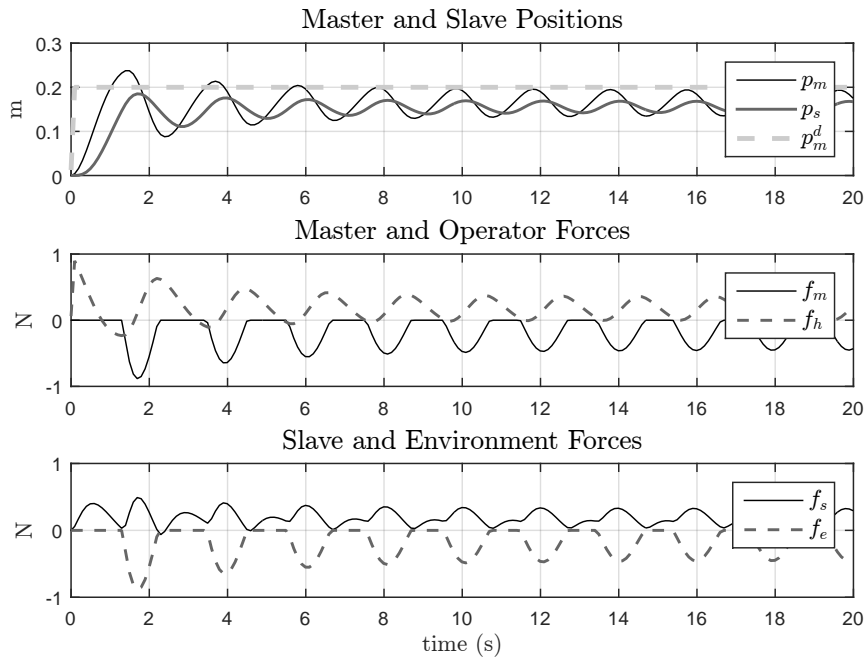

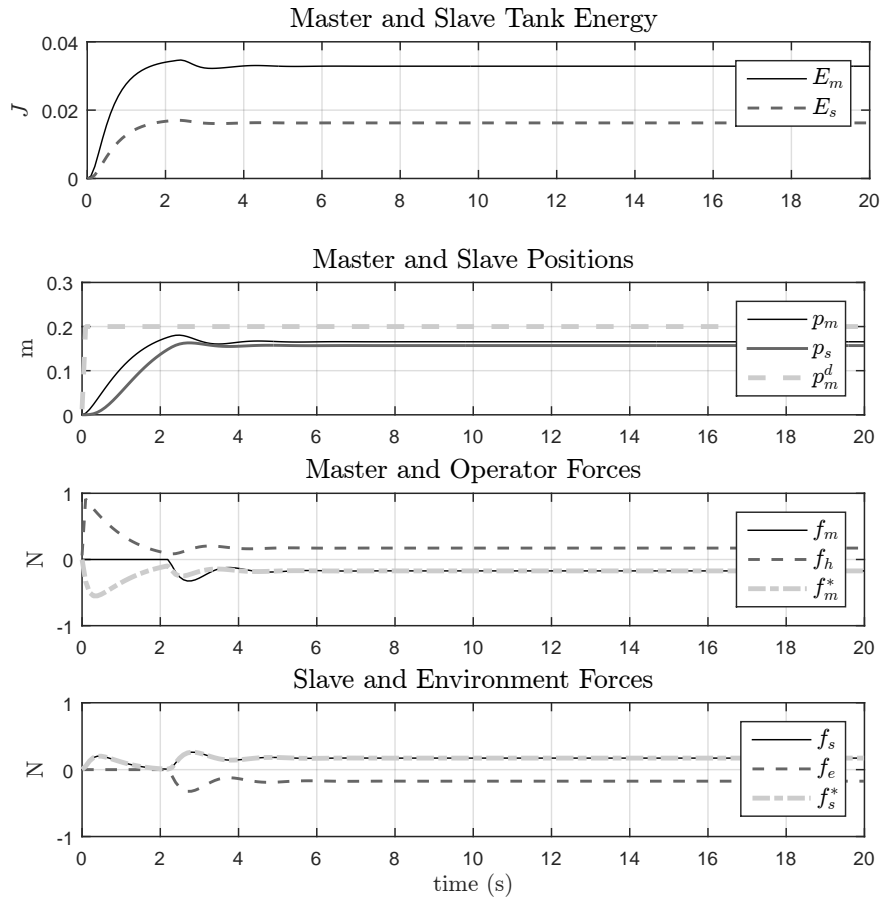Figure 4.8: Case 1, no time delays and inactive passivation, position and force errors.

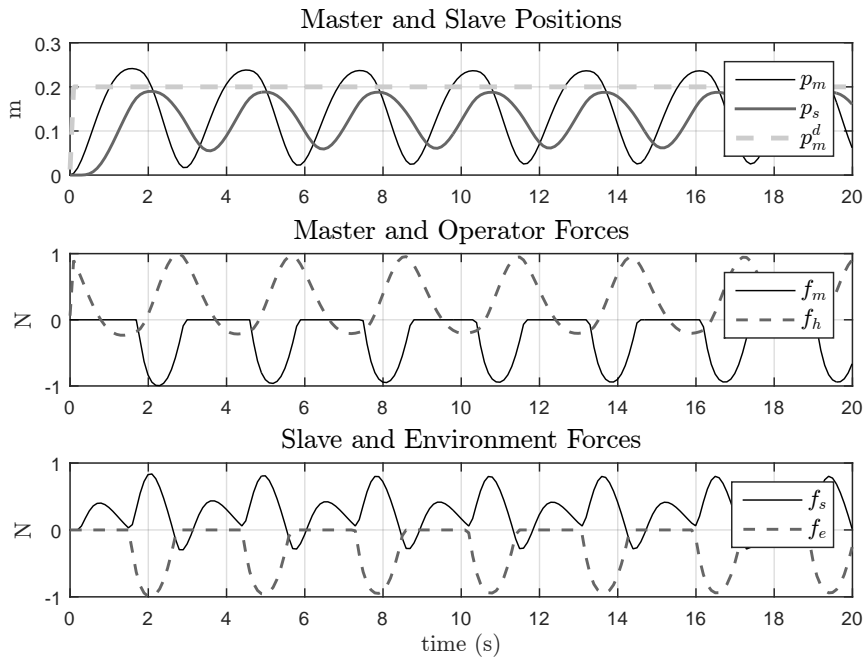Figure 4.9: Case 2, no time delays and active passivation.

Figure 4.10: Case 3, time delays of $0.2s$ and inactive passivation.
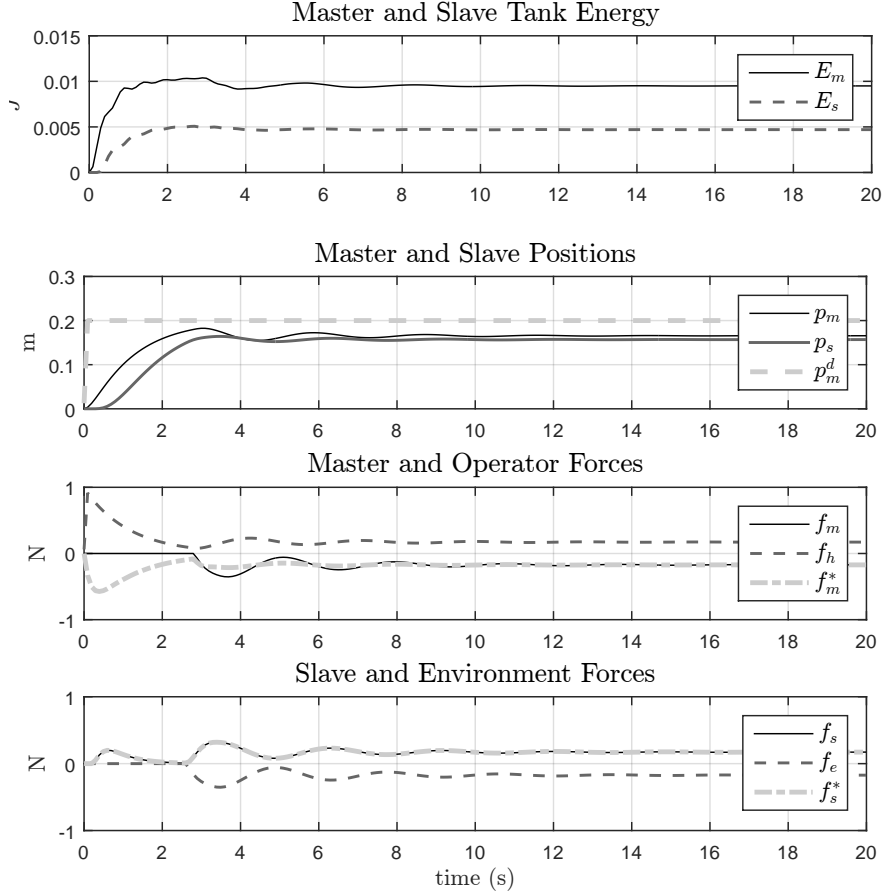
69

Figure 4.11: Case 4, time delays of $0.2s$ and active passivation.

4.1.4 Teleoperated Control of Cooperative Manipulator

In this section, the stability and performance of the proposed controller are illustrated by means of a numerical simulation. The control architecture is simulated considering a master a two slave three joints robots implemented in Simulink modeled according to Aldana et al. (2012).

The master follows a planar velocity trajectory given by $\dot{p}_o^d = \frac{0.1\pi}{16}\left[-\sin\frac{\pi t}{16}, \cos\frac{\pi t}{16}\right]$ while exerting a variable force (which is a function of the penetration in the virtual plane), here the operator actions is modeled with a PI controller.

In the slave side, the two slaves grasp an object with an stiffness of $500N/m$. Some noise is considered in the force measurement to better reflect actual values given by a force sensor. It is considered that he communication channel introduce time-delay of $50ms$ from master to slave and from slave to master. Table 4.2 shows the values of the constants used in the simulation.

The velocity,position and force errors are presented in Fig. 4.12, where it can be seen that the velocity error $\dot{p}_o$ and the force error $\tilde{f}$ tend to zero while the position error $\tilde{p}_o$ maintains its offset as expected because the velocities and forces

70

Table 4.2: Parameter values for the Simulation

Parameters	Symbol	Value
Kinematic control gain matrix	K_v	0.01
Cut-off frequency	λ_k	1
Dynamic control gain matrix	K_d	20
Dynamic adaptation gain	Λ_d	100
Kinematic adaptation gain	Λ_k	100
Transfer protocol constant	β	0.01
Level controller rate constant	α	20
Desired tank level	H_d	2

are controlled and not the position.
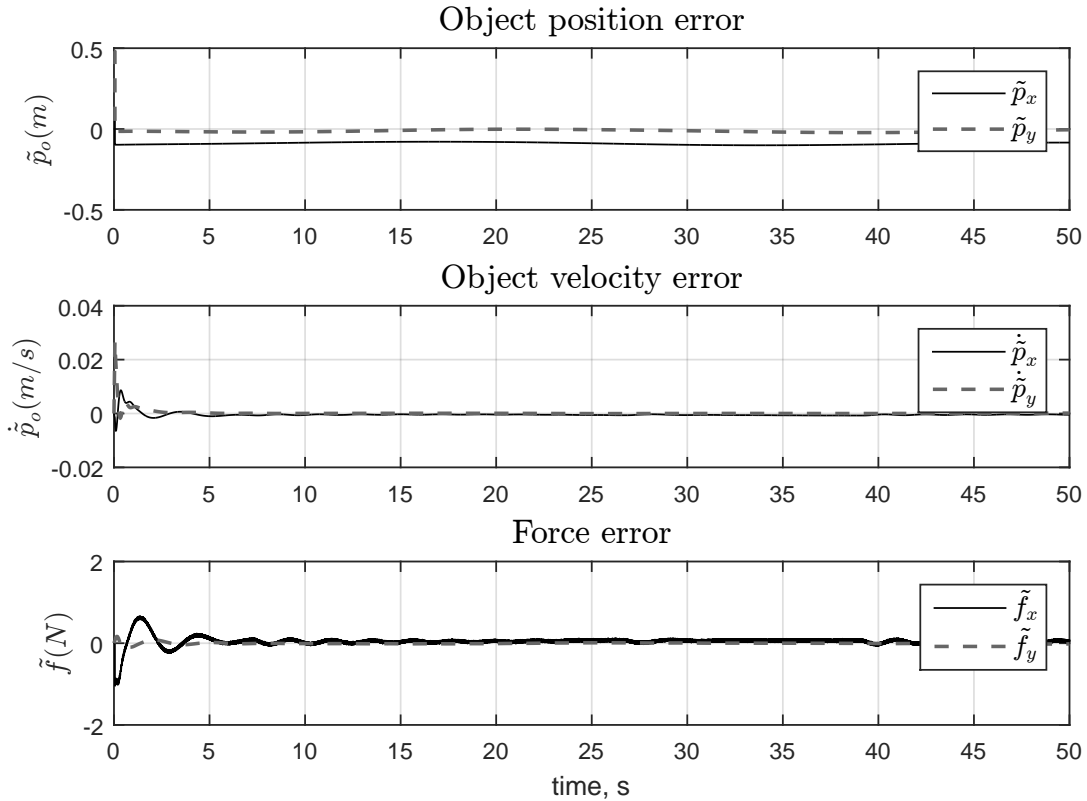
Figure 4.12: Position, velocity and force errors.

The tracking and adaptation errors are presented in Fig. 4.13. It is considered that the initial values of the kinematic and dynamic parameters are 10% higher than the actual values. Also, in the beginning of the simulation is considered that the master energy tank has $5J$, this is to avoid having to move the master to replenish its energy tank.
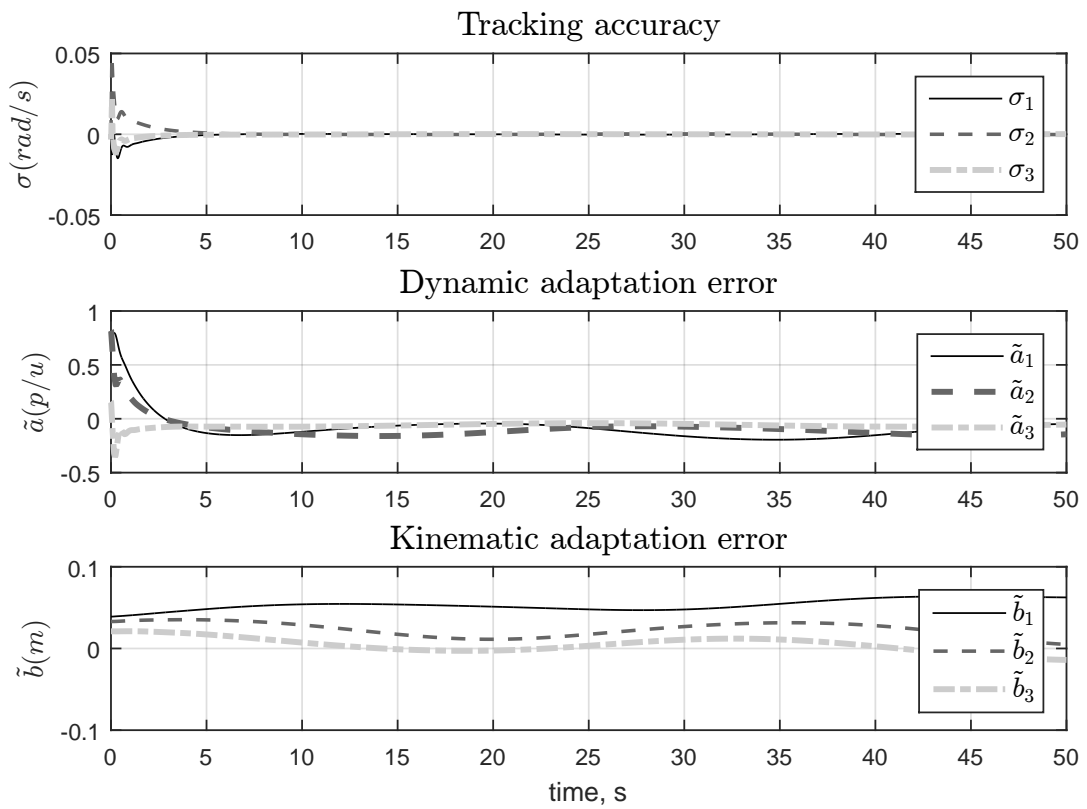
Figure 4.13: Tracking and adaptation errors.

4.2 Experiments

4.2.1 Cooperative Control: Object Manipulation - 3D

This experiment has the objective of manipulate an object held by a bimanual robotic manipulator considering the *cooperative task space* (Chiacchio et al. (1996)) formulation, which allows to describe the coordination task in terms of absolute and relative components.

It is considered that the control objective of the system is to follow the cooperative task space trajectory given by

$$p_a^d = p_a^o + d\sin\left(\frac{\pi t}{8}\right)\vec{m}, \tag{4.22a}$$

$$p_r^d = R_R L_c \vec{z}, \tag{4.22b}$$

$$R_a^d = R\left(\vec{r}, \phi^d\right) R_a^o, \tag{4.22c}$$

$$R_r^d = R_r^o, \tag{4.22d}$$

$$\phi^d = \frac{\pi}{8}\sin\left(\frac{\pi t}{8}\right) \tag{4.22e}$$

where $p_a^o = \begin{bmatrix} 0 & 0 & 1.8 \end{bmatrix}^\mathsf{T}$ is the initial position, $R_a^o \in \mathbb{R}^{3\times3}$ is the initial orientation, $R_1 \in \mathbb{R}^{3\times3}$ is the rotation matrix that represents the orientation of the first end-effector, $d = 0.1m$ is the half of the length of the desired linear trajectory of the absolute position and $L_c = 0.3m$ is the desired distance between end-effectors. $\vec{m}$ and $\vec{r}$ are vector that define the direction of linear movement and orientation of the desired rotation.

In turn, the desired velocities are given by

$$\dot{p}_a^d = d\frac{\pi}{8}\cos\left(\frac{\pi t}{8}\right), \tag{4.23}$$

$$\dot{p}_r^d = S\left(\vec{r}\dot{\phi}\right) R_a p_r^d, \tag{4.24}$$

$$\omega_a^d = \vec{r}\dot{\phi}^d, \tag{4.25}$$

$$\omega_r^d = \begin{bmatrix} 0 & 0 & 0 \end{bmatrix}^\mathsf{T}, \tag{4.26}$$

$$\dot{\phi}^d = \frac{\pi}{8}\cos\left(\frac{\pi t}{8}\right). \tag{4.27}$$

In order to have a soft control at the beginning of the experiment (have a desired velocity of zero), the initial position of the trajectories correspond to one of the extreme points of the line that the object has to swing around, where the desired velocities are zero. This is accomplished by setting the frequency of the trajectory equal to the frequency of the rotation, for all cases to the same value. Here that

73

frequency is set to $\frac{\pi}{8}$ such that the trajectories begin at $t = 4s$. This frequency allows to perform the experiment maintaining low joint velocities lower that $0.2\frac{rad}{s}$.

The reference individual trajectories and velocities of the end-effectors can be computed using (1.15a). For the control of the manipulators a gradient control law was considered, given by

$$v_1 = \begin{bmatrix} \dot{p}_1^d \\ \omega_1^d \end{bmatrix} - \begin{bmatrix} K_p \tilde{p}_1 \\ K_o \tilde{o}_1 \end{bmatrix}, \qquad v_2 = \begin{bmatrix} \dot{p}_2^d \\ \omega_2^d \end{bmatrix} - \begin{bmatrix} K_p \tilde{p}_2 \\ K_o \tilde{o}_2 \end{bmatrix}, \tag{4.28}$$

where K_p, K_o are the position and orientation gains, $\tilde{p}_1, \tilde{p}_2$ are the position errors, $\tilde{o}_1, \tilde{o}_2$ are the orientation errors given by the vectorial part of the quaternion of $R_1 R_1^{d\mathsf{T}}$ and $R_2 R_2^{d\mathsf{T}}$. Then, the control signal is given by

$$\dot{q} = J_M^{-1} \begin{bmatrix} v_1 \\ v_2 \end{bmatrix} \tag{4.29}$$

where J_M is the Jacobian of the two arm robotic manipulator with a torso, given in (D.3b).

A way to simplify the desired orientations is to multiply the values of the desired end-effectors orientations such that the resultant orientations are equal. By doing this the absolute orientation is given by the initial premultiplied orientation and the relative orientation is given by the identity matrix.

By example, consider the end-effectors described in Fig. 4.14, there the rotations can be described by the matrices $R_1 = \begin{bmatrix} \vec{z} & \vec{x} & \vec{y} \end{bmatrix}$ and $R_2 = \begin{bmatrix} \vec{z} & -\vec{x} & -\vec{y} \end{bmatrix}$. They can be multiplied by $R(\vec{x}, \frac{\pi}{2})$ and $R(\vec{x}, -\frac{\pi}{2})$ respectively such that the absolute orientation R_a is given by

$$R_a = R_1 R\left(\vec{x}, \frac{\pi}{2}\right) = R_2 R\left(\vec{x}, -\frac{\pi}{2}\right) = \begin{bmatrix} \vec{z} & \vec{x} & -\vec{y} \end{bmatrix}$$

and the relative orientation R_r is given by the identity matrix.
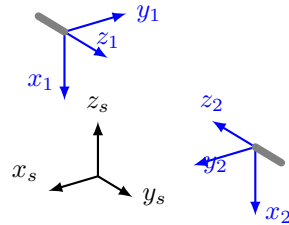
Figure 4.14: End-effectors facing each other.

In this experiment it was consider three cases, first, movement in the Y-Z axis and rotation in the Z-axis, second, movement in the X-Y axis and rotation in the X-axis, and finally, movement in the X-Y axis and rotation in the Y-axis. In all

cases the trajectories are follow for $40s$ with control gains given by $K_p = 10$ and $K_o = 10$.

The results are presented in Fig. 4.15 and Fig. 4.16 for the first case, in Fig. 4.17 and Fig. 4.18 for the second case and in Fig. 4.19 and Fig. 4.20 for the third case.
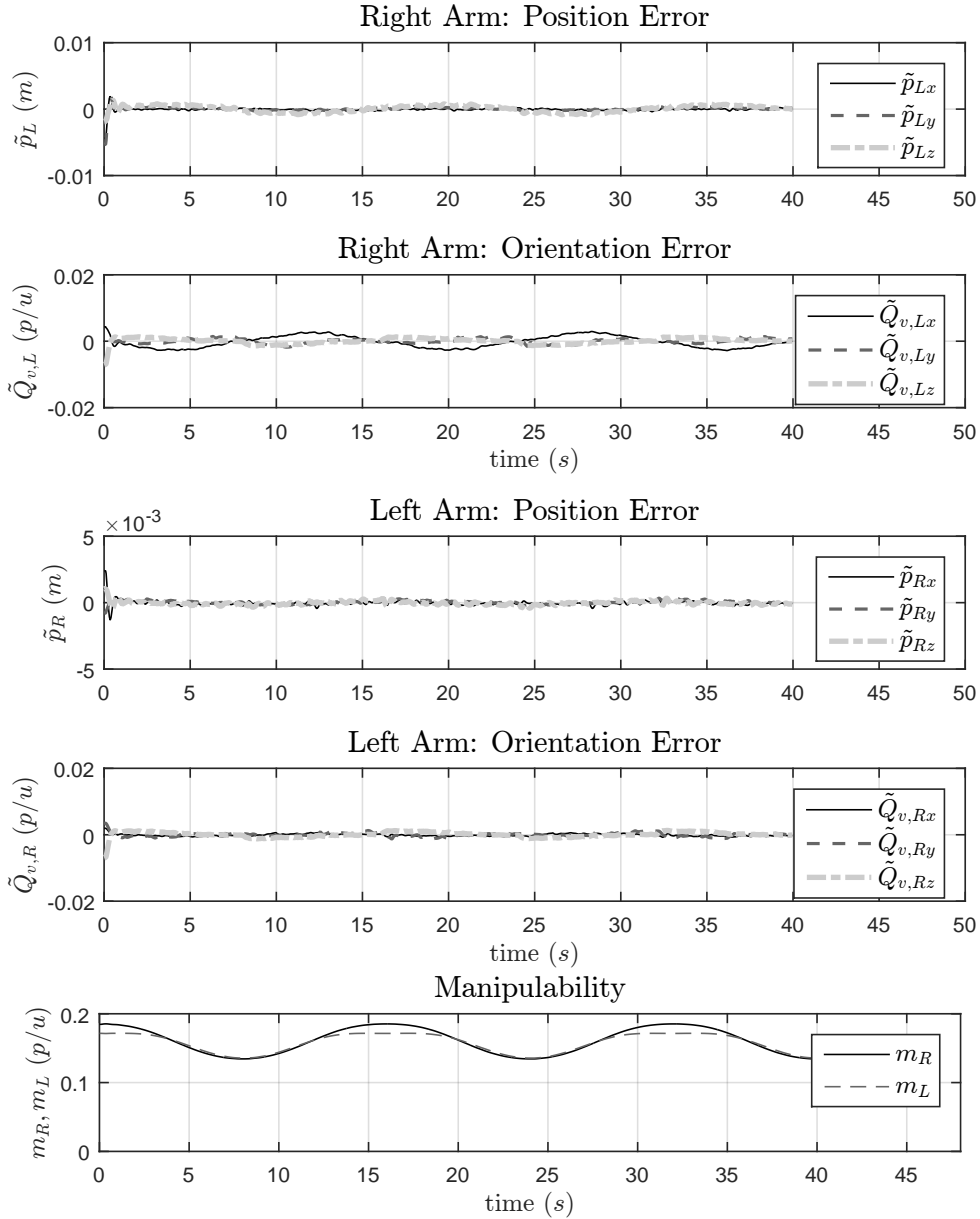
Figure 4.15: Case 1, Position and Orientation Errors and Manipulability.

In the three cases the object is made to follow a linear trajectory while rotating around an axis. The object is essentially swinging positions from one point to the other of a line of $0.2m$ of length.

The position and orientation tracking results (Fig. 4.15, 4.17, 4.19) show acceptable errors. This is considering that the position errors are small enough to

Figure 4.16: Case 1, Velocities and Positions of the Joints.
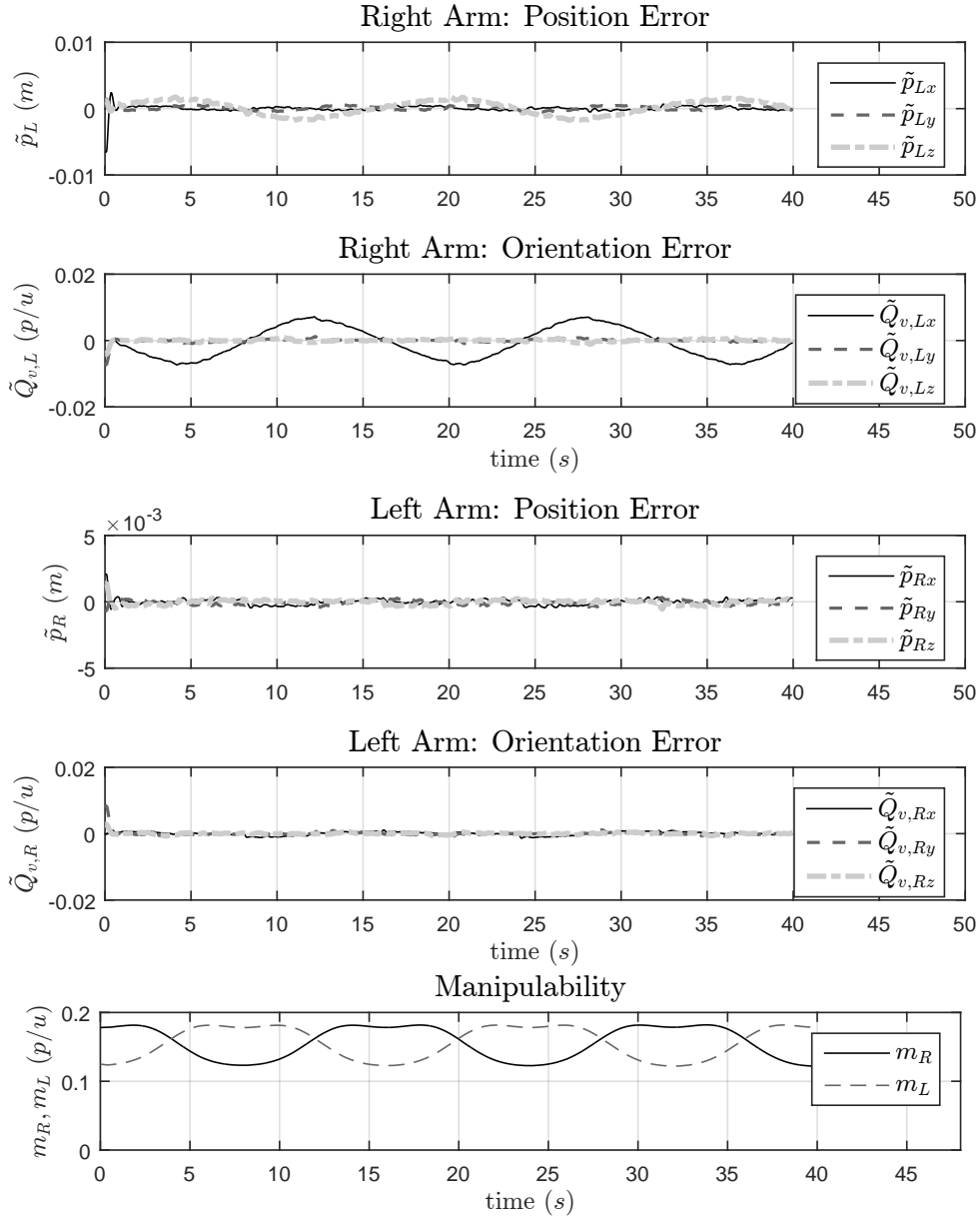
Figure 4.17: Case 2, Position and Orientation Errors and Manipulability.

avoid losing contact with the object. Also, the manipulability was maintained in values between 0.1-0.2, showing that the trajectories keep the end-effectors away from singular positions.

The joint velocities and positions (Fig. 4.16, 4.18, 4.20) results show that in all cases the joint velocities are kept at values lower than $0.2\frac{rad}{s}$.

Despite the fact that the initial velocities of the joints are set to be zero, there is a very small overshoot at the beginning of the experiments.
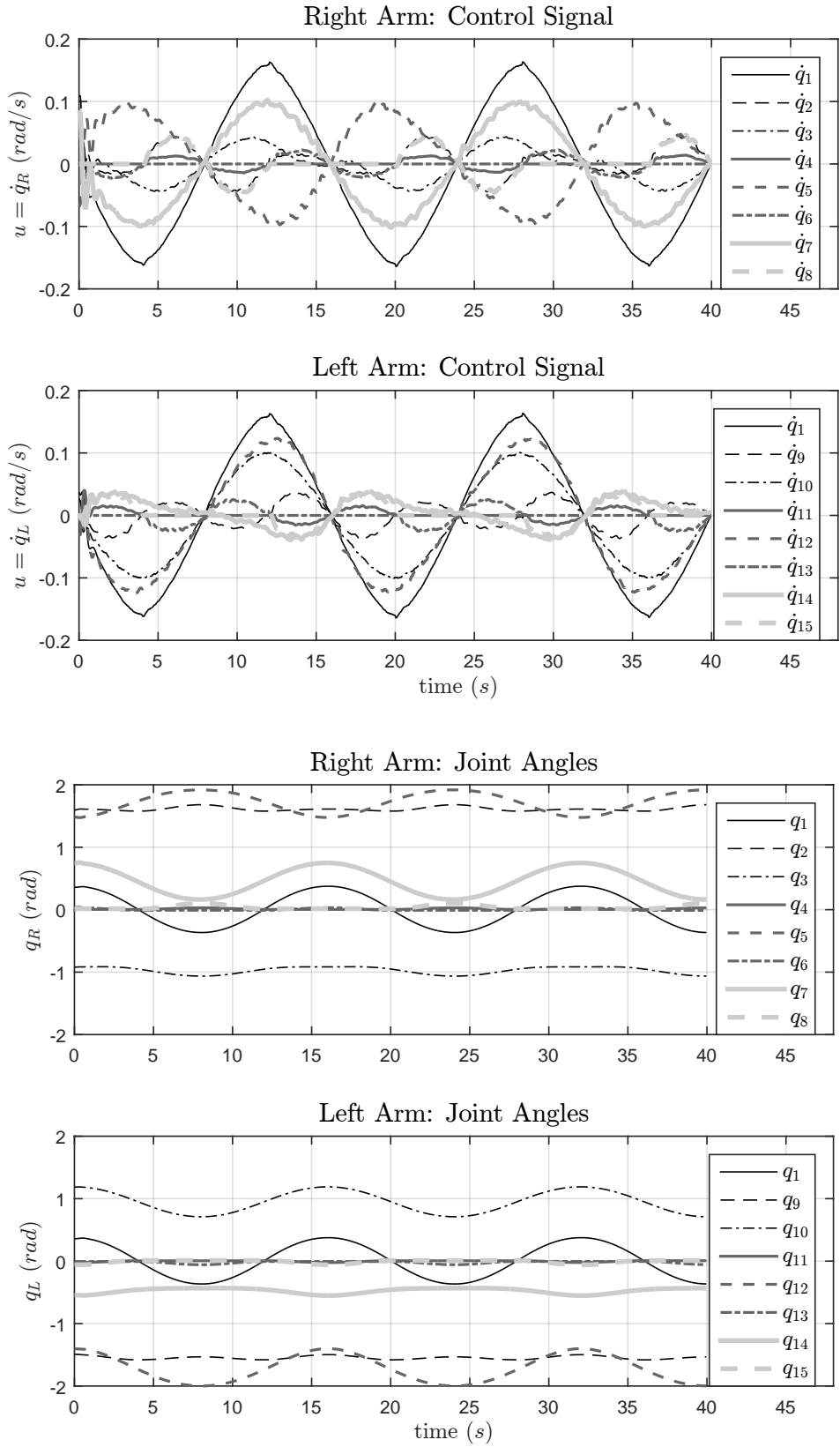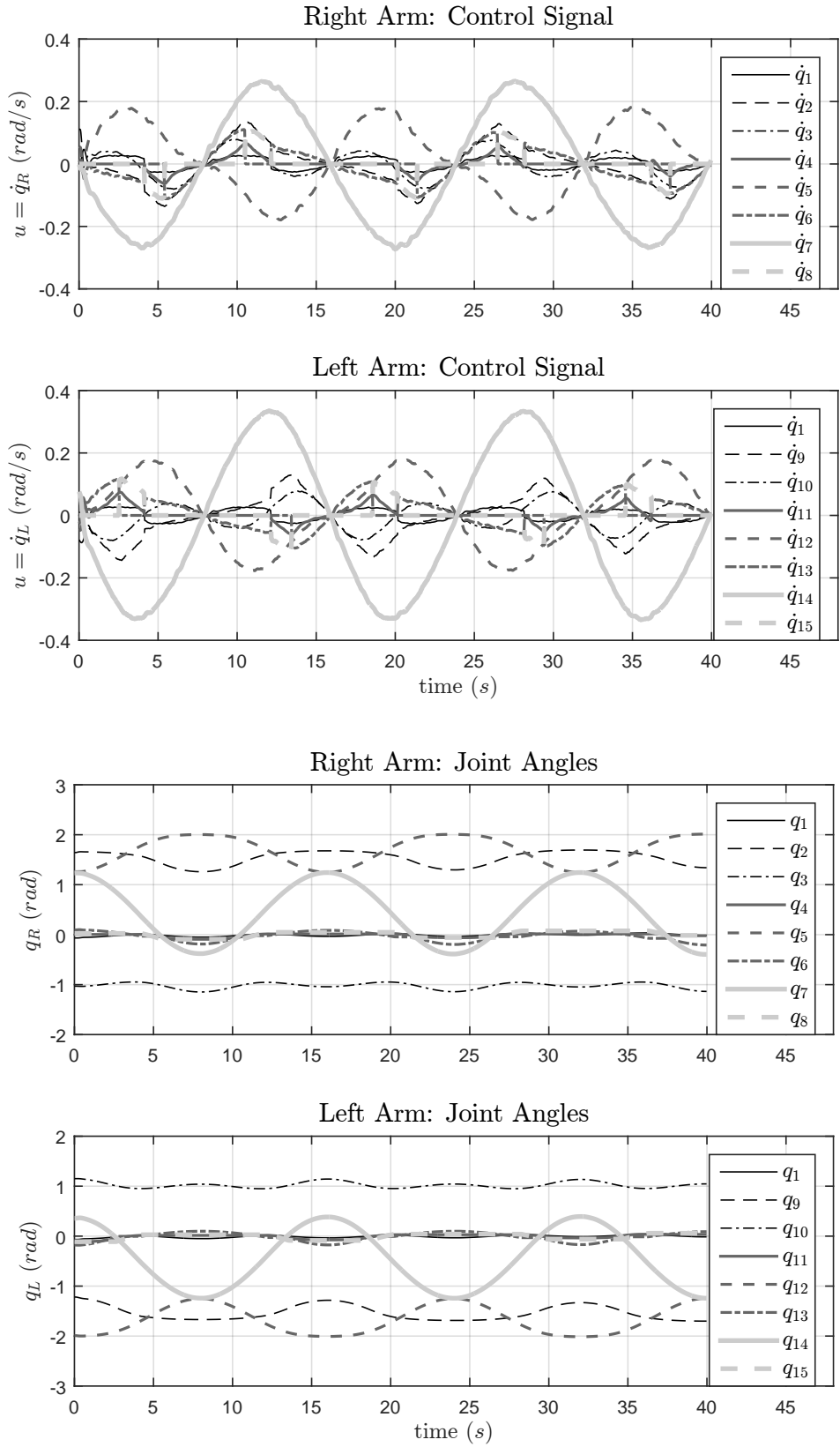
Figure 4.18: Case 2, Velocities and Positions of the Joints.
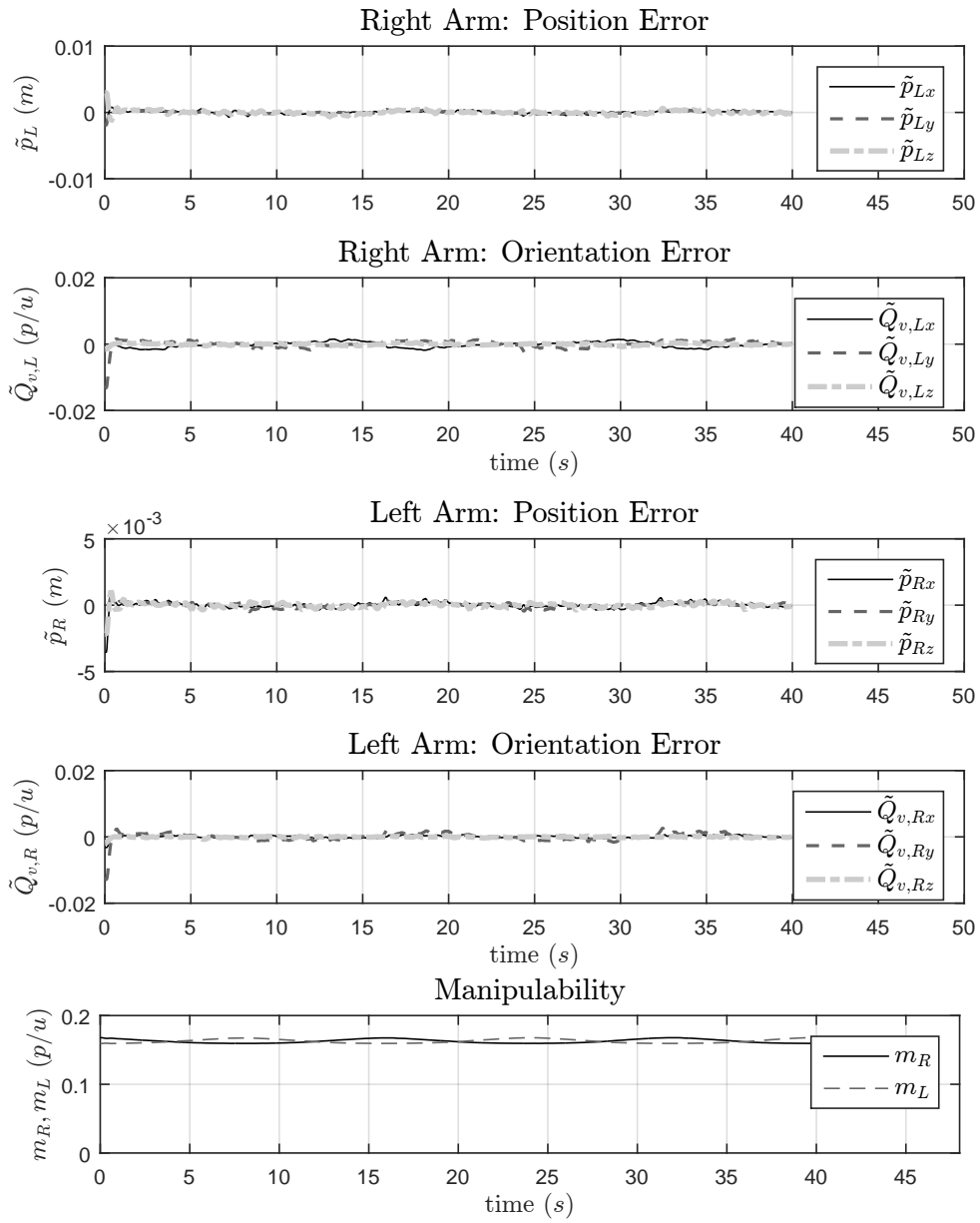
Figure 4.19: Case 3, Position and Orientation Errors and Manipulability.
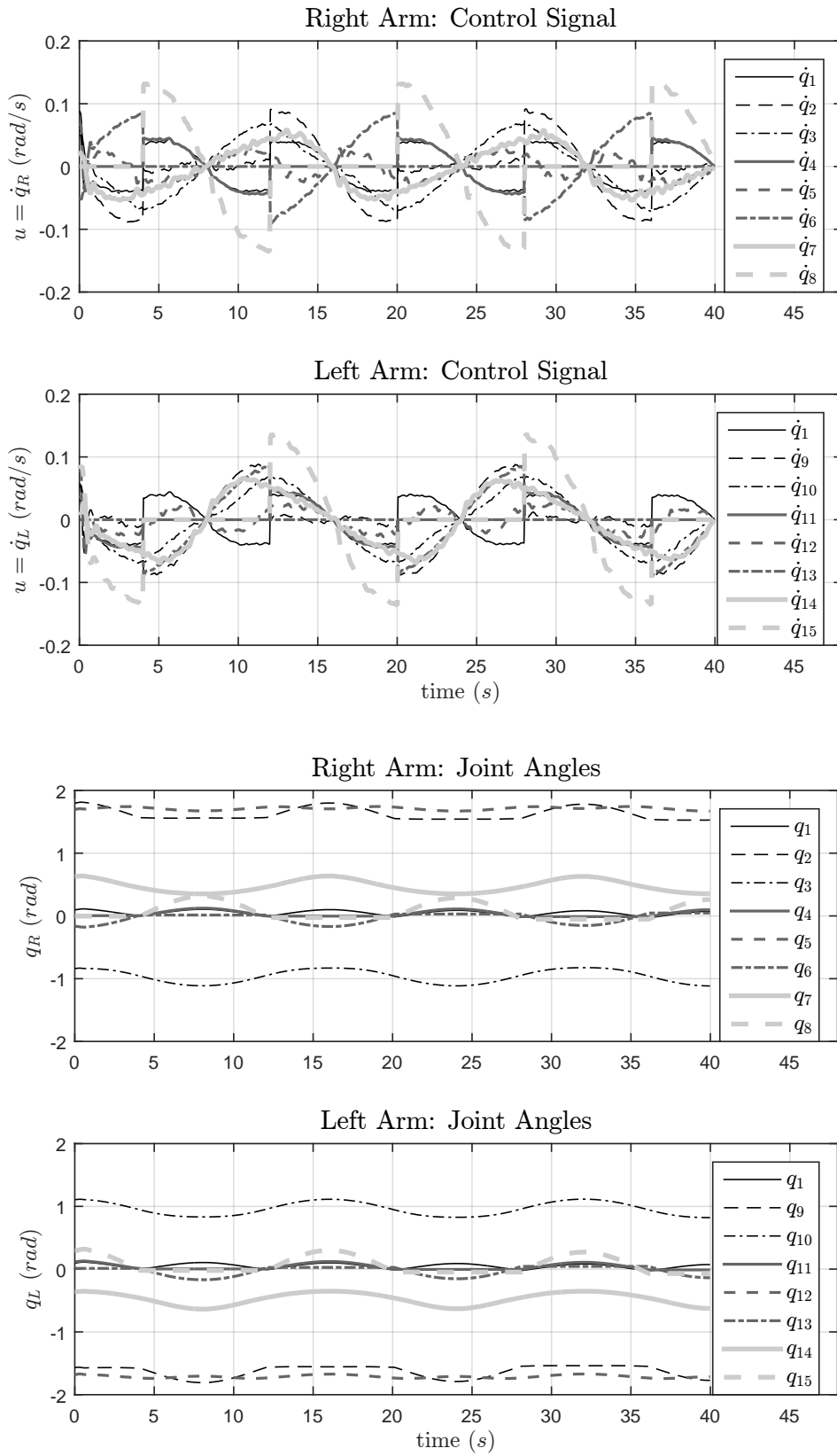
Figure 4.20: Case 3, Velocities and Positions of the Joints.

4.2.2 Cooperative Force Control

In this experiment the formation based control scheme developed is implemented in a two planar arm robotic manipulator. It is considered that the robotic manipulator is receiving velocity and force signals. Force control is applied in the X-axis, while the desired position in the Y-axis is integrated from the desired velocity signals. The orientations are kept at constant values.

The control objective is to track a circular trajectory of $0.1m$ of radius around the point $p_o = 0 \quad 0.5$.

The force was obtained as a function of the end-effector positions in order to represent the effect of force sensors. Consider that the end-effectors are holding an object of length L and that the end-effectors are located in the positions $p_R, p_L \in \mathbb{R}^2$ for the right and left arm, respectively. Then, the deformation δ suffered by the object by the end-effector forces in the X-axis can be represented by

$$\delta = \|p_{c,x} - p_{R,x}\| - \frac{L}{2}, \qquad p_{c,x} = \frac{p_{R,x} + p_{L,x}}{2}, \tag{4.30}$$

The orientation of the end-effectors was kept constant at $\phi_R = 0$ and $\phi_L = pi$, in order to maintain the end-effectors facing each other.

Then, the control laws $\dot{q}_R, \dot{q}_L$ are given by

$$v_R = \begin{bmatrix} p_{R,x}^d \\ p_{R,y}^d \\ \phi_R^d \end{bmatrix} + \begin{bmatrix} K_F \tilde{f}_{R,x} \\ K_p \tilde{p}_{R,y} \\ K_o \tilde{\phi}_R \end{bmatrix}, \qquad v_L = \begin{bmatrix} p_{L,x}^d \\ p_{L,y}^d \\ \phi_L^d \end{bmatrix} + \begin{bmatrix} K_F \tilde{f}_{L,x} \\ K_p \tilde{p}_{L,y} \\ K_o \tilde{\phi}_L \end{bmatrix}, \qquad \begin{matrix} \dot{q}_R = J_R^{-1} v_R, \\ \dot{q}_L = J_L^{-1} v_L, \end{matrix}$$

$$\tag{4.31}$$

where $q_R, q_L \in \mathbb{R}^3$ represent the joint of the right and left robotic manipulators.

The position of the end-effectors is given by

$$p_i = \begin{bmatrix} b_1 c_1 + b_2 c_{12} + b_3 c_{123} \\ b_1 s_1 + b_2 s_{12} + b_3 s_{123} \end{bmatrix} + B_i \tag{4.32}$$

where $B_i \in \mathbb{R}^2$ is the base of the planar manipulator, and the position Jacobian of the robotic planar manipulators is given by

$$J_p = \begin{bmatrix} -b_1 s_1 - b_2 s_{12} - b_3 s_{123} & -b_2 s_{12} - b_3 s_{123} & -b_3 s_{123} \\ b_1 c_1 + b_2 c_{12} + b_3 c_{123} & b_2 c_{12} + b_3 c_{123} & b_3 c_{123} \end{bmatrix}, \tag{4.33}$$

where $s_n = sin(q_n)$, $c_n = cos(q_n)$, $s_{12} = sin(q_1 + q_2)$, $c_{12} = cos(q_1 + q_2)$, $s_{123} = sin(q_1 + q_2 + q_3)$, $c_{12} = cos(q_1 + q_2 + q_3)$, and $b_1 = 0.39m, b_2 = 0.33m, b_3 = 0.21m$ represent the length of the link of the robotic arms.

Considering uncertain kinematic parameters, equation (3.8) can be used to obtain the forward kinematics regressor matrix Z_i, given by

$$Z_i = \begin{bmatrix} c_1 & c_{12} & c_{123} \\ s_1 & s_{12} & s_{123} \end{bmatrix} \tag{4.34}$$

likewise, equation (3.9) can be used to find differential kinematic regressor matrix W_i, given by

$$W_i = \begin{bmatrix} -s_1\dot{q}_1 & -s_{12}\dot{q}_{1+2} & -s_{123}\dot{q}_{1+2+3} \\ c_1\dot{q}_1 & c_{12}\dot{q}_{1+2} & c_{123}\dot{q}_{1+2+3} \end{bmatrix}, \quad b = \begin{bmatrix} b_1 \\ b_2 \\ b_3 \end{bmatrix}, \tag{4.35}$$

where $\dot{q}_{1+2} = \dot{q}_1 + \dot{q}_2$ and $\dot{q}_{1+2+3} = \dot{q}_1 + \dot{q}_2 + \dot{q}_3$.

The selected time duration of the experiment is $50s$ and the results of the experiment are presented in Fig. 4.21, Fig. 4.22 and Fig. 4.23.
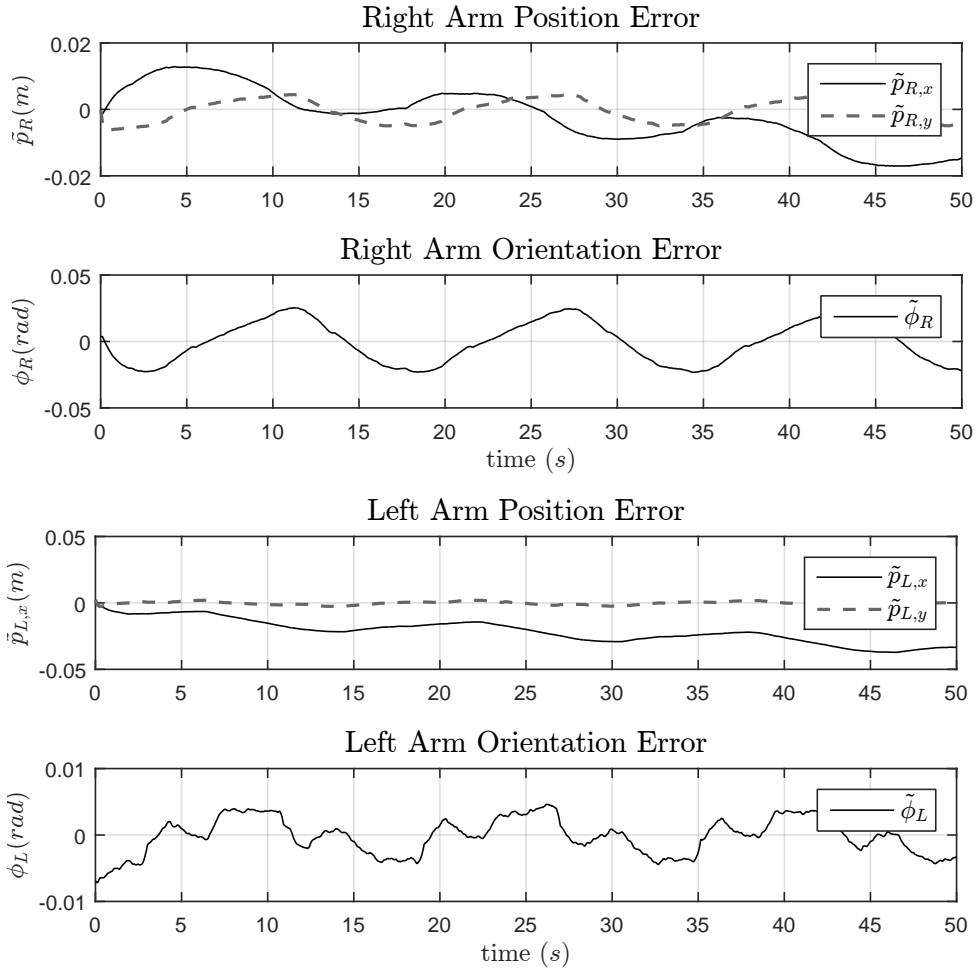
Figure 4.21: Position and Orientation Errors.

Figure 4.21 shows the position and orientation errors of the right and left end-

effectors. For the right arm both errors oscillate around $\pm 0.02m$, the error in the Y-axis present a periodic oscillation, while the error in X-axis shows a descending trajectory due to the fact that the desired force is exerting an elastic deformation in the object. Similar behavior is presented in the left arm but with higher position error and lower orientation error.
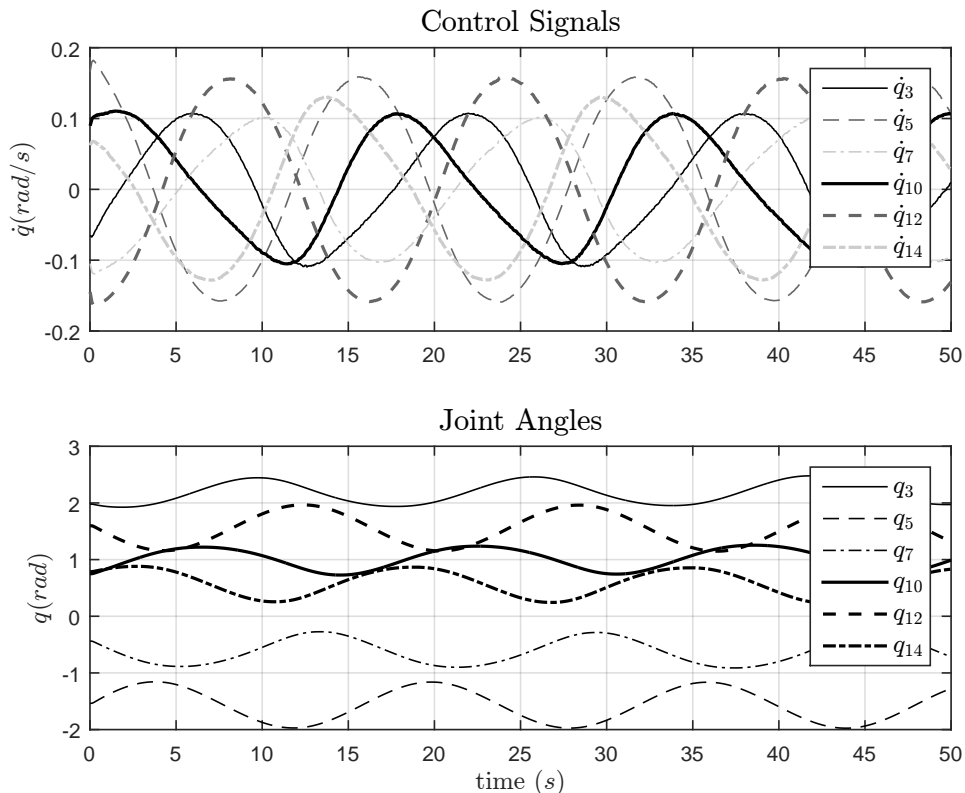
Figure 4.22: Velocities and Positions of the Joints.

Figure 4.22 shows joint velocities and positions. It can be seen that the joints describe periodical trajectories of less than $0.2\frac{rad}{s}$ of velocity, that correspond to the circular trajectory followed by the end-effectors.

Figure 4.23 shows the force errors, initially the error is high because in the initial position the end-effectors are grasping the object with a lesser force than the force desired. Then the system achieves the desired force in a time of $5s$ with errors of around $1N$ during the movement. Also, the manipulability of the end-effectors is kept around ± 0.12, which shows that the end-effectors are away from singularities.
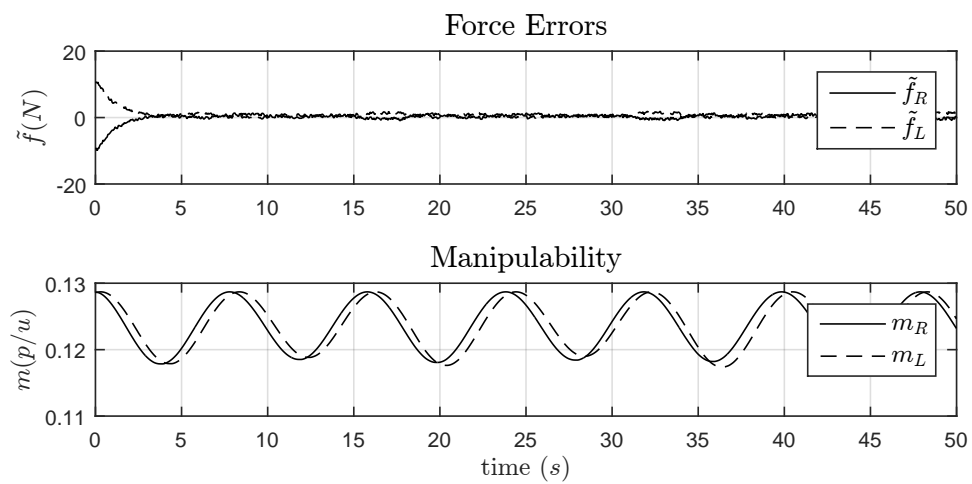
Figure 4.23: Force Error and Manipulability.

Chapter 5

Conclusions and Future Works

This work presents a Force/Velocity-Force (V/F-F) bilateral telemanipulation scheme for multiple robots grasping a deformable object.

A bilateral telemanipulation framework that enforces passivity based on a variation of the Time Domain Passivity Control (TDPC) approach is revised. This strategy use the concept of Energy Tanks to store energy in order to ration out damping to keep the overall system passivity. It consists of a two layer framework, where the top layer, called Transparency Layer (TL), enforces transparency of the teleoperation while the lower layer, called Passivity Layer (PL), enforces passivity of the system.

The Passivity Layer monitors the energy in the whole teleoperated system and in case of loss of passivity saturates the commands from the Transparency Layer to maintain passivity in the interaction with the system.

Two saturation functions are presented, one that gradually reduces the control signal received from the Transparency Layer when the system is losing passivity until, in the worst case scenario, the control signal is totally cancelled. The second saturation function considers a torque limit selected by the operator, which could be tuned to avoid excessive forces or velocities exerted by the slaves.

The proposed scheme considers the gradual injection of damping as a function of the energy of the system in order keep passivity while maintaining transparency. This is important because it prevents the excessive injection of damping that leads to sluggishness in the system. In the critical case when passivity is lost the saturated control signal turns to the gravity vector instead of zero torque, such that the robotic manipulators do not apply forces but try to keep their configurations.

Since the proposed scheme controls velocity with a grasping force error instead of position error could be considered as an advantage for the load transportation task in the case of packet loss in the communication channel. For position regulation, the loss of packets could lead to high position errors and in turn to high torque control signals. This could make the end-effectors lose contact with the object or to exert

excessive force damaging it.

With force regulation, a possible scenario could be a sudden change of direction of the object movement. In turn total loss of communication could lead to a sudden halt of movement and a gentle release of the object due to the fact that the default *zero* signal (the saturated signal provided by the passivity layer at the slave side) into the cooperative controller is the gravity compensation, which tries to keep the end-effectors positions but do not exert forces into the object.

The proposed cooperative control scheme for load transportation achieves convergence to the desired velocity and allows the operator to regulate the exerted desired grasping force in the held object and *feel* a haptic response in the form of the reaction force sensed by the slaves sensors and fed back to him through the communication channel.

First an operational space controller is proposed considering the formation-based control approach, where the force closure is implemented on a kinematic level on the slave side to guarantee a firm grasp of the object.

Then, by means of a cascade control strategy, the operational space controller is combined with an adaptive dynamical controller, ensuring the overall stability of the interconnected systems thanks to the inherent passivity properties of the cooperative robotic system. The fact that the operational space controller uses a filtered force signal leads to lack of need of the measurement of the time-derivative of the force to achieve the cascade control.

Two decentralized controllers were proposed. For the operational space controller it is considered that the kinematic parameters are uncertain, then an adaptive gradient-type composite law is proposed to estimate the kinematic parameters. Likewise, for the dynamic controller it is considered an adaptive gradient-type composite law for the kinematic parameters and an adaptive dynamic law for the dynamic parameters. The passivity properties and stability of the proposed theorems were proved using positive definite storage functions.

5.1   Future Works

In what follows we present a discussion of possible future work derived from this Thesis:

1. The Passivity-layer has several parameters that influence the performance of the two-layer framework. Each parameter is related to a specific function and as such independent of other parameters. Although this simplifies tuning it is recommended to derive a systematic tuning scheme for the parameters of the TLC and the energy transfer protocol, and the desired level of the energy tank

(Franken (2015)).

2. Two saturation functions are presented in Chapter 2. No general design criteria have been provided. Specific saturation functions to handle problematic situations in realistic applications should be designed, implemented, and evaluated to investigate the added benefit of such saturation functions.

3. Extension of the proposed cooperative adaptive control scheme to consider time-varying desired forces. For this class of desired force, only ultimately bounded results can be guaranteed.

4. Extension of the proposed cooperative adaptive control to consider the object orientation control problem in the cooperative control scheme.

5. Development of a visual servoing strategy approach for object grasping and manipulating tasks.

Bibliography

Adams, R. J. and Hannaford, B. (1999). Stable haptic interaction with virtual environments. *IEEE Transactions on Robotics and Automation*, 15(3):465–474.

Adorno, B., Fraisse, P., and Druon, S. (2010). Dual Position Control Strategies Using the Cooperative Dual Task-Space Framework. In *Proceedings of the IEEE/RSJ International Conference on Intelligent Robots and Systems*, pages 3955–3960.

Adorno, B. V. (2012). Manipulacao Cooperativa Descentralizada Usando o Espaco Dual de Cooperacao. In *Congresso Brasileiro de Automática*, pages 1436–1443.

Aghili, F. (2013). Adaptive Control of Manipulators Forming Closed Kinematic Chain with Inaccurate Kinematic Model. *IEEE Transactions on Mechatronics*, 18(5):1544–1554.

Ahmad, M., Ismail, K., and Mat, F. (2016). Impact Models and Coefficient of Restitution: A Review. *ARPN Journal of Engineering and Applied Sciences*, 11:6549–6555.

Albakri, A., Liu, C., and Poignet, P. (2013). Stability and Performance Analysis of Three-Channel Teleoperation Control Architectures for Medical Applications. In *Proceedings of the IEEE/RSJ International Conference on Intelligent Robots and Systems*, pages 456–462.

Aldana, C., Nuno, E., and Basanez, L. (2012). Bilateral Teleoperation of Cooperative Manipulators. In *IEEE International Conference on Robotics and Automation*, pages 4274–4279.

Aldana, C. I., Nuno, E., and Basanez, L. (2013). Control of Bilateral Teleoperators in the Operational Space without Velocity Measurements. In *Proceedings of the IEEE/RSJ International Conference on Intelligent Robots and Systems*, pages 5445–5450.

Anderson, R. J. and Spong, M. W. (1988). Bilateral Control of Teleoperators with Time Delay. In *IEEE International Conference on Decision and Control*, pages 167–173.

Anderson, R. J. and Spong, M. W. (1989). Bilateral Control of Teleoperators with Time Delay. *IEEE Transactions on Automatic Control*, 34(5):494–501.

Aracil, R., Buss, M., Cobos, S., Ferre, M., Hirche, S., Kuschel, M., and Peer, A. (2007). The Human Role in Telerobotics. In Ferre, M., Buss, M., Aracil, R., Melchiorri, C., and Balaguer, C., editors, *Advances in Telerobotics*, pages 11–24. Springer-Verlag.

Artigas, J., Preusche, C., and Hirzinger, G. (2007). Time Domain Passivity for Delayed Haptic Telepresence with Energy Reference. In *Proceedings of the IEEE/RSJ International Conference on Intelligent Robots and Systems*, pages 1612–1617.

Aziminejad, A., Tavakoli, M., Patel, R. V., and Moallem, M. (2008). Transparent Time-Delayed Bilateral Teleoperation Using Wave Variables. *IEEE Transactions on Control Systems Technology*, 16(3):548–555.

Bai, H., Arcak, M., and Wen, J. T. (2011). *Cooperative Control Design - A Systematic, Passivity-Based Approach*. Springer, 1st edition.

Bai, H. and Wen, J. T. (2010). Cooperative Load Transport: A Formation-Control Perspective. *IEEE Transactions on Robotics*, 26(4):742–750.

Bais, A. Z., Erhart, S., Zaccarian, L., and Hirche, S. (2015). Dynamic Load Distribution in Cooperative Manipulation Tasks. In *Proceedings of the IEEE/RSJ International Conference on Intelligent Robots and Systems*, pages 2380–2385.

Biagiotti, L. and Melchiorri, C. (2007). Environment Estimation in Teleoperation Systems. In Ferre, M., Buss, M., Aracil, R., Melchiorri, C., and Balaguer, C., editors, *Advances in Telerobotics*, pages 211–231. Springer-Verlag.

Bonitz, R. and Hsia, T. (1996). Internal Force-Based Impedance Control for Cooperating Manipulators. *IEEE Transactions on Robotics and Automation*, 12(1):78–89.

Buzan, F. T. and Sheridan, T. B. (1989). A Model-Based Predictive Operator Aid for Telemanipulators with Time Delay. In *International Conference on Systems, Man and Cybernetics Conference Proceedings*, pages 138–143 vol.1.

Caccavale, F., Chiacchio, P., and Chiaverini, S. (1999). Stability Analysis of a Joint Space Control Law for a Two-Manipulator System. *IEEE Transactions on Automatic Control*, 44(1):85–88.

Caccavale, F., Chiacchio, P., and Chiaverini, S. (2000). Task-Space Regulation of Cooperative Manipulators. *Automatica*, 36:879–887.

Caccavale, F., Chiacchio, P., Marino, A., and Villani, L. (2008). Six-DOF Impedance Control of Dual-Arm Cooperative Manipulators. *IEEE Transactions on Mechatronics*, 13(5):576–586.

Caccavale, F. and Uchiyama, M. (2016). Cooperative Manipulators. In Siciliano, B. and Khatib, O., editors, *Springer Handbook of Robotics*, pages 989–1006. Springer International Publishing.

Caccavale, F. and Villani, L. (1999). Impedance Control of Cooperative Manipulators. *Mach. Intell. Robot. Control*, 2:51–57.

Cavusoglu, M. C., Sherman, A., and Tendick, F. (2002). Design of Bilateral Teleoperation Controllers for Haptic Exploration and Telemanipulation of Soft Environments. *IEEE Transactions on Robotics and Automation*, 18(4):641–647.

Cheah, C. C., Liu, C., and Slotine, J. J. E. (2006a). Adaptive Jacobian Tracking Control of Robots with Uncertainties in Kinematic, Dynamic and Actuator Models. *IEEE Transactions on Automatic Control*, 51(6):1024–1029.

Cheah, C. C., Liu, C., and Slotine, J. J. E. (2006b). Adaptive Tracking Control for Robots with Unknown Kinematic and Dynamic Properties. *The International Journal of Robotics Research*, 25:283–296.

Chiacchio, P., Chiaverini, S., and Siciliano, B. (1996). Direct and Inverse Kinematics for Coordinated Motion Tasks of a Two-Manipulator System. *Journal of dynamic systems measurements and control*, 118:691–697.

Chopra, N. and Spong, M. (2007). Adaptive Synchronization of Bilateral Teleoperators with Time Delay. In Ferre, M., Buss, M., Aracil, R., Melchiorri, C., and Balaguer, C., editors, *Advances in Telerobotics*, pages 257–270. Springer-Verlag.

Chopra, N., Spong, M. W., and Lozano, R. (2008). Synchronization of Bilateral Teleoperators with Time Delay. *Automatica*, 44:2142–2148.

Colgate, J. E. and Brown, J. M. (1994). Factors affecting the z-width of a haptic display. In *IEEE International Conference on Robotics and Automation*, pages 3205–3210.

Dauchez, P., Delebarre, X., Bouffard, Y., and Degoulange, E. (1991). Task modeling and force control for a two-arm robot. In *Proceedings. 1991 IEEE International Conference on Robotics and Automation*, pages 1702–1707 vol.2.

Dauchez, P., Delebarre, X., and Jourdan, R. (1990). Force control of a two-arm robot: implementation on a multiprocessor architecture. In *EEE International Workshop on Intelligent Robots and Systems, Towards a New Frontier of Applications*, pages 487–492.

Dietrich, A., Ott, C., and Stramigioli, S. (2016). Passivation of Projection-Based Null Space Compliance Control Via Energy Tanks. *IEEE Robotics and Automation Letters*, 1(1):184–191.

Dietrich, A., Wu, X., Bussmann, K., Ott, C., Albu-Schäffer, A., and Stramigioli, S. (2017). Passive Hierarchical Impedance Control Via Energy Tanks. *IEEE Robotics and Automation Letters*, 2(2):522–529.

Diftler, M. A., Mehling, J. S., Abdallah, M. E., Radford, N. A., Bridgwater, L. B., Sanders, A. M., Askew, R. S., Linn, D. M., Yamokoski, J. D., Permenter, F. A., Hargrave, B. K., Platt, R., Savely, R. T., and Ambrose, R. O. (2011). Robonaut 2 - The First Humanoid Robot in Space. In *IEEE International Conference on Robotics and Automation*, pages 2178–2183.

Erhart, S. and Hirche, S. (2013). Adaptive Force/Velocity Control for Multi-Robot Cooperative Manipulation under Uncertain Kinematic Parameters. In *Proceedings of the IEEE/RSJ International Conference on Intelligent Robots and Systems*, pages 307–314.

Erhart, S. and Hirche, S. (2016). Model and Analysis of the Interaction Dynamics in Cooperative Manipulation Tasks. *IEEE Transactions on Robotics*, 32(3):672–683.

Erhart, S., Sieber, D., and Hirche, S. (2013). An Impedance-Based Control Architecture for Multi-Robot Cooperative Dual-Arm Mobile Manipulation. In *Proceedings of the IEEE/RSJ International Conference on Intelligent Robots and Systems*, pages 315–322.

Erickson, D., Weber, M., and Sharf, I. (2003). Contact Stiffness and Damping Estimation for Robotic Systems. *Automatica*, 22:41–57.

Faria, R. (2016). Hybrid Kinematic Control of Dual-Arm Cooperative Robots for Object manipulation. Master's thesis, Universidade Federal do Rio de Janeiro.

Faria, R. O., Kucharczak, F., Freitas, G. M., Leite, A. C., Lizarralde, F., Galassi, M., and From, P. J. (2015). A Methodology for Autonomous Robotic Manipulation of Valves Using Visual Sensing. *2nd IFAC Workshop on Automatic Control in Offshore Oil and Gas Production*, pages 227–234.

Ferraguti, F., Preda, N., Manurung, A., Bonfè, M., Lambercy, O., Gassert, R., Muradore, R., Fiorini, P., and Secchi, C. (2015). An Energy Tank-Based Interactive Control Architecture for Autonomous and Teleoperated Robotic Surgery. *IEEE Transactions on Robotics*, 31(5):1073–1088.

Ferraguti, F., Secchi, C., and Fantuzzi, C. (2013). A Tank-Based Approach to Impedance Control with Variable Stiffness. In *IEEE International Conference on Robotics and Automation*, pages 4948–4953.

Ferre, M., Barrio, J., Melchiorri, C., Bogado, J. M., Castedo, P. L., and Ibarra, J. M. (2007). Experimental Results on Bilateral Control Using an Industrial Telemanipulator. In Ferre, M., Buss, M., Aracil, R., Melchiorri, C., and Balaguer, C., editors, *Advances in Telerobotics*, pages 163–176. Springer-Verlag.

Franken, M. (2015). *Control of haptic Interaction - An Energy-Based Approach.* PhD thesis, Technische Universiteit Eindhoven.

Franken, M., Misra, S., and Stramigioli, S. (2012). Stability of Position-Based Bilateral Telemanipulation Systems by Damping Injection. In *IEEE International Conference on Robotics and Automation*, pages 4300–4306.

Franken, M., Stramigioli, S., Misra, S., Secchi, C., and Macchelli, A. (2011). Bilateral Telemanipulation With Time Delays: A Two-Layer Approach Combining Passivity and Transparency. *IEEE Transactions on Robotics*, 27(4):741–756.

Franken, M., Stramigioli, S., Reilink, R., Secchi, C., and Macchelli, A. (2009). Bridging the Gap between Passivity and Transparency. In *Proc. of Robot.: Sci. and Syst.*, Seattle, WA.

Freitas, G. M., Leite, A. C., and Lizarralde, F. (2011). Kinematic Control of Constrained Robotic Systems. *SBA: Controle & Automacao Sociedade Brasileira de Automatica*, 22:559–572.

G.Niemeyer and Slotine, J.-J. E. (2004). Telemanipulation with Time Delays. *International Journal of Robotic Research*, 23(9):873–890.

Guenther, R. and Hsu, L. (1993). Variable Structure Adaptive Cascade Control of Rigid-Link Electrically-Driven Robot Manipulators. In *IEEE International Conference on Decision and Control*, pages 2137–2142 vol.3.

Guo, J., Liu, C., and Poignet, P. (2015). Enhanced Position-Force Tracking of Time-Delayed Teleoperation for Robotic-Assisted Surgery. In *2015 37th Annual International Conference of the IEEE Engineering in Medicine and Biology Society (EMBC)*, pages 4894–4897.

Hannaford, B. (1989). A Design Framework for Teleoperators with Kinesthetic Feedback. *IEEE Transactions on Robotics and Automation*, 5(4):426–434.

Hannaford, B. and Fiorini, P. (1988). A Detailed Model of Bi-lateral Teleoperation. In *International Conference on Systems, Man and Cybernetics Conference Proceedings*, volume 1, pages 117–121.

Hannaford, B. and Ryu, J.-H. (2001). Time Domain Passivity Control of Haptic Interfaces. In *IEEE International Conference on Robotics and Automation*, volume 2, pages 1863–1869.

Hashtrudi-Zaad, K. and Salcudean, S. E. (2001). Analysis of Control Architectures for Teleoperation Systems with Impedance/Admittance Master and Slave Manipulators. *International Journal of Robotic Research*, 20(6):419–445.

Hashtrudi-Zaad, K. and Salcudean, S. E. (2002). Transparency in Time-Delayed Systems and the Effect of Local Force Feedback for Transparent Teleoperation. *IEEE Transactions on Robotics and Automation*, 18(1):108–114.

Hayati, S. (1986). Hybrid Position/Force Control of Multi-Arm Cooperating Robots. In *IEEE International Conference on Robotics and Automation*, volume 3, pages 82–89.

Heck, D., Kostic, D., Denasi, A., and Nijmeijer, H. (2013). Internal and External Force-Based Impedance Control for Cooperative Manipulation. In *European Control Conference*, pages 2299–2304.

Heck, D. J. F. (2011). *Delayed Bilateral Teleoperation: A Direct Force-Reflecting Control Approach*. PhD thesis, University of Twente.

Heck, D. J. F., Saccon, A., and Nijmeijer, H. (2015). A Two-Layer Architecture for Force-Reflecting Bilateral Teleoperation with Time Delays. In *IEEE International Conference on Decision and Control*, pages 1509–1514.

Hoeckelmann, M., Rudas, I. J., Fiorini, P., Kirchner, F., and Haidegger, T. (2015). Current Capabilities and Development Potential in Surgical Robotics. *International Journal of Advanced Robotic Systems*.

Hogan, N. (1985). Impedance Control: An Approach to Manipulation: Parts I-II. *ASME Journal of Dynamic Systems, Measurement and Control*, 107:1–24.

Hokayem, P. F. and Spong, M. W. (2006). Bilateral Teleoperation: An Historical Survey. *Automatica*, 42(12):2035–2057.

Hsu, L., Costa, R. R., and Lizarralde, F. (2007). Lyapunov/Passivity-Based Adaptive Control of Relative Degree Two MIMO Systems with an Application to Visual Servoing. *IEEE Transactions on Automatic Control*, 52(2):364–371.

Hua, C., Yang, Y., and Liu, P. X. (2015). Output-Feedback Adaptive Control of Networked Teleoperation System With Time-Varying Delay and Bounded Inputs. *IEEE Transactions on Mechatronics*, 20(5):2009–2020.

Jazar, R. N. (2011). *Advanced Dynamics: Rigid Body, Multibody, and Aerospace Applications*. John Wiley & Sons, Inc., 1st edition.

Jean, J.-H. and Fu, L.-C. (1993). An Adaptive Control Scheme for Coordinated Multimanipulator Systems. *IEEE Transactions on Robotics and Automation*, 9(2):226–231.

Kelly, R., Davila, V. S., and Perez, J. A. L. (2005). *Control of Robot Manipulators in Joint Space*. Springer, 1st edition.

Khalil, H. K. (2002). *Nonlinear Systems*. Prentice Hall, Inc., 3rd edition.

Khatib, O., Yeh, X., Brantner, G., Soe, B., Kim, B., Ganguly, S., Stuart, H., Wang, S., Cutkosky, M., Edsinger, A., Mullins, P., Barham, M., Voolstra, C. R., Salama, K. N., L'Hour, M., and Creuze, V. (2016). Ocean One: A Robotic Avatar for Oceanic Discovery. *IEEE Robotics Automation Magazine*, 23(4):20–29.

Kruse, D., Radke, R. J., and Wen, J. T. (2013). A Sensor-Based Dual-Arm Tele-Robotic Manipulation Platform. In *International Conference on Automation Science and Engineering*, pages 350–355.

Kruse, D., Wen, J. T., and Radke, R. J. (2015). A Sensor-Based Dual-Arm Tele-Robotic System. *IEEE Transactions on Automation Science and Engineering*, 12(1):4–18.

Kuban, D. P. and Martin, H. L. (1984). An Advance Remotely Maintenable Force-Reflecting Servomanipulator Concept. In *National Topical Meeting on Robotics and Remote Handling in Hostile Environments*.

Lawrence, D. A. (1992). Stability and Transparency in Bilateral teleoperation. In *IEEE International Conference on Decision and Control*, pages 2649–2655.

Lawrence, D. A. (1993). Stability and Transparency in Bilateral Teleoperation. *IEEE Transactions on Robotics and Automation*, 9(5):624–637.

Lee, D. and Spong, M. (2006). Passibe Bilateral Teleoperation with Time Delays. *IEEE Transactions on Robotics*, 22(2):269–281.

Leite, A. C. (2011). *Servovisao adaptativa e controle de forca para robos manipuladores com cinematica e dinamica incertas interagindo com ambientes nao-estruturados*. PhD thesis, Universidade Federal do Rio de Janeiro.

Leite, A. C. and Lizarralde, F. (2016). Passivity-Based Adaptive 3D Visual Servoing without Depth and Image Velocity Measurements for Uncertain Robot Manipulators. *International Journal of Adaptive Control and Signal Processing*, 30(8-10):1269–1297.

Leite, A. C., Zachi, A., Lizarralde, F., and Hsu, L. (2011). Adaptive 3d visual servoing without image velocity measurement for uncertain manipulators. *IFAC Proceedings Volumes (18th IFAC World Congress)*, 44(1):14584–14589.

Li, H. and Kawashima, K. (2016). Bilateral Teleoperation with Delayed Force Feedback Using Time Domain Passivity Controller. *Robotics and Computer-Integrated Manufacturing*, 37:188–196.

Liu, Y. C. and Khong, M. H. (2015). Adaptive Control for Nonlinear Teleoperators with Uncertain Kinematics and Dynamics. *IEEE Transactions on Mechatronics*, 20(5):2550–2562.

Lizarralde, F., Leite, A. C., Hsu, L., and Costa, R. R. (2013). Adaptive Visual Servoing Scheme Free of Image Velocity Measurement for Uncertain Robot Manipulators. *Automatica*, 49(5):1304–1309.

Llewellyn, F. B. (1952). Some fundamental properties of transmission systems. *Proceedings of the IRE*, 40(3):271–283.

Mehling, J. S., Strawser, P., Bridgwater, L., Verdeyen, W. K., and Rovekamp, R. (2007). Centaur: NASA's Mobile Humanoid Designed for Field Work. In *Proceedings 2007 IEEE International Conference on Robotics and Automation*, pages 2928–2933.

Melchiorri, C. (2003). Robotic Telemanipulation Systems: An Overview on Control Aspects. *International Federation of Automatic Control*.

Mendoza, M., Bonilla, I., Gonzalez-Galvan, E., and Reyes, F. (2016). Impedance Control in a Wave-Based Teleoperator for Rehabilitation Motor Therapies Assisted by Robots. *Comput Methods Programs Biomed*, 123:54–67.

Mohajerpoor, R., Sharifi, I., Talebi, H. A., and Rezaei, S. M. (2013). Adaptive Bilateral Teleoperation of an Unknown Object Handled by Multiple Robots under Unknown Communication Delay. In *Proc. of IEEE/ASME Int. Conf. Adv. Intel. Mech.*, pages 1158–1163.

Montemayor, G. and Wen, J. T. (2004). Multiple Robot Force Control with Delayed Force Measurements. In *Proceedings of the IEEE International Conference on Control Applications*, volume 1, pages 327–332.

Munir, S. and Book, W. J. (2002). Internet-Based Teleoperation Using Wave Variables with Prediction. *IEEE Transactions on Mechatronics*, 7(2):124–133.

Ni, L. and Wang, D. W. L. (2002). Contact Transition Stability Analysis for a Bilateral Teleoperation System. In *IEEE International Conference on Robotics and Automation*, pages 3272–3277.

Niemeyer, G., Preusche, C., Stramigioli, S., and Lee, D. (2016). Telerobotics. In Siciliano, B. and Khatib, O., editors, *Springer Handbook of Robotics*, pages 1085–1108. Springer International Publishing.

Niemeyer, G. and Slotine, J. J. E. (1991). Stable Adaptive Teleoperation. *IEEE Journal of Oceanic Engineering*, 16(1):152–162.

Nudehi, S. S., Mukherjee, R., and Ghodoussi, M. (2005). A Shared-Control Approach to Haptic Interface Design for Minimally Invasive Telesurgical Training. *IEEE Transactions on Control Systems Technology*, 13(4):588–592.

Nuno, E., Basanez, L., de Alba-Padilla, C., and Lopez-Franco, C. (2012a). An Adaptive Controller for Bilateral Teleoperators: Transatlantic Experiments Using the Internet. In *World Automation Congress 2012*, pages 1–6.

Nuno, E., Basanez, L., and G. Obregon-Pulido and, G. S.-P. (2011a). Bilateral Teleoperation Control without Velocity Measurements. In *International Federation of Automatic Control*, pages 332–337, Milano, Italy.

Nuno, E., Basanez, L., and Ortega, R. (2011b). Passivity-Based Control for Bilateral Teleoperation: A Tutorial. *Automatica*, 47(3):485–495.

Nuno, E., Basanez, L., Ortega, R., and Obregon-Pulido, G. (2010a). Position Tracking Using Adaptive Control for Bilateral Teleoperators with Time-Delays. In *IEEE International Conference on Robotics and Automation*, pages 5370–5375.

Nuno, E., Basanez, L., Ortega, R., and Spong, M. W. (2009a). Position Tracking for Non-Linear Teleoperators with Variable Time Delay. *International Journal of Robotic Research*, 28(7):895–910.

Nuno, E., Basanez, L., and Prada, M. (2009b). Asymptotic Stability of Teleoperators with Variable Time-Delays. In *2009 IEEE International Conference on Robotics and Automation*, pages 4332–4337.

Nuno, E., Ortega, R., Barabanov, N., and Basanez, L. (2008). A Globally Stable PD Controller for Bilateral Teleoperators. *IEEE Transactions on Robotics*, 24(3):753–758.

Nuno, E., Ortega, R., and Basanez, L. (2010b). An Adaptive Controller for Nonlinear Teleoperators. *Automatica*, 46:155–159.

Nuno, E., Sarras, I., and Basanez, L. (2013a). Consensus in Networks of Nonidentical Euler–Lagrange Systems Using P+d Controllers. *IEEE Transactions on Robotics*, 29(6):1503–1508.

Nuno, E., Sarras, I., and Basanez, L. (2014a). An Adaptive Controller for Bilateral Teleoperators: Variable Time-Delays Case. In *International Federation of Automatic Control*, pages 9341–9346, Cape Town, South Africa.

Nuno, E., Sarras, I., Basanez, L., and Kinnaert, M. (2012b). A Proportional Plus Damping Injection Controller for Teleoperators with Joint Flexibility and Time-Delays. In *IEEE International Conference on Robotics and Automation*, pages 4294–4299.

Nuno, E., Sarras, I., Basanez, L., and Kinnaert, M. (2014b). Control of Teleoperators with Joint Flexibility, Uncertain Parameters and Time-Delays. *Robotics and Autonomous Systems*, 62(12):1691–1701.

97

Nuno, E., Valle, D., Sarras, I., and Basanez, L. (2013b). Bilateral Teleoperation of Flexible-Joint Manipulators with Dynamic Gravity Compensation and Variable Time-Delays. In *Proceedings of the IEEE/RSJ International Conference on Intelligent Robots and Systems*, pages 5439–5444.

P. Arcara, C. M. (2002). Control Schemes for Teleoperation with Time Delay: A Comparative Study. *Robotics and Autonomous Systems*, 38:49–64.

Panzirsch, M., Balachandran, R., and Artigas, J. (2015). Cartesian Task Allocation for Cooperative, Multilateral Teleoperation Under Time Delay. In *IEEE International Conference on Robotics and Automation*, pages 312–317.

Passenberg, C., Peer, A., and Buss, M. (2010). A Survey of Environment-, Operator-, and Task-Adapted Controllers for Teleoperation Systems. *Mechatronics*, 20:787–801.

Petit, A., Lippiello, V., Fontanelli, G. A., and Siciliano, B. (2017"). Tracking elastic deformable objects with an rgb-d sensor for a pizza chef robot. *Robotics and Autonomous Systems*, 88:187 – 201.

Ribeiro, G. C. M. (2013). Teleoperacao Bilateral de Multiplos Robos Aplicada ao Transporte de Carga. Master's thesis, Universidade Federal do Rio de Janeiro.

Ribeiro, G. C. M., Lizarralde, F., and Hsu, L. (2014). Bilateral Teleoperation of Multiple Cooperative Robots for Load Transport. In *Congresso Brasileiro de Automática*, pages 1498–1505, Belo Horizonte.

Ryu, J.-H., Artigas, J., and Preusche, C. (2010). A Passive Bilateral Control Scheme for a Teleoperator with Time-Varying communication delay. *Mechatronics*, 20:812–823.

Ryu, J.-H., Kim, Y. S., and Hannaford, B. (2004). Sampled- and Continuous-Time Passivity and Stability of Virtual Environments. *IEEE Transactions on Robotics*, 20(4):772–776.

Ryu, J. H. and Preusche, C. (2007). Stable Bilateral Control of Teleoperators Under Time-varying Communication Delay: Time Domain Passivity Approach. In *IEEE International Conference on Robotics and Automation*, pages 3508–3513.

Salvietti, G., Meli, L., Gioioso, G., Malvezzi, M., and Prattichizzo, D. (2017). Multicontact Bilateral Telemanipulation With Kinematic Asymmetries. *IEEE Transactions on Mechatronics*, 22(1):445–456.

Sarras, I., Nuno, E., Kinnaert, M., and Basanez, L. (2012). Output-Feedback Control of Nonlinear Bilateral Teleoperators. In *Proceedings of the IEEE American Control Conference*, pages 3490–3495.

Satici, A. C., Ruggiero, F., Lippiello, V., and Siciliano, B. (2016). A coordinate-free framework for robotic pizza tossing and catching. In *2016 IEEE International Conference on Robotics and Automation (ICRA)*, pages 3932–3939.

Schindlbeck, C. and Haddadin, S. (2015). Unified Passivity-Based Cartesian Force/Impedance Control for Rigid and Flexible Joint Robots Via Task-Energy Tanks. In *IEEE International Conference on Robotics and Automation*, pages 440–447.

Schneider, S. A. and R. H. Cannon, J. (1992). Object Impedance Control for Co-operative Manipulation: Theory and Experimental Results. *IEEE Transactions on Robotics and Automation*, 8(3):383–394.

Shahbazi, M., Atashzar, S. F., Talebi, H. A., and Patel, R. V. (2015). Novel Co-operative Teleoperation Framework: Multi-Master Single-Slave System. *IEEE Transactions on Mechatronics*, 20(4):1668–1679.

Sherman, A., Cenk, M., and Tendick, F. (2000). Comparison of Teleoperator Cconrol Architectures for Palpation Task. In *Symp. on Haptic Interfaces for Virtual Environment and Teleoperator Systems*.

Siciliano, B., Sciavicco, L., Villani, L., and Oriolo, G. (2009). *Robotics: Modelling, Planning and Control.* Springer-Verlag London, 1st edition.

Sieber, D., Deroo, F., and Hirche, S. (2013). Formation-Based Approach for Multi-Robot Cooperative Manipulation Based on Optimal Control Design. In *Proceedings of the IEEE/RSJ International Conference on Intelligent Robots and Systems*, pages 5227–5233.

Sieber, D., Musić, S., and Hirche, S. (2015). Multi-Robot Manipulation Controlled by a Human with Haptic Feedback. In *Proceedings of the IEEE/RSJ International Conference on Intelligent Robots and Systems*, pages 2440–2446.

Slotine, J. J. E. and Li, W. (1988). Adaptive Manipulator Control: A Case Study. *IEEE Transactions on Automatic Control*, 33(11):995–1003.

Slotine, J. J. E. and Li, W. (1991). *Applied Nonlinear Control.* Prentice Hall Inc., 1 edition.

Smith, C., Karayiannidis, Y., Nalpantidis, L., Gratal, X., Qi, P., Dimarogonas, D. V., and Kragic, D. (2012). Dual Arm Manipulatio - A Survey. *Robotics and Autonomous Systems*, 60:1340–1353.

Stramigioli, S., Mahony, R., and Corke, P. (2010). A Novel Approach to Haptic Tele-Operation of Aerial Robot Vehicles. In *IEEE International Conference on Robotics and Automation*, pages 5302–5308.

Stuart, H., Wang, S., Khatib, O., and Cutkosky, M. R. (2017). The Ocean One Hands: An Adaptive Design for Robust Marine Manipulation. *The International Journal of Robotics Research*, pages 1–17.

Sun, D., Naghdy, F., and Du, H. (2014). Application of Wave-Variable Control to Bilateral Teleoperation Systems: A Survey. *Annual Reviews in Control*, 38:12–31.

Tadele, T. S., de Vries, T. J. A., and Stramigioli, S. (2014). Combining Energy and Power Based Safety Metrics in Controller Design for Domestic Robots. In *IEEE International Conference on Robotics and Automation*, pages 1209–1214.

Tanner, N. A. and Niemeyer, G. (2004). Online Tuning of Wave Impedance in Telerobotics. In *IEEE Conference on Robotics, Automation and Mechatronics*, volume 1, pages 7–12 vol.1.

Tinos, R., Terra, M. H., and Ishihara, J. Y. (2006). Motion and Force Control of Cooperative Robotic Manipulators with Passive Joints. *IEEE Transactions on Control System Technology*, 14(4):725–734.

Uchiyama, M. and Dauchez, P. (1988). A Symmetric Hybrid Position/Force Control Scheme for the Coordination of Two Robots. In *IEEE International Conference on Robotics and Automation*, pages 350–356 vol.1.

Uchiyama, M., Iwasawa, N., and Hakomori, K. (1987). Hybrid Position/Force Control for Coordination of a Two-Arm Robot. In *Robotics and Automation. Proceedings. 1987 IEEE International Conference on*, volume 4, pages 1242–1247.

Vittorias, I. and Hirche, S. (2010). Stable Teleoperation with Communication Unreliabilities and Approximate Human/Environment Dynamics Knowledge. In *Proceedings of the IEEE American Control Conference*, pages 2791–2796.

Wang, H. (2013). Passivity Based Synchronization for Networked Robotic Systems with Uncertain Kinematics and Dynamics. *Automatica*, 49:755–761.

Wang, H. and Xie, Y. (2009). Adaptive Inverse Dynamics Control of Robots with Uncertain Kinematics and Dynamics. *Automatica*, 45:2114–2119.

Wen, J. T. and Kreutz-Delgado, K. (1992). Motion and Force Control of Multiple Robotic Manipulators. *Automatica*, 28:729–743.

Wikipedia (2017). Network delay. https://en.wikipedia.org/wiki/Network_delay. Accessed: 2017-09-05.

Willaert, B., Corteville, B., Reynaerts, D., Brussel, H. V., and Poorten, E. B. V. (2010). Transparency Trade-Offs for a 3-Channel Controller Revealed by the Bounded Environment Passivity Method. In *2010 Third International Conference on Advances in Computer-Human Interactions*, pages 66–72.

Willaert, B., D. Reynaerts, H. v. B., and Poorten, E. B. V. (2014). Bilateral Teleoperation: Quantifying the Requirements for and Restrictions of Ideal Transparency. *IEEE Transactions on Control Systems Technology*, 22(1):387–395.

Yang, X., Hua, C., Yan, J., and Guan, X. (2016). An Exact Stability Condition for Bilateral Teleoperation with Delayed Communication Channel. *IEEE Transactions Systems, Man, and Cybernetics: Systems*, 46(3):434–439.

Yanque, I., Lizarralde, F., and Leite, A. C. (2016). Bilateral Teleoperation for Uncertain Robot Manipulators Based on the Formation Control Approach. In *Proceedings of the IEEE International Conference on Control Applications*, pages 911–916, Buenos Aires, Argentina.

Yokokohji, Y., Imaida, T., and Yoshikawa, T. (1999). Bilateral teleoperation under time-varying communication delay. In *Proceedings of the IEEE/RSJ International Conference on Intelligent Robots and Systems*, volume 3, pages 1854–1859.

Yokokohji, Y. and Yoshikawa, T. (1994). Bilateral Control of Master-Slave Manipulators for Ideal Kinesthetic Coupling-Formulation and Experiment. *IEEE Transactions on Robotics and Automation*, 10(5):605–620.

Appendix A

A.1 Uncertain kinematic Prediction Error

Replacing (3.16) in (3.10) gives

$$
\begin{aligned}
\dot{p}_i &= J_i(q_i)\hat{J}_i^\dagger(q_i)(v_i + \omega_1), \\
&= J_i(q_i)\left(\hat{J}_i^\dagger(q_i) + J_i^\dagger(q_i) - J_i^\dagger(q_i)\right)(v_i + \omega_1), \\
&= v_i + \omega_1 + \underbrace{J_i(q_i)\left(\hat{J}_i^\dagger(q_i) - J_i^\dagger(q_i)\right)(v_i + \omega_1)}_{\epsilon_i},
\end{aligned}
$$

where $\epsilon_i \in \mathbb{R}^3$ is a vanishing perturbation term

$$
\begin{aligned}
\epsilon_i &= \left(J_i(q_i)\hat{J}_i^\dagger(q_i) - I\right)(v_i + \omega_1), \qquad I = \hat{J}_i(q_i)\hat{J}_i^\dagger(q_i), \\
&= \left(J_i(q_i) - \hat{J}_i(q_i)\right)\underbrace{\hat{J}_i^\dagger(q_i)(v_i + \omega_1)}_{\beta_i}, \\
&= J_i(q_i)\beta_i - \hat{J}_i(q_i)\beta_i,
\end{aligned}
$$

then ϵ_i can be parameterized as in (3.9), which gives

$$
\begin{aligned}
\epsilon_i &= W_i(q_i, \beta_i)b_i - W_i(q_i, \beta_i)\hat{b}_i, \\
&= W_i(q_i, \beta_i)\tilde{b}_i.
\end{aligned}
$$

where $\tilde{b}_i$ is the parameter estimation error and β_i in (3.18) is given by

$$
\beta_i = \hat{J}_i^\dagger(q_i)(v_i + \omega_1). \tag{A.1}
$$

A.2 Positive Definite Storage Function

To prove the presented theorems an energy motivated storage function based on the one proposed by Bai and Wen (2010) is used. The Taylor series of the Potential

function of the deformation $P(\delta_i)$, considering the assumption (3.6), is given by

$$P(\delta_i) = P(\delta_i^d) + \nabla P(\delta_i^d)\tilde{\delta} + \frac{1}{2}\nabla^2 P(\hat{\delta}_i)\tilde{\delta}_i^2, \quad \hat{\delta}_i \in [\delta_i, \delta_i^d]$$

then the following energy motivated storage function can be considered

$$\begin{aligned} V_{A1} &= \frac{1}{2}\nabla^2 P(\hat{\delta}_i)\tilde{\delta}_i^2, \\ &= P(\delta_i) - P(\delta_i^d) - \nabla P(\delta_i^d)\tilde{\delta}_i > 0. \end{aligned}$$

Appendix B

Proofs of Theorems

B.1   Proof of Theorem 3

First, let $V_1(x_1)$ and $V_2(x_2)$ be the storage functions for the interconnected subsystems Σ_1 and Σ_2. Now, we consider

$$V(x) = V_2(x_2) + \alpha V_1(x_1), \tag{B.1}$$

as the storage function for the feedback connection.

The time-derivative of $V(x)$ along the trajectories of the subsystems Σ_1 and Σ_2, considering $\omega_2 = 0$, is given by

$$\dot{V} \leq -\lambda_2 \|y_2\|^2 - \alpha\lambda_1\|y_1\|^2 + \alpha c_1\|y_1\|\|y_2\|, \qquad \alpha > 0, \tag{B.2}$$

$$\dot{V} \leq \begin{bmatrix} \|y_1\| & \|y_2\| \end{bmatrix} \begin{bmatrix} -\alpha\lambda_1 & \frac{1}{2}\alpha c_1 \\ \frac{1}{2}\alpha c_1 & -\lambda_2 \end{bmatrix} \begin{bmatrix} \|y_1\| \\ \|y_2\| \end{bmatrix}, \tag{B.3}$$

a Shur's complement property states that

$$\begin{bmatrix} S_1 & S_2 \\ S_2^\mathsf{T} & S_3 \end{bmatrix} < 0 \iff S_3 < 0, \quad S_1 - S_2^\mathsf{T} S_3^{-1} S_2 < 0, \tag{B.4}$$

then from (B.3), $\dot{V} < 0$ if

$$-\lambda_2 < 0, \qquad -\alpha\left(\lambda_1 + \frac{\alpha c_1^2}{4\lambda_2}\right) < 0, \tag{B.5}$$

then for some value of $\alpha > 0$, sufficiently small, implies that $\dot{V}(x)$ is negative definite with respect to outputs y_1 and y_2. As a consequence, we have $x_1, x_2 \in \mathcal{L}_\infty$ and $\dot{x}_1, \dot{x}_2 \in \mathcal{L}_\infty$. The inequality equation for $\dot{V}(x)$ implies that $y_1, y_2 \in \mathcal{L}_2 \cap \mathcal{L}_\infty$. From Barbalat's lemma (Slotine and Li (1991), p.122), it results that $\lim_{t\to\infty} y_1(t) = 0$

and $\lim_{t\to\infty} y_2(t) = 0$, which demonstrates the global asymptotic stability of the closed-loop interconnected subsystems.

Appendix C

Representation of Orientation

The orientation of a robotic manipulator can be obtained by resorting to four parameters expressing a rotation of a given angle $\vartheta \in \mathbb{R}$ about an axis $r \in \mathbb{R}^3$ in space (Siciliano et al. (2009)). Let $r = [r_x \ r_y \ r_z]^\mathsf{T}$ be the unit vector of a rotation axis with respect to the reference frame $\mathbb{E}_s$ as in Fig. C.1.
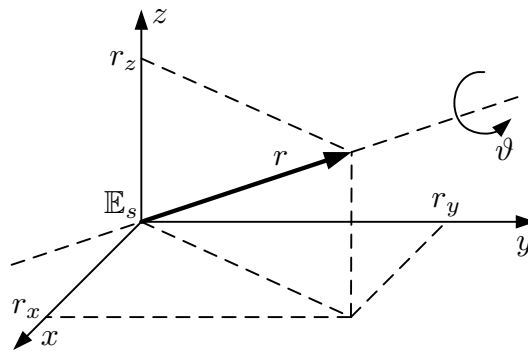

Figure C.1: Rotation around an arbitrary axis

C.1 Rotation Matrix

The orientation can be represented by a rotation matrix $R(\vartheta, r)$ given by

$$R(\vartheta, r) = \begin{bmatrix} r_x^2 m_\vartheta + c_\vartheta & r_x r_y m_\vartheta - r_z s_\vartheta & r_x r_z m_\vartheta + r_y s_\vartheta \\ r_x r_y m_\vartheta + r_z s_\vartheta & r_y^2 m_\vartheta + c_\vartheta & r_y r_z m_\vartheta - r_x s_\vartheta \\ r_x r_z m_\vartheta - r_y s_\vartheta & r_y r_z m_\vartheta + r_x s_\vartheta & r_z^2 m_\vartheta + c_\vartheta \end{bmatrix} \tag{C.1}$$

where $s_\vartheta = \sin \vartheta$, $c_\vartheta = \cos \vartheta$ and $m_\vartheta = 1 - \cos \vartheta$.

Likewise, consider the rotation matrix R given by

$$R = \begin{bmatrix} r_{11} & r_{12} & r_{13} \\ r_{21} & r_{22} & r_{23} \\ r_{31} & r_{32} & r_{33} \end{bmatrix},$$
(C.2)

the respective angle ϑ and axis r can be computed by

$$\vartheta = \cos^{-1}\left(\frac{r_{11} + r_{22} + r_{33} - 1}{2} \right), \qquad r = \frac{1}{2s_\vartheta} \begin{bmatrix} r_{32} - r_{23} \\ r_{13} - r_{31} \\ r_{21} - r_{12} \end{bmatrix},$$
(C.3)

for $s_\vartheta \neq 0$. If $s_\vartheta = 0$, the expressions (C.3) become meaningless. Notice that when $\vartheta = 0$ the unit vector r is arbitrary.

C.2 Unit Quaternion

Another representation of the orientation that overcomes the drawbacks angle/axis is given by the unit quaternion $Q(\vartheta, r)$. It is a four element vector that describes the orientation difference between two systems separated by a rotation of an angle ϑ (in rad) around a unit vector r. It is given by a scalar $Q_s \in \mathbb{R}$ and a vector $Q_v \in \mathbb{R}^3$, defined as follows

$$Q(\vartheta, r) = \{Q_s, Q_v\}, \qquad Q_s = \cos\frac{\vartheta}{2}, \qquad Q_v = \sin\frac{\vartheta}{2}r,$$
(C.4)

where $Q_v = [Q_{vx} \; Q_{vy} \; Q_{vz}]^\mathsf{T}$. It is subject to the following restriction

$$Q_s^2 + Q_v^\mathsf{T} Q_v = 1.$$
(C.5)

A rotation by $-\vartheta$ about $-r$ gives the same quaternion as that associated with a rotation by ϑ about r.

Consider two quaternions $Q_1 = \{Q_{s1}, Q_{v1}\}$ and $Q_2 = \{Q_{s2}, Q_{v2}\}$ that correspond to the rotations R_1 and R_2 respectively. The quaternion corresponding to the product $R_1 R_2$ is given by

$$Q_1 * Q_2 = \left\{ Q_{s1} Q_{s2} - Q_{v1}^\mathsf{T} Q_{v2} \;,\; Q_{s1} Q_{v2} + Q_{s2} Q_{v1} + Q_{v1} \times Q_{v2} \right\},$$
(C.6)

where $\times$ denotes the cross product.

Also, the quaternion related to $R(\vartheta, r)^{-1} = R(\vartheta, r)^\mathsf{T}$ is denoted as Q^{-1} and is given by $Q^{-1} = \{Q_s, -Q_v\}$.

C.3 Relation between the unit quaternion and the rotation matrix

A rotation matrix can be related with its corresponding quaternion by

$$R(Q_s, Q_v) = (2Q_s^2 - Q_v^\mathsf{T} Q_v)I + 2(Q_v Q_v^\mathsf{T} - Q_s S(Q_v)) \tag{C.7}$$

where $S(.)$ is the vectorial product operator and $I \in \mathbb{R}^{3 \times 3}$ is the identity matrix, which results in

$$R(Q_s, Q_v) = \begin{bmatrix} 2(Q_s^2 + Q_{vx}^2) - 1 & 2(Q_{vx}Q_{vy} - Q_s Q_{vz}) & 2(Q_{vx}Q_{vz} + Q_s Q_{vy}) \\ 2(Q_{vx}Q_{vy} + Q_s Q_{vz}) & 2(Q_s^2 + Q_{vy}^2) - 1 & 2(Q_{vy}Q_{vz} - Q_s Q_{vx}) \\ 2(Q_{vx}Q_{vz} - Q_s Q_{vy}) & 2(Q_{vy}Q_{vz} + Q_s Q_{vx}) & 2(Q_s^2 + Q_{vz}^2) - 1 \end{bmatrix} \tag{C.8}$$

Likewise, the quaternion q that correspond to the rotation R given by

$$R = \begin{bmatrix} r_{11} & r_{12} & r_{13} \\ r_{21} & r_{22} & r_{23} \\ r_{31} & r_{32} & r_{33} \end{bmatrix} \tag{C.9}$$

can be compute in the following way

$$Q_s = \frac{1}{2}\sqrt{tr(R) + 1}, \qquad Q_v = \frac{1}{2} \begin{bmatrix} sgn(r_{32} - r_{23})\sqrt{r_{11} - r_{22} - r_{33} + 1} \\ sgn(r_{13} - r_{31})\sqrt{r_{22} - r_{33} - r_{11} + 1} \\ sgn(r_{21} - r_{12})\sqrt{r_{33} - r_{11} - r_{22} + 1} \end{bmatrix}, \tag{C.10}$$

where conventionally $sgn(x) = 1$ for $x \geq 0$ and $sgn(x) = -1$ for $x < 0$ and $tr(.)$ is the trace function. Notice that in (C.10) it has been implicitly assumed $Q_s \geq 0$, this corresponds to an angle $\vartheta \in [-\pi, \pi]$, and thus any rotation can be described.

Appendix D

Robotic Manipulator

D.1   Description of the Motoman DIA10

For the simulations and experiments presented in this work the model of the Motoman DIA10 (Fig. D.1) was adopted. It is a robotic manipulator that consist in two anthropomorphic robotic arms (with 7 revolution joints each) and a common rotating base, which results in a 15 revolution joint robotic system where all joints can be controlled independently (Ribeiro (2013)). Each arm can withstand a payload of 10kg at the end-effector.
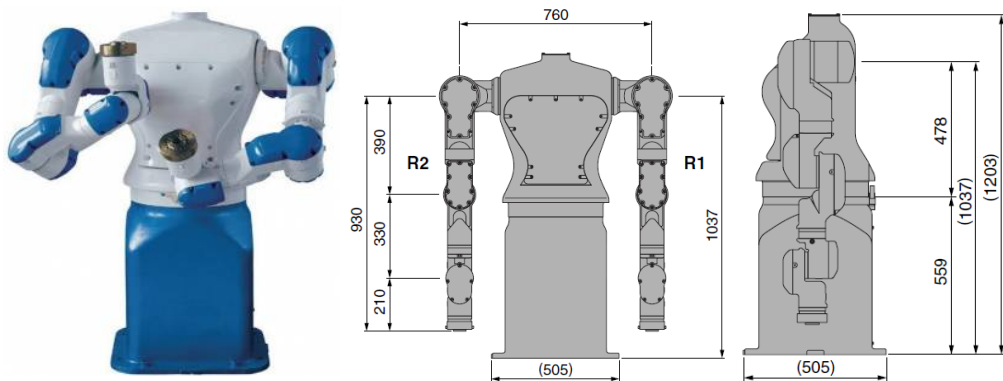

Figure D.1: Photo and schematics of the Motoman DIA10 with dimmentions in mm.

D.2   Control Architecture of Motoman

The devices and software used to control the Motoman are briefly commented in this section.

NX100

The Motoman is controlled though the industrial controller NX100, where the drivers of the servo motors are located. The NX100 is connected though three power

cables and two signal cables to read the encoders. A industrial three-phase power outlet of 248 V, 435 KVA energy source is used.

Teach Pendant

The Teach Pendant is used to configure the NX100 and control the Motoman DIA10. It is a handheld device wired to the NX100 that serves as a control box for programming the motions of the robot, it can be set to the modes *remote*, *learn* or *play*. When the *play* mode is enabled the controller is set in automatic mode and can receive external control signals from a computer though the HSC.

High Speed Controller (HSC)

The High Speed Controller (HSC) is used to control the Motoman DIA10 thought a computer with the industrial network Star Fabric. It reconciles the real time control of the industrial controller with the control implemented in a computer. A common two-way Ethernet wiring is used, one for the transmission and the other for the reception of data, requiring a special network interface controller.

The HSC sets a system similar to a share memory allowing that the NX100 and the computer to have access the same data, even at different times. The NX100 considers the actual and desired positions of the joints in encoder's pulses. The conversion from pulses to degrees is obtain thought a parameter that corresponds to each joint, that conversion is done directly to radians using a communication library written according the recommendations for the Motoman. This library can be accessed by any computer in the network using a program in RR.

Robot Raconteur (RR)

The Robot Raconteur (RR) is a communication library for applications in robotic and automation, it is used to make avaliable the access to the Motoman by any computer in the same network. Every program is a node in a network formed in a single computer or distributed in different devices. Each node can have different objects, properties and methods that can be accessed and called by the other nodes. The RR supports different programming languages, among them Matlab and C++.

To connect a node is necessary to know its the address (IP and gate). During the connection the client node receives a description of the characteristics of the server though a text message. The node has an object with two properties, one for the access to the current positions of the joints (ActualRobotJointAngles) and the other to define the desired angles (DesiredRobotJointAngles). This reference goes to a position control loop designed in Simulink, compiled and executed by the node in a frequency of 500 Hz.

The overall architecture of the Motoman DIA10 is presented in Figure D.2 and a detailed explanation of the architecture control and the steps for its operation can be found in (Ribeiro (2013)).
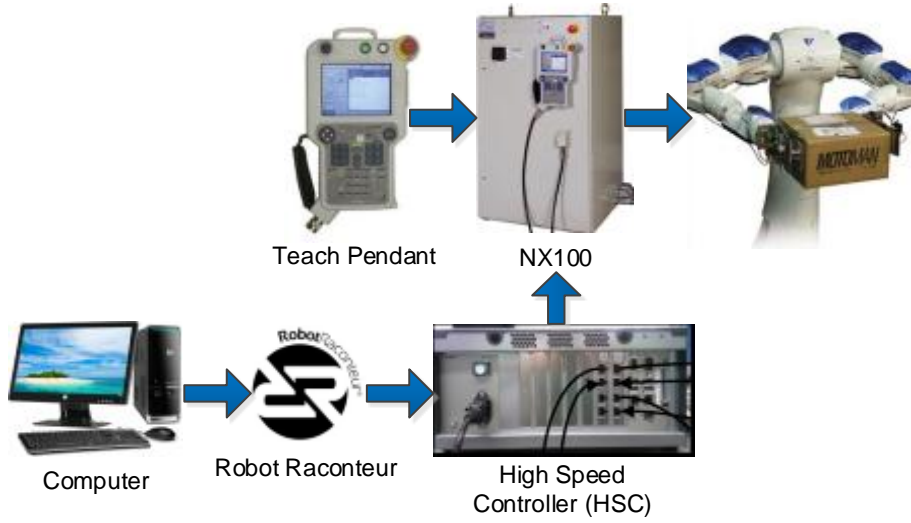

Figure D.2: Architecture of the Motoman DIA10.

D.3   Denavit-Hartenberg parameters of Motoman

Considering a initial position where the arms are wide open, the Denavit-Hartenberg (DH) representation of each arm was considered to obtain a representation of the direct kinematics of the Motoman. The adopted convention is the DH Standard. The DH parameters in Table D.1 and the schematics of the axis and frames considered is presented in Figure D.3. Notice that each arm is represented separately albeit both arms share the same torso, i.e. the rotation of the first joint is always the same for both arms.

Table D.1: Standard Denavit-Hartenberg Parameters of Motoman.

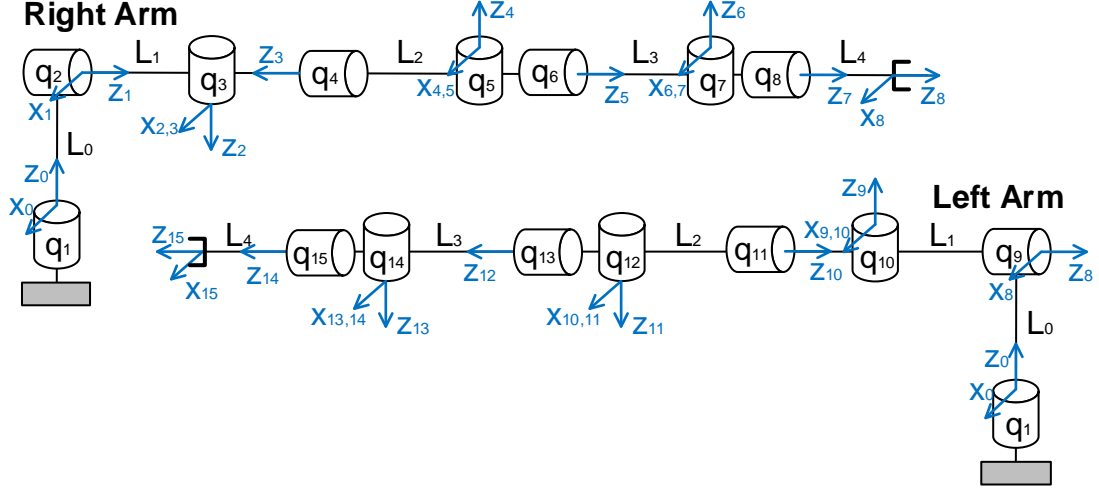| DH Right Arm					DH Left Arm			
i	q_i	d_i	a_i	α_i	i	q_i	d_i	a_i	α_i
1	q_1	1.337	0	$-\pi/2$	1	q_1	1.337	0	$-\pi/2$
2	q_2	0.380	0	$-\pi/2$	2	q_9	-0.380	0	$\pi/2$
3	q_3	0	0	$-\pi/2$	3	q_{10}	0	0	$-\pi/2$
4	q_4	-0.390	0	$-\pi/2$	4	q_{11}	-0.390	0	$-\pi/2$
5	q_5	0	0	$-\pi/2$	5	q_{12}	0	0	$-\pi/2$
6	q_6	0.330	0	$\pi/2$	6	q_{13}	0.330	0	$\pi/2$
7	q_7	0	0	$-\pi/2$	7	q_{14}	0	0	$-\pi/2$
8	q_8	0.210	0	0	8	q_{15}	0.210	0	0

Figure D.3: Denavit-Hartenberg Diagram of Motoman.

D.4 Differential Kinematics of the Motoman

Let $p_R \in \mathbb{R}^3$ and $p_L \in \mathbb{R}^3$ denote the position and $Q_R \in \mathbb{R}^4$ and $Q_L \in \mathbb{R}^4$ denote the orientation (represented with unit quaternions) of the end-effectors of the Motoman, where R and L stands for left and right, respectively. The orientation can also be represented using rotation matrices for the left $R_R \in \mathbb{R}^{3\times3}$ and right $R_L \in \mathbb{R}^{3\times3}$ arms

Then, the pose of the arms can be expressed in terms of operational space vectors x_R and x_L given by

$$x_R = k_R(q_R) = \begin{bmatrix} p_R(q_R) \\ Q_R(q_R) \end{bmatrix}, \qquad x_L = k_L(q_L) = \begin{bmatrix} p_L(q_L) \\ Q_L(q_L) \end{bmatrix}, \qquad (\text{D.1})$$

where k_R, k_L are the direct kinematic functions and $q_R = [q_1 \quad q_2 \ldots q_8]$ and $q_L = [q_1 \quad q_9 \ldots q_{15}]$ denote the joint position vectors of the left and right arms (as in Fig.D.3). Notice that q_R and q_L share the joint q_1 which corresponds to the rotating torso of the Motoman.

Consider that linear velocity $\dot{p}_R, \dot{p}_L \in \mathbb{R}^3$ and angular velocity $\omega_R, \omega_L \in \mathbb{R}^3$ can be collected in the generalized velocity vector $\vee_R, \vee_L \in \mathbb{R}^6$, as in (Caccavale and Uchiyama (2016)).

Then, the differential direct kinematics of the arms can be expressed as

$$\vee_R = \begin{bmatrix} \dot{p}_R \\ \omega_R \end{bmatrix} = J_R(q_R)\dot{q}_R, \qquad \vee_L = \begin{bmatrix} \dot{p}_L \\ \omega_L \end{bmatrix} = J_L(q_L)\dot{q}_L, \qquad (\text{D.2})$$

where $J_R, J_L \in \mathbb{R}^{6\times8}$ denote the geometric Jacobians of the right and left arm, respectively.

Let $J_M \in \mathbb{R}^{12\times15}$ be the Jacobian matrix that maps the 15 joint velocities to the

12 spatial velocities (angular and linear) of both end-effectors (Kruse et al. (2015)), such that

$$
\begin{bmatrix} v_R \\ v_L \end{bmatrix} = J_M(q_M)\,\dot{q}_M, \qquad q_M = [\overbrace{q_1}^{\text{Torso}} \quad \overbrace{q_2 \dots q_8}^{\text{Right Arm}} \quad \overbrace{q_9 \dots q_{15}}^{\text{Left Arm}}]^\mathsf{T}, \tag{D.3a}
$$

$$
J_M = \begin{bmatrix} J_{R1} & J_{R2} \dots J_{R8} & 0 \\ J_{L1} & 0 & J_{L2} \dots J_{L8} \end{bmatrix}, \tag{D.3b}
$$

where J_{Ri}, J_{Li} with $i = 1, \dots, 8$, denote the ith column of the Jacobian matrices J_R, J_L, respectively.